

https://dspace.org/

Optimization of the Integrated Gasification Combined Cycle using mathematical modelling

Mvelase, Bongani Ellias

2016

http://hdl.handle.net/10539/20992

Mvelase, Bongani Ellias (2016) Optimization of the Integrated Gasification Combined Cycle using advanced mathematical modelling, University of Witwatersrand, Johannesburg, <http://wiredspace.wits.ac.za/handle/10539/20992>

Downloaded from a DSpace repository. https://dspace.org/



Optimization of the Integrated Gasification Combined Cycle Using Advanced Mathematical Modelling

by

Bongani Ellias Mvelase (920982)

A thesis submitted in partial fulfillment of the requirements for the degree of

Doctor of Philosophy (Chemical Engineering)

Submitted to

School of Chemical and Metallurgical Engineering, Faculty of Engineering and the Built Environment, University of the Witwatersrand, Johannesburg, South Africa

Supervisor: Prof. Thokozani Majozi

May 2016

Synopsis

The Integrated Gasification Combined Cycle (IGCC) is a promising technology in the power generation industry to increase efficiency and reduce environmental emissions associated with fossil fuels. The performance of the gasifier and its economic feasibility largely depends on the gasifier island and many problems experienced during gasification are associated with extreme operating conditions. There is, however, no evidence that the extreme operating conditions in the gasifier yield the maximum possible fuel gas heating value.

The main objective of this research was, therefore, to develop a mathematical model to simulate and optimize the performance of the IGCC, particularly focusing on maximizing the fuel gas heating value. The work carried out in this thesis was divided into three parts. The first part presented a 1-D simulation model for a dry-fed entrained flow gasifier with oxygen and steam used as oxidizing agents. The model was then validated against published models for a similar reactor configuration and then extended to an existing entrained flow gasifier of Elcogas IGCC power plant in Puertollano, Spain. The second part presented the optimization model in which the objective function was to maximize the fuel gas heating value. The last part combined gasifier and the gas turbine models and evaluated the overall performance of the gas path.

The formulated mathematical model which consisted of mass and energy balances of the system was solved in gPROMS platform in order to determine the optimum conditions of the gasifier. Multiflash for Windows was used to obtain the thermodynamic properties of gas phase. The model was first used to replicate three published simulation models, particularly focusing on the carbon conversion, cold gas efficiency, gasification peak temperature and gasifier exit gas temperature. The results obtained during optimization of the Elcogas entrained flow gasifier showed a 14% increase in fuel gas heating value was realized with a decrease of 519K in operating temperature. The pressure did not have a significant impact on the fuel gas heating value, with only less than 2% increase in heating value being achieved by changing the pressure from 2MPa to 5MPa.

Owing to a decrease in operating temperature, the conversion was reduced from 97% to about 63% and that led to a decrease of almost 60% in O_2 and 50% in steam used in the gasifier. The results also indicate an almost 2% increase in the efficiency of the gas turbine when burning the gas of the higher heating value. This was mainly due to the increase in the expander inlet temperature. The gas turbine exhaust temperature and the exhaust gas heat capacity also

increased, thereby, increasing the amount of heat available in the heat recovery steam generator. There was also a 7% notable increase of the overall gas path efficiency. A reduction in operating temperature and pressure of the gasifier, therefore, guarantee an extended operating cycle of the gasifier, thereby, improving commercial attractiveness and competitiveness of the technology compared to other available power generation technologies. These new proposed operating conditions, which are less severe, therefore, signify a possible improvement availability and reliability of the IGCC power plant.

Declaration

I, **Bongani Ellias Mvelase**, with student number **920982**, declare in terms of **Rule G27** that:

1. I understand what plagiarism is and I am aware of the University policy in this regard.

2. This thesis is my own original work. Where other people's work has been used (either from a printed source, Internet or any other source), this has been properly acknowledged and referenced in accordance with departmental requirements.

3. This thesis and all of its contents has not been used as a submission for any other degree or submitted at any other university.

4. I have not used work previously produced by another student or any other person to hand in as my own.

5. I have not allowed, and will not allow, anyone to copy my work with the intention of passing it off as his or her own work.

_____

Signature

_____

Date

Acknowledgements

I would like to express my sincere gratitude to Professor Thokozani Majozi for his guidance, support and motivation throughout the course of this study. I would like to thank him for his patience and time that he devoted in helping me to achieve the objectives of this thesis.

I would also like to thank Eskom Generation Division, particularly Camden Power Station and Coal III Management for affording me an opportunity to develop myself as an Engineer and a Scientist. I would like to particularly mention the Station Management that gave me this opportunity in 2011, Anthony Kuzelj and Zweli Witbooi (now Power Station and Senior Technical Plant Managers, respectively, at Duvha Power Station), Hazel Mthembu and Pumla Mthombeni (former and current Boiler Engieering Managers, respectively). I would also like to also thank Mandla Mthembu (Senior Engineering Manager at Eskom PEIC), Dr. Titus Mathe (Mentor), Linda Maqhashalala & Pro Mkhize (both Camden Middle Managers); your support and faith you have had in me from the beginning has been amazing.

To my lovely wife, Nonhlanhla Ngesi Mvelase, and my beautiful kids, Nonjabulo, Khwezi and Bandile, it was never easy being so far away from you. I want to thank you for the inspiration, encouragement and support that you constantly gave me throughout my studies.

Many thanks also go to my colleagues at Sustainable Systems Process Engineering (SUSPE) at the University of Witwatersrand whom became my sisters and brothers while conducting my research. I would like to thank Dr. Vincent Gololo and Dr. Mkhokeli Ndlovu for always lending me their ears whenever I wanted to bounce my ideas and for their support during the compilation of this Thesis. To Musah (My Oga) Abbass, for everything we have been through or went through, "God Knows" and "We shall prevail"……

Special thanks also go to my mother, Agnes (uMaZulu) Zulu for keeping me motivated all the time. I thank God for giving me such a wonderful mother and I'm really grateful for the support and love that you have given me. Mrs Mamlo Ngesi and Mrs Dudu Maseko, God Blessed me with more mothers in you!

To my friends, Sholo Noko, Simo Thango, Thokozani Ngcamu, Bhabha Hlophe, Xolani Bhengu, Lwazi Magwetshu, Nkanyiso Shozi, Dumisani Zuma, Sithokozile Hlongwa, Charlene Naicker, just to mention a few, thank you for being part of my life.

Above all, without the Almighty God, this work would have not been a success.

TABLE OF CONTENT

1. Introduction 1

1.1 Background 1

1.2 Problem analysis 2

1.3 Research objectives 3

1.4 Scope of work 3

1.5 Thesis structure 5

References 6

2. Literature Review 7

2.1 Introduction 7

2.1.1 Energy Efficiency 11

2.1.2 Environmental Impacts 13

2.2 Process Integration 14

2.3 Process Design Considerations 15

2.4 Advantages of IGCC 17

2.5 Disadvantages of IGCC 17

2.6 Gasification Technology Options 18

2.6.1 Entrained – flow Gasifier 19

2.6.2 Fluidized Bed Gasifier 20

2.6.3 Moving Bed Gasifier 21

2.7 Gasification Process Description 21

2.8 Chemical Reactions 23

2.9 The Synthesis Gas 25

2.10 Gasifier Performance 26

2.10.1 Effect of temperature 26

2.10.2 Effect of pressure 27

2.11 Existing Mathematical Models 29

2.11.1 Simulation Models 30

2.11.2 Optimization Models 33

References 35

3. Model Development 40

3.1 Introduction 40

3.2 Model description 41

3.2.1 Devolatilization Model 41

3.2.2 Homogeneous Gas Phase Kinetic Model 42

3.2.3 Heterogeneous Gas-Solid Reactions 44

3.2.4 Mathematical formulation 46

3.3 Gasifier flowsheet and key modelling assumptions 53

3.3.1 Mass balance assumptions 55

3.3.2 Energy Balance Assumptions *55*
3.4 Modelling Platform 56
3.4.1 gPROMS *56*
3.4.2 Multiflash *56*
3.5 Optimization Model 57
3.6 Gasifier Performance 58
3.7 Solution Procedure 58
Reference 61
4. Case Studies 63
4.1 Entrained Flow Reactor Model 63
4.1.1 Modelling of an entrained flow gasifier (Vamvuka et al., 1995) *63*
4.1.2 A simple process modelling for a dry-feeding entrained bed coal gasifier (Lee et al., 2011) *65*
4.1.3 Techno-Economic Assessment of Co-gasification of Coal-Petcoke and Biomass in IGCC Power Plant (Sofia et al., 2013) *66*
4.1.4 Elcogas IGCC power plant *68*
Simulation model *68*
Optimization Model *70*
4.2 Overall performance 73
4.3 Conclusions 76
Reference 77
5. Conclusions 78
6. Recommendations 80
Nomenclature 82
Gasifier: Greek Symbols **..... 83**
Gas Turbine: Greek Symbols **..... 85**
APPENDIX A: Mass and Energy Balance 86
APPENDIX B 1: gPROMS Model 90
APPENDIX B2: Optimization Model 116
APPENDIX C: Model Input data 118
APPENDIX D: gPROMS Results 123

LIST OF FIGURES

Figure 2.1: IGCC power plant without CCS 9
Figure 2.2: IGCC power plant with CCS 10
Figure 2.3: IGCC for poly-generation 10
Figure 2.4: Evolution of coal-based electricity generation in non-OECD countries 11
Figure 2.5: Improvements in Siemens Gas Turbine Combine Cycle 12
Figure 2.6: Natural gas price in nominal US $ 12
Figure 2.7: World CO2 emissions by sector 13
Figure 2.8: Gasification technologies 18
Figure 2.9: Gasifier Modelling Approaches 29
Figure 3.1: Gas turbine unit 51
Figure 3.3: Mathematical model solution procedure 60
Figure 4.1: Temperature and Conversion profiles of an original simulated gasifier 70
Figure 4.3: Temperature and Conversion profiles of an optimized gasifier 72
Figure 4.4: Composition profiles of an optimized gasifier 72

LIST OF TABLES

Table 2.1: Technology suppliers for gasification 8
Table 2.2: Feedstock used in gasification 19
Table 2.3: Dominant chemical reactions in a gasifier 24
Table 2.4: Approximate relative rate of solid-gas 25
Table 2.5: Composition and syngas heating values 28
Table 3.1: Homogeneous phase reaction kinetics 43
Table 3.2: Homogeneous gas phase reaction orders 44
Table 3.3: Heterogeneous reaction kinetics 45
Table 3.4: Heterogeneous reaction parameters 46
Table 4.1: Feed data of the gasifier 64
Table 4.2: Gasifier performance model comparison with Vamvuka et al. (1995) 64
Table 4.3: Gasifier performance model comparison 66
Table 4.4: Proximate Analysis of fuel 67
Table 4.5: Gasifier performance model comparison with Sofia et al. (2013) 67
Table 4.6: Elcogas Power Plant main operating data 68
Table 4.7: Raw gas analysis of Elcogas 69
Table 4.8: Elcogas Power Plant performance data 69
Table 4.9: Performance of the gas turbine 74
Table 4.10: Fuel gas composition 75
Table 4.11: Overall performance of the gas path 76

1. Introduction

1.1 Background

The Integrated Gasification Combined Cycle (IGCC) is considered to be the most promising technology in producing cleaner electricity at higher efficiency. The gasification process is not a new technology since coal gasification was first developed in 1729 to produce town gas (Basu, 2006) and the combined cycle power plants have been in existence for decades. The integration of these technologies however, has only been recent (Barnes, 2013). The term IGCC, therefore, refers to the integration of the gasifier to the combined cycle power plant. It can therefore be appreciated that most of the components/systems making up the IGCC plant have been used in industry for many years but for different purposes. The major sub-plants that make up an IGCC power plant include the air separating unit (ASU), gasifier, gas cooling and gas cleaning units, gas turbine, heat recovery steam generator (HRSG) and steam turbine. It is the integration of these major components that has promised significant improvement in the efficiency and reduction in environmental emissions associated with power generation using fossil fuel. The largest IGCC power plants that have been built for demonstration and commercial purposes are shown in **Figure 1.1**.

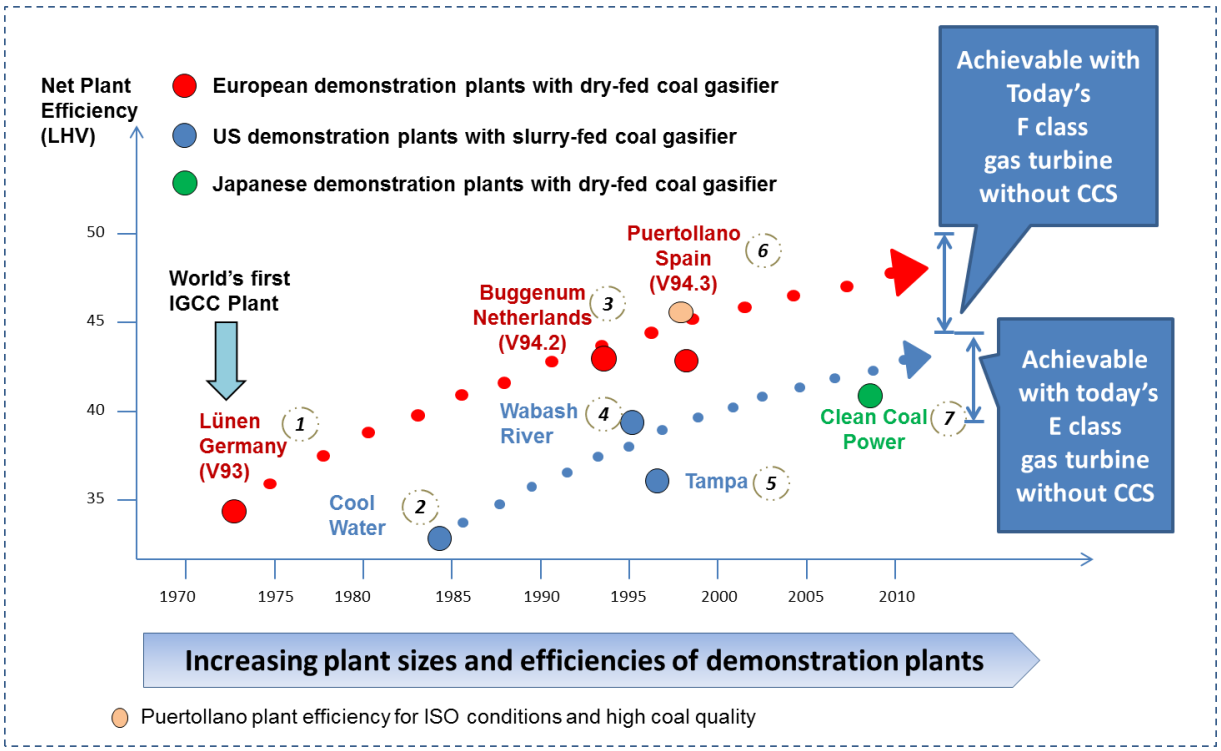

Figure 1.1: Available IGCC power plants around the world (Karg, 2009)

Similar to the conventional power plant whose overall cycle efficiency depends on the boiler and steam turbine efficiencies (taking into account of the auxiliary power requirements), the overall efficiency of the IGCC power plant largely depends on the efficiencies of the integrated components. The IGCC power plant has been described to have superior efficiencies compared to conventional coal-fired power plants. The highest actual gross efficiency of an IGCC power plant has been reported at 47% (Elcogas, 2005) compared to 44% reported for Super-Critical (SC) power plants (Beér, 2009). Recent studies have also demonstrated that this efficiency (of 47%) can be potentially increased to 55% through process integration techniques (Madzivhandila *et al*., 2010). The conventional coal-fired power plants have also experienced positive developments recently that were aimed at improving the efficiency and environmental impact through the introduction of SC and Ultra SC Units with Flue Gas Desulphurization (FGD) and integrated CO_2 capture. However, IGCC has continued to demonstrate superior performance when it comes to emissions such as particulates, carbon dioxide and the oxides of sulphur and nitrogen (Klara and Wimer, 2007).

The IGCC has two paths, i.e., gas and steam paths. The gas path focuses on the fuel gas generation in the gasifier, removal of impurities in the gas cleaning circuit and its combustion in the gas turbine. Steam path involves the heat recovery from gasifier jacketed-walls, gas cooling units and gas turbine exhaust Heat Recovery Steam Generator (HRSG). A number of simulation models to study the performance of an IGCC power plant that focus on the gasifier have been developed. These range from a simple 1-dimensional model to complex 2-D and 3-D Computational Fluid Dynamics (CFD) models. However, most of the developed models on the entrained flow gasifier have mainly focused on the simulation of the gasifier to predict the gas product composition at given operating conditions, i.e., temperature and pressure, and maximizing carbon conversion.

1.2 **Problem analysis**

The performance of an IGCC plant and its economic feasibility mainly depend on the cost of the gasifier island (Campbell *et al.*, 2000). The majority of problems experienced during gasifier operation are associated with an increase in temperature (Ruiz *et al.*, 2013) and the refractory life and material of construction of components have been identified as a limiting factor in worldwide use of this technology (Schnake, 2013). It can, therefore, be construed that lowering the operating temperature, especially the peak temperature could extend the refractory life.

The entrained flow gasifier, which is commonly used in IGCC, is known to operate under extreme conditions, such as temperatures up to 2000°C (Sun *et al.*, 2012) and pressures in excess of 8MPa (Majoumerd *et al.*, 2014). The entrained flow gasifier, therefore, achieves very high conversions of up to 99%. However, these extreme conditions impact negatively on the capital and operational investments of the gasifier and the downstream units.

Published literature has divided the work that has been carried out in IGCC optimization to increase efficiency into steam and gas paths. Based on the extensive work that has been carried out on the steam path of the process, there seems to be no scope in further improving the system efficiency. While significant work has also been carried out on the gas path of the process, there are still opportunities available, especially in understanding the performance of the gasifier. Thus far a number of researchers have put significant effort in the simulation of the gasification unit, mostly studying the performance of the gasifier under different operating conditions such as temperature, pressure and oxidising agent-to-fuel ratios and coal quality.

1.3 **Research objectives**

Thus far, there has been no corroboration in published literature indicating that the extreme conditions are the optimum conditions at which the gasifier should be operated, especially, when the fuel gas (syngas) produced has to be processed in the gas turbine to produce power. This work, therefore, aims at investigating if there are any less severe operating conditions of the gasifier that could result in the highest possible heating value of the fuel gas. The possibility of milder operating temperature and pressure of the gasifier could guarantee an extended operating cycle of the gasifier, thereby, improving commercial attractiveness and competitiveness of the technology compared to other available power generation technologies.

1.4 **Scope of work**

The main objective of this research is to develop a mathematical model to simulate and optimize the performance of the IGCC, particularly focusing on maximizing the fuel gas heating value. The work to be carried out in this thesis will be divided into three parts. The first part presents a 1-D simulation model for a dry-fed entrained flow gasifier with oxygen used as oxidizing agent. The model is then validated against published models for a similar reactor configuration and then extended to an existing entrained flow gasifier for an IGCC power plant in Puertollano, Spain. The second part presents the optimization model in which the objective function is to maximize the fuel gas heating value. The last part combines gasifier and the gas

turbine models and evaluate the overall performance of the gas path. The formulated mathematical model which consists of mass and energy balances of the system is solved in the *g*PROMS platform in order to determine the optimum conditions of the gasifier. Multiflash for Windows is used to obtain the thermodynamic properties of gas phase.

The mathematical models mentioned in Section 1.2, together with other available models on the subject will form the basis for the current work. The Elcogas power plant in Puertollano, Spain, as shown in **Figure 1.2** will also be used for model validation and as a case study. The choice of this power plant is twofold; the highest efficiency and the availability of data. This power plant has a capability of generating about 200MWe from the gas turbine and 135MWe from a steam turbine.

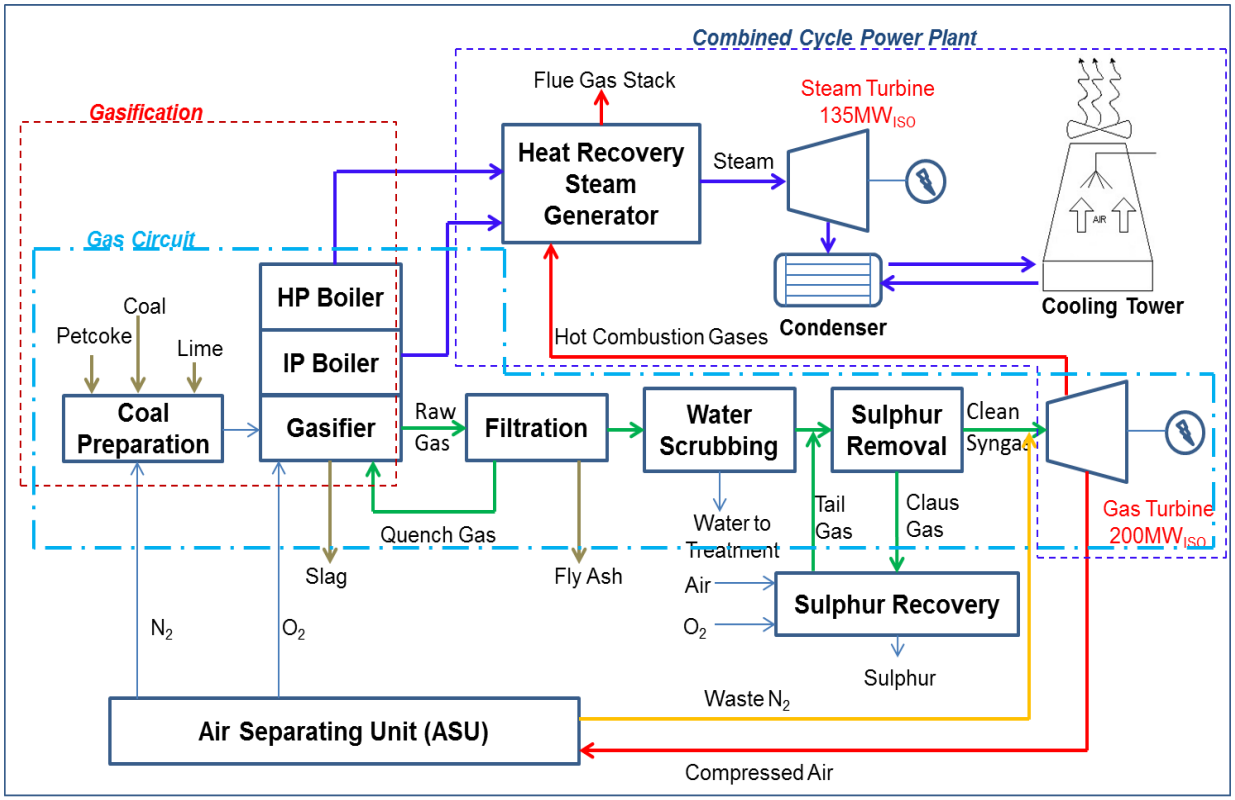

Figure 1.2: Process flowsheet of Elcogas power plant

This plant uses PRENFLO gasification technology and a Siemens V94.3 gas turbine. The plant configuration consists of a two-stage dry feed entrained flow gasifier, waste heat recovery boiler (WHRB), gas cleaning plant, gas turbine, steam turbine and an air separation unit. The plant has an overall thermal efficiency of 47%.

1.5 Thesis structure

The thesis is arranged as outline below:

Chapter 2 provides a comprehensive literature review, particularly focusing on the gas path of the IGCC. Existing simulation and optimization models to study the performance of the system are discussed in greater detail, concentrating on their strengths and short-comings.

Chapter 3 focuses on the mathematical model formulation used in this work. This is divided into the gasifier and gas turbine models. Mathematical modelling equations, together with the adopted assumptions that describe performance of these two main units are also presented.

Chapter 4 presents the mathematical model validation where the model developed in this work is compared against other published models. A case study is then presented where the new model is used to determine the optimum operating conditions of the Elcogas power plant.

Chapter 5 provides conclusions derived from the current work and ***Chapter 6*** highlights the recommendations for future work

References

Barnes, I., *Recent operating experience and improvement of commercial IGCC*, CCC/222, ISBN 978-92-9029-542-6, 2013, pp 52

Basu, P., *Combustion and Gasification in Fluidized Beds*, Taylor & Francis Group, LLC, 2006

Beér, J. M., *Higher Efficiency Power Generation Reduces Emissions (MIT)*, National Coal Council, 2009

Campbell, P.E., McMullan, J.T., Williams, B.C., *Concept for competitive coal fired integrated gasification combined cycle power plant*, Fuel, 2000, 79 (9), 1031-1040

Elcogas, *Operating experience and current status of Puertollano IGCC power pla*nt, International Freiberg Conference on IGCC & Xtl Technologies, (www.elcogas.es), 2005

Karg, J., *IGCC experience and further developments to meet CCS market*, Siemens AG, Energy Sector, Fossil Power Generation Division, Coal-Gen Europe, 2009

Klara, J. M., Wimer, J. G, *Cost and Performance Baseline for Fossil Energy Plants*, 2007, Vol.1 DOE/NETL-2007/1281

Madzivhandila, V., Majozi, T., Zhelev, T., *Recovery of Flue Gas Energy in Heat-Integrated gasification Combined Cycle (IGCC) Power Plants Using the Contact Economizer*, Energy & Fuels, 2011, 25(4), 1529-1536

Majoumerd, M. M., Rass, H., De, S., Assadi, M., *Estimation of performance variation of future generation IGCC with coal quality and gasification process – Simulation results of EU H2-IGCC project*, Applied Energy, 2014, 13, 452-462

Ruiz, J.A., Juarez, M.C., Morales, M.P., Munoz, P., Mendvil, M.A., *Biomass gasification for electricity generation: Review of current technology barriers*, Renewable and Sustainable Energy Reviews, 2013, 18, 174-183

Schnake, M. *Slagging Gasifier Refractories: A New Pathway to Longer Refractory Life*. Cleaner Combustion and Sustainable World, 2013, 881 – 884

Sun, Z., Dai, Z., Zhou, Z., Xu, J., Yu, G., *Comparative Study of Gasification Performance between Bituminous Coal and Petroleum Coke in the Industrial Opposed Multi-burner Entrained Flow Gasifier*, Energy & Fuels, 2012, 26, 6792 – 6802

2. Literature Review

2.1 Introduction

In 1900 fuel conversion efficiency into electricity was less than 5% (Pouris, 1985) and recently, a conventional coal-fired thermal power plant efficiency is estimated at 45% (Roth, 2005 and Beér, 2009). An increase in efficiency of the conventional power plant is largely influenced by an increase in steam temperatures for fixed pressure operating units. The generation of steam at higher temperatures, in the region of 600°C and above, compels the use of more expensive material of construction which results in extremely high capital investment of the power plant. After the recent developments of supercritical (SC) and ultra-supercritical (USC) units, there seem to be no scope in further increasing the overall efficiency of the conventional power plant. Integrated Gasification Combined Cycle (IGCC) has however indicated a lot of potential in terms of overall cycle efficiency improvement, with the latest developments showing a prospective efficiency of 57 % by the year 2030 (Kawabata *et al.*, 2012).

IGCC is, therefore, a technology to increase efficiency and reduce environmental emissions associated with fossil fuel firing. It efficiently converts a number of low-value solid and liquid fossil fuels into other useful fuels with less impact on the environment as opposed to conventional technologies. IGCC power plant combines two matured technologies, the combined cycle power plant and gasification to produce electricity. Combined cycle power plant generally use natural gas to generate hot gases, also referred to as flue gas, which is used to power the gas turbine. In an IGCC power plant, the gasifier produces the fuel gas, also referred to as synthesis gas or syngas, which is used as a substitute gas for natural gas in the gas turbine of the combined cycle power plant to generate power. A number of IGCC power plants have been built worldwide by different technology suppliers as shown in **Table 2.1**, while also a significant number are also at pilot stage (Minchener, 2005). The performance of an IGCC plant and its economic feasibility mainly depends upon the cost of the gasifier island (Campbell *et al.*, 2000 and USDoE, 2001). The majority of problems experienced during gasifier operation are associated with an increase in temperature (Ruiz *et al.*, 2013). The refractory life has been identified as a limiting factor in worldwide use of this technology (Schnake, 2012, Puente-Ornelas *et al.*, 2012).

Table 2.1: Technology suppliers for gasification (Minchener, 2005)

Technology Supplier	Gasifier Type	Feed Type	Oxidizing Agent	Major Installations
Chevron Texaco (USA)	Entrained Flow	Water Slurry	O2	Tampa Electric IGCC Plant, Cool Water Plant, Chevron Texaco Eldorado IGCC Plant, Eastman Chemical, Ube Industries, Motiva Enterprises, Deer Park
Global Energy E-Gas (USA)	Entrained Flow	Water Slurry	Oxygen	Wabash River IGCC Plant and Louisiana Gasification Technology IGCC Plant
Shell, USA/The Netherlands	Entrained Flow	Dry	O2	Demkolec IGCC Plant (Buggenum, Netherlands) Shell Pernis IGCC Plant, Netherlands, Harbug
Lurgi (Germany)	Moving Bed	Dry	Air	Sasol Chemical Industries and Great Plains Plant
British Gas/Lurgi Germany, UK	Moving Bed	Dry	O2	Global energy power/methanol plant, Germany
PRENFLO/Uhde (Germany)	Entrained Flow	Dry	O2	Elcogas, Puertollano IGCC Plant (Spain), Furstenhausen in Saarland
Noell/GSP (Germany)	Entrained Flow	Dry	O2	Schwarze Pumpe, Germany
KRW (USA)	Fluidized Bed	Dry	Air/O2	Sierra Pacific (Nevada, USA)

IGCC has been widely used to convert low value hydrocarbon feedstock to high value products such as chemicals, hydrogen and power generation (Tennant, 2012, Lu and Wang, 2014). The gasifier type and flowsheet arrangement generally depend on the type of final product application. Three process flowsheets of the IGCC have been presented in literature, and these are; IGCC without carbon capture, with carbon capture and poly-generation (Breault, 2010), as shown in **Figures 2.1, 2.2** and **2.3**. A number of IGCC configurations exist and different levels of integrations between processing equipment are also possible.

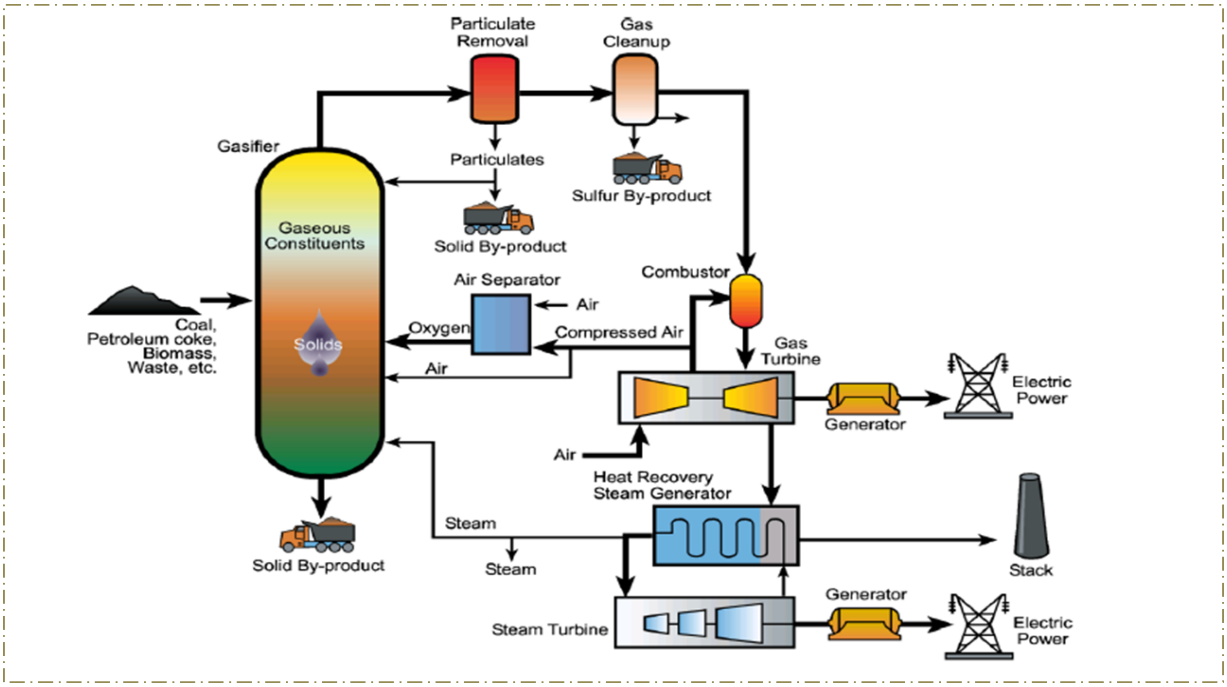

Figure 2.1: IGCC power plant without CCS (Breault, 2010)

Major equipments in the IGCC flowsheet include the gasifier, Air Separating Unit (ASU), gas turbine, steam turbine and the Heat Recovery Steam Generator (HRSG). The gasifier, gas cleaning and the gas turbine forms part of the gas path of the IGCC. The heat recovery from gasifier wall cooling, fuel gas cooling, HRSG and subsequent power production from the steam turbine forms part of the steam path. There are two main by-products that are produced during solid fuel gasification, and these are, slag from the gasifier and the solid sulphur from the gas cleaning plant.

The earlier flowsheets of the power plants did not include the carbon capture and storage (CCS) as shown in **Figure 2.1**. This arrangement, therefore, resulted in a relatively higher amount of CO_2 emissions. The fuel gas burnt in the gas turbine has, however, less SO_x and particulate because of the gas cleaning unit. The air required by the ASU is taken from the gas turbine compressor and therefore eliminates an additional compressing unit that will only supply the ASU. The CO-to-H_2 ratio is only determined by the feedstock and gasifier operating conditions in the configuration since there are no shift reactors.

The flowsheet of the IGCC with CCS as presented in **Figure 2.2** includes shift reactors and gas separator in addition to all equipment existing in **Figure 2.1**. The main objective of the shift reactors is to adjust and control the CO-to-H_2 ratio. This may be important for gas turbine designed with a specific range of CO-to-H_2 ratio. Since this flowsheet has CCS, the flue gas produced in this arrangement will have less CO_2.

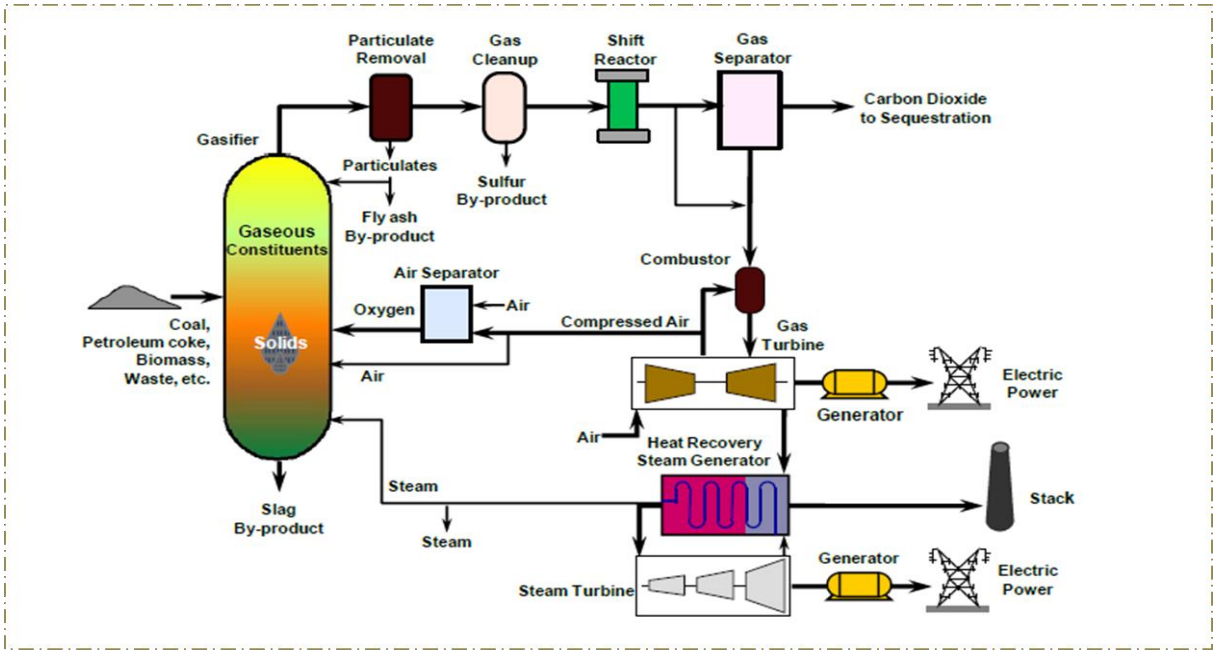

Figure 2.2: IGCC power plant with CCS (Breault, 2010)

The poly-generation flowsheet refers to IGCC process that is used for multipurpose. In this flowsheet, as shown in **Figure 2.3**, chemicals, hydrogen and electric power can be produced.

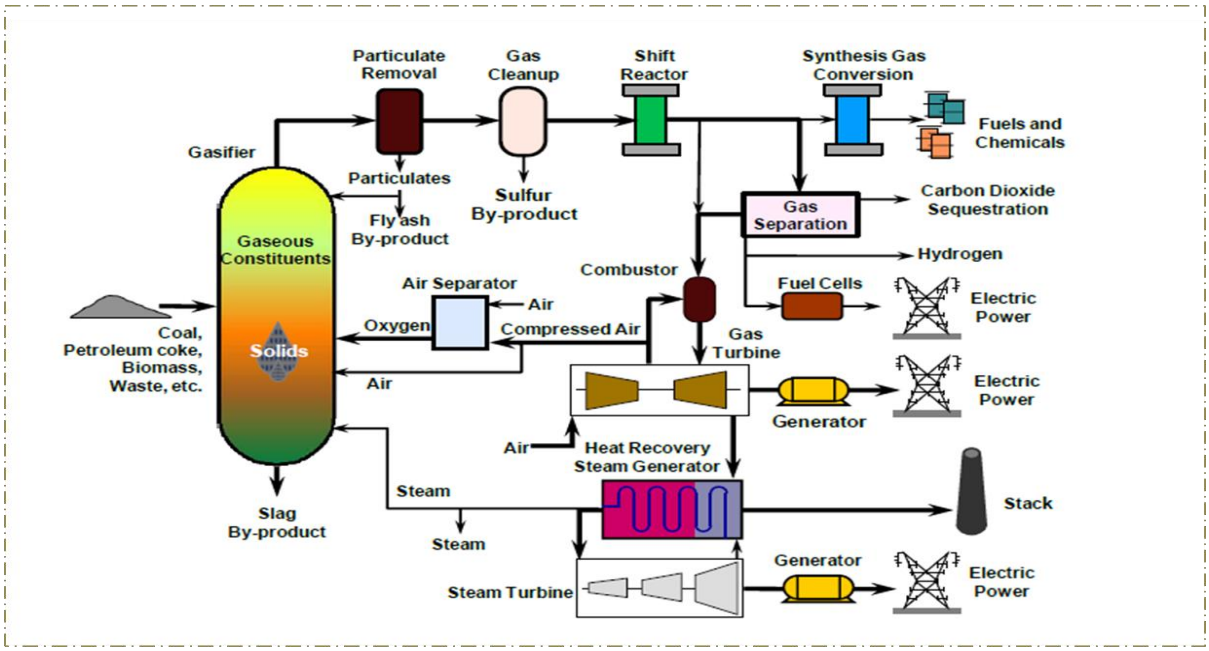

Figure 2.3: IGCC for poly-generation (Breault, 2010)

In addition to the IGCC power plant flowsheet with CCS, the poly-generation includes the Synthesis Gas Conversion and the Gas Separation units which are added for the purpose of producing fuels, chemicals and hydrogen. The hydrogen produced in the gas separator can be used in the fuel cells to produce electricity and could be used for transportation fuels.

2.1.1 **Energy Efficiency**

Increasing the efficiency of the coal fired power plant still remains at the forefront in continuing to utilise coal as an energy source. Two-thirds of the total fuel reserves in the world is coal and it is expected to last more than 150 years (SRWE, 2012). **Figure 2.4** shows the amount of electricity generated from coal by non-Organization for Economic Co-operation and Development (OECD), in which South Africa is part of.

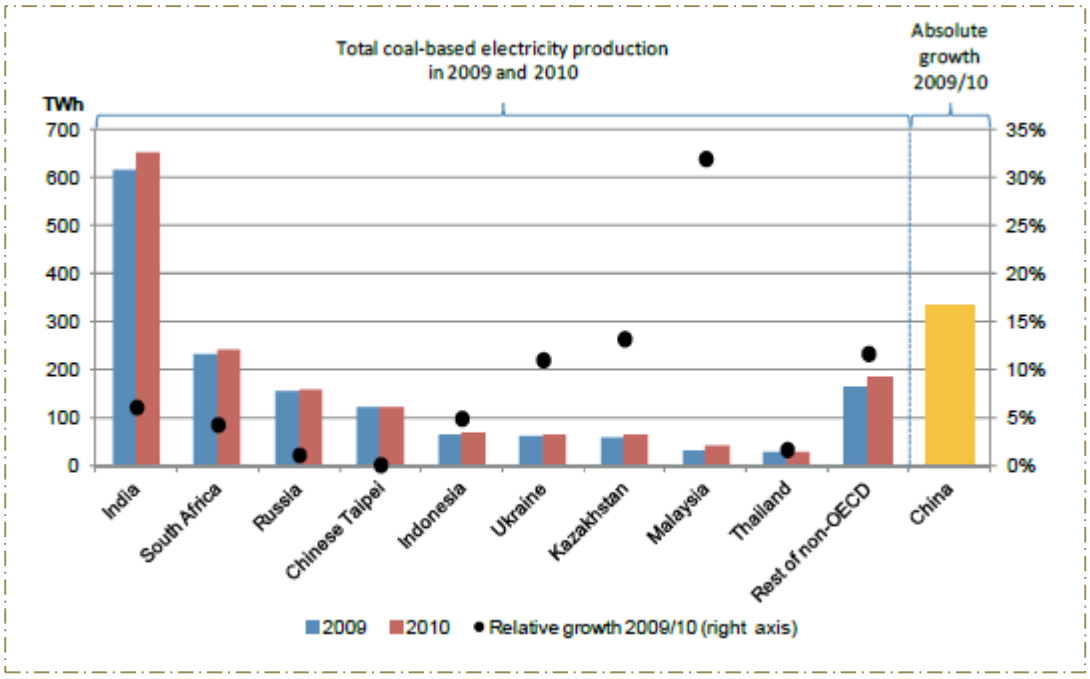

Figure 2.4: Evolution of coal-based electricity generation in non-OECD countries (OECD/IEA, 2012)

South Africa, currently, has 24 power stations, of which 13 of them are coal fired power stations. These power stations are very old, dating as back as 1960's and the average cycle efficiency of these power stations is now at about 27%. In 2007/8, poor efficiencies of these power generating units coupled with already known Eskom's insufficient power generating capacity resulted in load-shedding. Since then, Eskom is increasing its capacity, where they are building super critical units that will convert the abundant coal available in the country more efficiently compared to the existing units. They are also exploring Underground Coal Gasification (UCG) to address both efficiency and emissions but this technology still posses a serious threat in water pollution (van der Riet, 2008). The gas produced from UCG is expected to be used in the existing Coal-Fired Boiler through proper modification of the burners.

The high energy prices, the high demand and stringent environmental regulations are challenging process designers to propose processes that are highly efficient with high

availability, reliability and less harmful to the environment. In the most recent years, an increase in combined cycle gas turbine power plants using natural gas as fuel has been experienced and this has been mainly because of their high efficiencies, up to 61.5% (Hada *et al*., 2012). **Figure 2.5** shows the developments in Siemens combined cycle power plant since 1992.

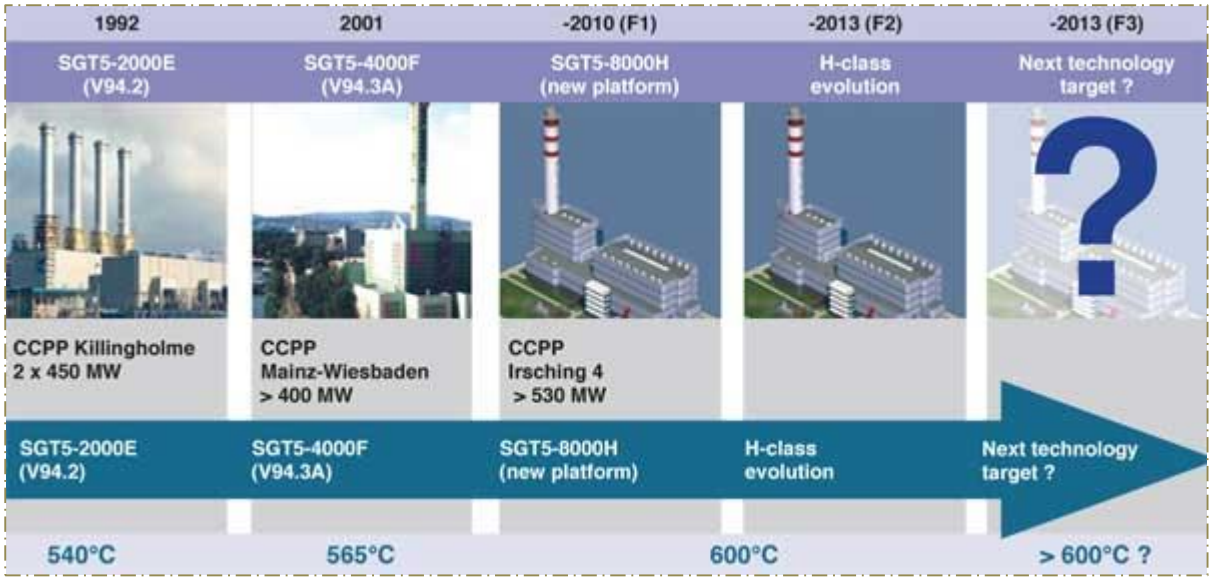

Figure 2.5: Improvements in Siemens Gas Turbine Combine Cycle (COSPP, 2014)

With the natural gas prices increasing as shown in **Figure 2.6** and its reserves depletion, using syngas as a substitute fuel in gas turbine has more economic and environmental benefits. About 20% of the IGCC for power production around the world use coal as a feedstock (USDoE, 2001).

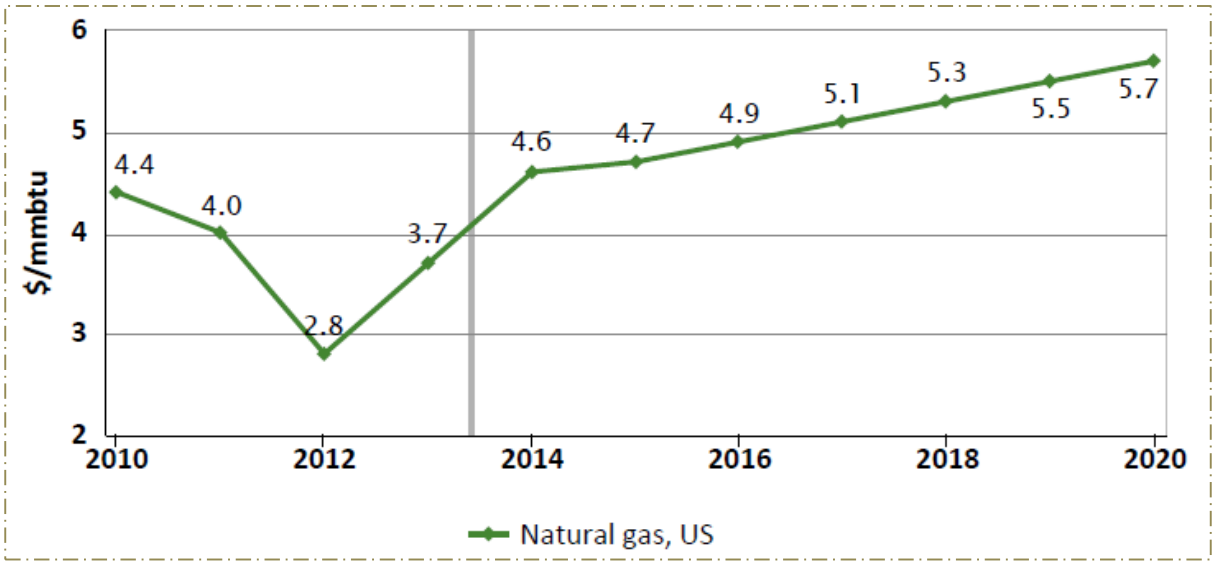

Figure 2.6: Natural gas price in nominal US $ (WBC, 2014)

In a typical IGCC power plant, the higher the efficiency of the plant is, the less is the electricity unit cost (Vamvuka *et al*., 1995). IGCC power plants have the highest thermal efficiencies compared to the traditional power plants. The highest efficiency in the world for an IGCC power plant is that of Elcogas power plant of 47% (Zaporowski, 2003).

2.1.2 **Environmental Impacts**

Stringent environmental emission regulations have compelled industries into pursuing technologies that are sustainable and less detrimental to the environmental. Coal is estimated to provide about 30.3% of global energy needs and generates about 42% of the world electricity (Xu *et. al*., 2014). By the year 2010, coal had continued to dominate global CO_2 emissions with 43%, while 36% came from oil and 20% from gas (IEA, 2012). **Figure 2.7** shows the CO_2 by sector as of the year 2010. The Copenhagen Accord stated that significant changes were necessary in order to keep the global temperature increase below 2°C (UNFCCC, 2009). The reduction of the emissions, especially the greenhouse gases, is currently forming a basis of any process innovation and future technologies. In 2011, South Africa hosted a 17th Conference of Parties (COP 17) which was a climate change conference, where developed and developing countries committed themselves in extending the Kyoto Protocol to reduce their carbon emissions.

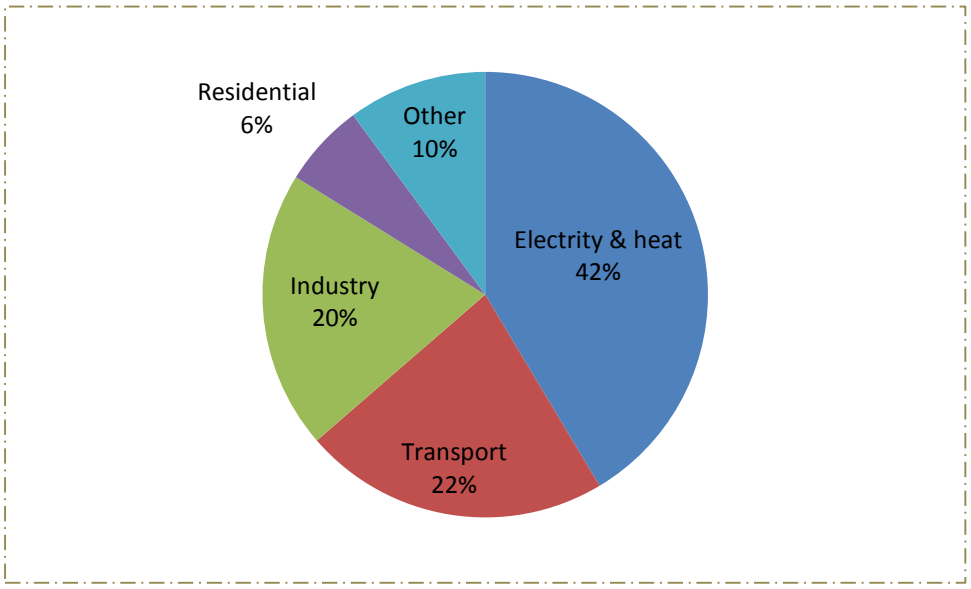

Figure 2.7: World CO2 emissions by sector (IEA, 2012)

World energy demand continues to increase and in 2007, a 60% increase was forecasted by the year 2037 (Christou *et al*., 2007). Currently about 90% of the South Africa's electricity comes from the burning of coal, with the balance being generated from Nuclear, Hydro and

Wind (Eskom, 2014). South Africa has an estimated 32 billion tonnes of coal reserves and this will remain the most abundant energy source for the next 30 years (Aasberg-Petersen, *et al*., 2004 and OSACVC, 2011). The challenge remains when coal is being converted to other useful forms of energy, in which, in conventional conversion, results in significant CO_2 emissions. Thus far, flue gas desulphurization and UCG are the technologies that Eskom is considering to address the environmental concerns. Retrofitting an existing system to comply with environmental standards also introduces other disadvantages because an increase in auxiliary systems that require electricity in order to operate and, therefore, this may reduce the thermal efficiency of the power plant.

IGCC power plants that have been built since 1990 have demonstrated the superiority of this technology when it comes to reducing the emissions such as NO_x, SO_x particulate matter, waste and slag (Higman 2006). Combined cycle systems yield lower rates of CO_2 emissions per kWh of electricity produce and this is mainly due to higher efficiencies (Vamvuka *et al*., 1995). IGCC can also achieve from 99% up to complete removal of sulphur and particulates through a process of wet scrubbing of the raw syngas before the combustion turbine (Vamvuka *et al*., 1995 and Korens *et al*., 2002). Sulphur present in the fuel is mainly converted to hydrogen sulphide (H_2S) with small percentage being converted to carbonyl sulphide (COS).

The process of cleaning up the syngas before combusting it on the gas turbine ensures that the exhaust gas has less environmental harm and even further reduction on the GHG emissions are possible with carbon capture and storage (CCS) on the IGCC. Power generation units with CCS technology can reduce CO_2 emissions by up 90% (Chyou, 2010 and Leung *et al*., 2014). On the IGCC units that are on demonstration phase, significant reduction in air toxic compounds, negligible contaminated water discharges, with solid wastes produced as vitrified material impervious to leaching in storage have been proven (Minchener, 2005). They also use less water as compared to traditional coal fired power plants, and this is in the region of 20-50% less (Thompson, 2005). Apart from its ability to reuse wastewater (CATF, 2014), most of the power (about 60%) is generated from the gas turbine as compared to the traditional pulverized coal (PC) power plant where all the power is generated from the steam turbine.

2.2 **Process Integration**

IGCC allows for the use of well-established technology to maximize efficiency and reduce environmental impact associated with fossil fuel firing. The overall efficiency of the IGCC

power plant is determined by the power produced by the gas turbine and steam turbine as shown in equation 2.1.

$$\eta_{Thermal} = \frac{W_{GT} + W_{ST}}{\dot{m}_c HV_c} \; x \; 100 \qquad (2.1)$$

W_{GT} and W_{ST} are the amounts of energy produced by gas turbine and steam turbine respectively, while $\dot{m}_c$ is the mass flowrate of coal fed into the gasifier and HV_c is the coal heating value. The power split in an IGCC is about 60:40 between the gas turbine and steam turbine, respectively (Pruschek, 1998). Conventional coal-fired power plants produces almost similar the overall IGCC efficiencies, however, IGCC has the edge since it has lower emission pollutant gases and residual (Prescheck 1998). The success of the IGCC plant lies on the proper and optimal integration of the major components that makes up the plant. The integration of the gasifier to the combined cycle power plant replaces the need for natural gas in the gas turbine, which is substituted with fuel gas.

The recent work by Madzivhandila *et al.* (2009) indicated that integrating the low heat recovery unit called contact economizer from the exhaust of the HRSG has the prospective of increasing the overall plant efficiency by almost 4%. A gas turbine compressor may be used to supply the total air required in an IGCC power plant, and this air includes, air to the ASU required for oxygen production that will be during gasification and the air required in the combustion chamber of the gas turbine. Lowering ambient air temperature through possible integration of the gas turbine to cold process stream such as LNG vaporization could lower the energy required to drive the compressor and, therefore, increase the cycle efficiency. It is also known that about 55% to 65% of the power produced by the expander of the gas turbine is used to drive the compressor (Wartsila, 2014), and this could vary with ambient air temperature. The CCS also improves the environmental attractiveness of the IGCC which has demonstrated a lot of potential in decreasing CO_2 emissions (Leung, 2014).

2.3 **Process Design Considerations**

The high costs associated with an entrained flow gasifier of an IGCC power plant are associated with high temperature operation of the gasifier (Ruiz *et al.*, 2013). The severe operating conditions, especially, temperature, which warrants the use of more expensive material of construction, have been identified as the major constraint in the popularity of the worldwide use of this technology (Minchener, 2005 and Schnake, 2012). The gasifier and the gas cooling

units are largely affected by these high temperatures. The gas cooling process can be either carried out as a cold or hot process and therefore this will result is a trade-off between the cost of material of construction and plant efficiency. The cold and hot gas cooling processes take place at 38°C and 537°C, respectively (Zaporowski, 2003). These two processes, by their significant difference in temperatures, affect the production of steam and, therefore, the overall plant efficiency.

Design feedstock and feedstock flexibility affect gasifier efficiency and the fuel gas production. Entrained flow gasifiers are popular due to their flexibility in processing a variety of feedstock, ranging from coal, biomass and solid waste (Brdar and Jones, 2000). A lot problems, though, have been encountered regarding the feed handling system, especially, when it comes to dry-feed handling system (van der Drift *et al.*, 2004, Minchener, 2005). IGCC power plants with ASU and therefore, using pure oxygen as an oxidizing agent, achieves better conversion than those using normal air (Silaen and Wang, 2010). During the plant design stage, the trade-off between higher conversion and the capital and operational costs of the ASU must be properly evaluated. Economic evaluations are also required to evaluate the use of the gas turbine compressor to supply the total air required in ASU for gasification and gas turbine combustion chamber versus providing a separate compressor for the ASU. Design ambient conditions and site elevation are also important, more especially, when it comes to gas turbine performance. An increase in ambient temperature increases the power requirements to drive the compressor of the gas turbine, reduces the net power produced by the gas turbine and therefore the overall cycle efficiency.

The expander inlet temperature constraints the firing temperature on the combustion chamber of the GT and this is due to material construction. While there have been developments in material of construction to allow the expander inlet temperatures up 1600°C with the Mitsubishi J-Series (Hada *et al*., 2012), the old gas turbine frames still have a limitation in firing H_2 rich fuels (Minchener, 2005). The challenge of meeting the emission limits or standards also allow the consideration of CCS during the design stage where proper assessments of the benefits of the CCS can be evaluated. There is also trade-off between efficiency and environmental benefits of the IGCC power plant, especially in relation CO_2 emissions. While the CCS can reduce CO_2 emissions by almost 90%, the net plant efficiency based on high HV can also be reduced by approximately 5.7% (DOE/NETL, 2007).

The integration of the low heat recovery unit downstream the HRSG has a potential of increasing the overall IGCC thermal efficiency (Madzivhandila *et al.*, 2009). This, however, may introduce backpressure on the system, especially on the gas turbine. Backpressure is known to affect the power output from the gas turbine and therefore the benefits have to be properly assessed (Smith, 2005). While severe operating temperatures impacts negatively on the gasifier operation due to downtimes and high capital investment, a large amount steam is be generated on the gasifer walls and in gas cooling units. The optimal ratio of the power generated from gas turbine and steam turbine has to be determined in order to optimize the operating conditions. Elcogas power plant has a design power ratio of 67.5-to-32.5 of gas turbine-to-steam turbine (Pena, 2005), and ratios up to 60-to-40 of gas turbine-to-steam turbine power have been reported (Pruschek, 1998, Sofia *et al.*, 2013).

2.4 **Advantages of IGCC**

Most notable advantages of IGCC are improved efficiencies and less environmental harm when compared to traditional power generation processes associated with coal firing. IGCC can be used to produce a number of products with a wide applications and these include synthesis chemicals (Beath, 1996), hydrogen (Christou *et al.*, 2007) and syngas to be used as fuel in either boilers or gas turbines. Gasification process has the ability to convert a number of solid and liquid feedstock into useful combustible or synthesis gaseous products. Feedstock that is widely used in gasification plants includes *biomass* in Integrated Biomass Gasification Combined Cycle (IBGCC), *coal* in Integrated Coal Gasification Combined Cycle (ICGCC), heavy oils or refinery residue and natural gas for reforming applications. The new IGCC power plants can be built with superior gas cleaning units including Carbon Capture and Storage (CCS), and this ensures that even lower CO_2 emissions are achieved (Holt *et al.*, 2003, Rutkowski *et al.*, 2003, and Minchener, 2005). Power generation units with CCS technology can reduce CO_2 emissions by up 90% (Chyou, 2010, Leung *et al.*, 2014).

2.5 **Disadvantages of IGCC**

IGCC power plants are associated with high capital investments and uncertainty concerning its operational track record. The challenges that need to be addressed for IGCC to be commercially viable are best summarized by Minchener, 2005 as outlined below:

- Gasifier component development, *including improved materials of construction for refractories* and HRSGs, improved feeding and handling systems

- Gas turbine combustor development to ensure the efficient use of hydrogen rich fuels
- Ancillary component development, including lower cost air separation units
- *Complementary design and optimization studies, including full integration of CO2 capture.*
- Associated level playing field techno-economic studies, taking into account the global market possibilities.

2.6 **Gasification Technology Options**

Gasification is a term used for partial combustion of carbon-based fuel into fuel gas, also known as syngas. This is an endothermic process and the required heat is supplied by the combustion of volatiles and a certain fraction of the carbon in the feed. Only about 30% of the oxygen required for complete combustion is supplied for gasification process (Chyou, 2010 and Silaen & Wang, 2010). Three variants of gasifier technologies are commercially available depending on the feed type and product gas application, and these include traditional *moving* bed also known as Sasol-Lurgi or *fixed* bed, *fluidized* bed and *entrained* flow gasifiers as shown in **Figure 2.8**. Gasifiers are also classified according to feedstock inflow into to the gasifier, and these are counter-current flow, co-current flow, updraft and downdraft. They may also be categories according to the oxidising agent being used and these categories are oxygen or air blown gasifiers. There are twelve gasifier designs that are currently available in the world and these are summarized by Breault (2010).

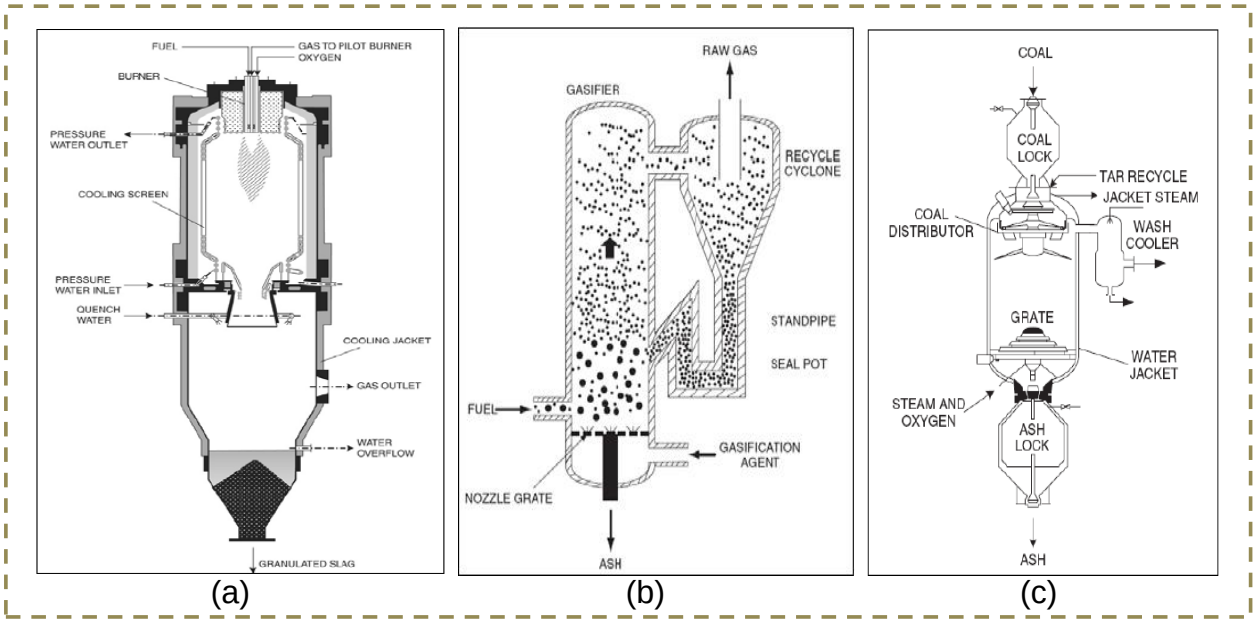

Figure 2.8: Gasification technologies: (a) Entrained Flow, (b) Fluidized Bed, (c) Moving Bed

These gasifiers can process different types of feedstock as shown in **Table 2.2**, at different operating conditions and they can achieve different conversions, and therefore may be only limited to specific applications, e.g., production of hydrogen, electricity, ammonia, oxy-chemicals, syngas and methanol (USDoE, 2001). In the year 2001, out of the total of 160 operating gasifiers around the world, about 120 of these were entrained flow gasifiers with a significant number being Lurgi moving bed (Simbeck and Johnson, 2001). Gasifier feedstock may include but not limited to coal, petroleum coke, refinery residues, biomass and municipal waste (Choyou, 2010).

Table 2.2: Feedstock used in gasification (USDoE, 2001, Minchener, 2005)

Feedstock	Operational Plant	Planned Plant
Coal	27	14
Coal/Petcoke	3	1
Petcoke	5	7
Natural Gas	22	0
Biomass	12	3
Fuel Oil/Heavy Petroleum Residue	29	2
Municipal Waste	5	0
Naphtha	5	0
Vacuum Residue	12	2
Unknown	40	6

A brief summary about each type of the gasifier is provided below, however, more details can also be found in literature including Higman and van der Burgt (2007) and Bell *et al.* (2010).

2.6.1 **Entrained – flow Gasifier**

There are seven different types of entrained flow gasifiers (also sometimes referred to as continuous flow reactors) and these are Texaco, PRENFLO, Hitachi, SCGP, BBP, MHI and E-gas (Simbeck and Johnson, 2001 and Collot, 2002). Entrained flow gasification refers to a process in which the fuel and oxidizing agents (air or relatively pure oxygen) are injected in the same position on the gasifier and flow co-currently as the chemical reactions take place. Two available feeding options of entrained flow reactors have been reported in literature and

these are slurry and dry feed designs. Entrained flow gasifier are characterized by their ability to process any type of coal, from lignite (Maxim *et al.*, 2010) to highest quality coal like anthracite. Fuel types that can be processed in this type of gasifier include sewage sludge, lignite, petroleum coke, sludge, natural gas, distillate and black coal. Entrained flow gasifiers can process very fine coal particles, from as low as 41 µm (Vamvuka *et al.*, 1995), 100 µm (Maurstad, 2005 and Gue *et al.*, 2007) and up to 150 µm (Xu *et al.*, 2014) and this together with very high temperatures (above slagging temperature of coal) ensures that the gasifier achieves very high conversions, in excess of 99% (Gue *et al.*, 2007). Operating temperatures between 1250°C and 2000°C for this gasifier type have been reported in literature (Zaporowski, 2003, Zheng and Furinsky (2005), Phillips, 2010, Xu *et al.*, 2014) and they are often operated at pressures between 2 – 8 MPa with most of the large plants operating at around 2.5 MPa (Minchener, 2005).

Two types of configurations for the entrained flow gasifier designs have been reported in literature and these are single stage and two-stage feed. In a two-stage feed gasifier, fuel is split between the two stages and the percentage split can range from 25-75% and 50-50% split between the two stages, with the latter achieving a better conversion (Silaen and Wang, 2010). Entrained flow gasifiers are also characterized by their simple mechanical designs and their ability to process higher throughputs per reactor volume. Shorter residence times, in the order of seconds or tens of seconds make these types of gasifiers very popular (Phillips, 2010). Entrained flow gasifiers produce fuel gas that is free of tars and phenols. While this type of a gasifier can process mostly any type of coal, low ash content coals are preferred for the main three reasons associated with efficiency, slag production and disposal (Boyd *et al.*, 1998 and Ploeg, 2001). The conversion and the cold gas efficiency achieved in entrained flow gasifiers are largely associated with the feeding type (slurry or dry), with dry feeding configuration achieving higher conversions and cold gas efficiency.

2.6.2 **Fluidized Bed Gasifier**

There are six classes of gasification technologies classified under fluidized bed and these are BHEL, HTW, IDCC, KRW, Transport reactor, Mitsui Babcock ABGC (Tabberer, 1998 and Collot, 2002). In a fluidized bed gasifier, feed fuel and oxidising agent flow counter-currently as shown in **Figure 2.8**(b). Fluidized bed gasifiers operate at uniform and moderate temperatures in order to avoid sintering of coal particles and loss of fluidity of the bed; and these temperatures are normally below the ash melting temperature, which is below 1200°C

(Phillips, 2010). Syngas leaves the gasifier at an average temperature of about 500°C (Puente-Ornelas *et al.*, 2012). Fluidized bed gasifiers have relatively much longer residence time compared to entrained flow gasifiers, between 10-50 seconds (Paul *et al.*, 1992).

Fluidized bed gasifiers have the ability to process coals with high ash fusion temperatures and the fuel types suitable for these gasifiers include biomass, pulp mill sludge, peat and black coal. Coal particles entrainment into the product gas is one of the disadvantages of this gasifier, therefore, just sufficient flow of gases into the gasifier (recycled gas, oxidant and steam) should be maintained in order to float coal particles within the bed. These gasifiers, therefore, have a limitation when it comes to particle sizes and between 0.5 and 5mm coal particles have been reported in literature (Minchener, 2005). Fluidized bed gasifiers can process reactive coals such as lignite, sub-bituminous and brown coals (Anderson *et al.*, 1998 and Baltas, 1999) and are also characterized by their ability to operate at variable loads.

2.6.3 **Moving Bed Gasifier**

Moving bed gasifiers are considered to be the oldest design type and most matured gasification technology that currently exists. An example of a moving bed gasifier as shown in **Figure 2.8**(c) is the *Lurgi* gasifier which is now known as *Sasol-Lurgi*, after Sasol had acquired the rights from a Lurgi, a German firm, and after a number of positive modifications on the original design, Lurgi is now often referred to as Sasol-Lurgi (Bell *et al.*, 2010). Other commercially available moving bed gasifiers are BGL and BHEL. In general, moving bed gasifiers operate at moderate temperatures of less than 1250°C and they are mainly used in the production of synthetic liquid fuels from coal (Phillips, 2010). Moving bed gasifiers are only suitable for solid fuels such as coal, biomass and waste. Pulverized fuel (coal) and the oxidising and gasifying agents (air and steam) flow counter-current, where fuel enters at the top of the gasifier while air and steam entering at the bottom. Originally, moving bed gasifiers were characterised by low temperature and low carbon conversion. Low temperatures ensure a reduced slag formation during the gasification process, however, significant amount of tars are formed at the lower temperatures (Beath, 1996).

2.7 **Gasification Process Description**

Coal Gasification takes place in oxygen deficient environment and in general, only about 30% of the oxygen required for complete combustion is supplied (Silaen & Wang, 2010). The gasification of coal is described by two-step process: pyrolysis and char gasification. These

steps include chemical reactions such as coal devolatilization, solid-gas and gas-gas reactions. Gasification is an endothermic process, and the heat required for gasification reactions is supplied by complete combustion reactions of char and volatiles that are also taking place in the gasifier. Coal is ground into fine particles from as small as 41 µm (Vamvuka et *al.*, 1995) up to between 70 and 100 µm (Maurstad, 2006 and Gue et *al.*, 2007). The relatively fine coal particles, also referred to as Pulverized Fuel (PF), are then mixed with limestone to improve the resulting slag flow properties. In this process, the PF is conveyed into the gasifier using nitrogen as transport gas. Air or pure oxygen may be used as an oxidizing agent depending on the plant configuration. In the case where pure oxygen is used as an oxidizing agent, air is drawn from the atmosphere and compressed on the gas turbine compressor and transported into the ASU where it is separated into O_2 and N_2. In other possible configurations, both external and gas turbine compressors may be used to supply specified fractions of the air requirements (Christou *et al.*, 2007).

A number of feed arrangements exist depending on the type of gasifier being used (entrained flow, fixed or moving bed types). In an entrained flow arrangement, oxidizing agents (oxygen or air) and the mixture of coal and limestone are fed at the top of the reactor. The devolatilization, heterogeneous solid-gas reactions and homogeneous gas-gas reactions takes place as the raw materials flow co-currently down the reactor producing fuel gas at very high temperature and sometimes high pressure. The gas is then cooled down in a Waste Heat Boiler (WHB) to generate steam. The cooled gas is piped into a gas cleaning unit where all the impurities such as SO_x, NH_3, COS, are removed from the gas. The cleaned gas is then transported to the combustion chamber of the gas turbine unit where it is combusted with air in the presence of steam or nitrogen that is used to control the flame temperature and thus prohibits the formation of NO_x and excessive high temperatures.

The high temperature, high pressure, flue gas from the combustion chamber of the gas turbine is passed through the turbine where mechanical work is produced. The exhaust gas from the turbine still contains a significant amount of heat and it is, therefore, passed through the HRSG where the available heat is absorbed to produce steam. Once the sensible heat present in the flue gas has been recovered, the gas is then released to atmosphere via stack. Madzivhandila *et al.* (2010) proposed the integration of a low heat recover unit called *contact economiser* between the gas turbine exhaust and the stack to further recovery heat from the gas using the dew point as the final target temperature for maximum heat recovery. In their work, they

suggested that, through the integration of the *contact economiser*, the overall efficiency of the IGGC could be improved from 47% to 51%.

2.8 **Chemical Reactions**

Gasification is known to be an endothermic process. When coal is subjected to high temperatures, it undergoes physical separation called, devolatilization, where char and volatiles are produced. The volatiles mainly consist of CH_4, CO, H_2 and tars (Wen and Chaung, 1979, Lee *et al.*, 2011, Kasule *et al.*, 2012). In the presence of oxidizing agent such as oxygen or air, and suitable operating conditions, the volatiles completely combusts and release the heat required by the endothermic gasification reactions. Therefore, there are two main reactions taking place in the gasifier; homogeneous gas-phase reactions and heterogeneous solid-gas reactions. The homogeneous gas-phase reactions involve volatiles combustion and water-gas shift reaction. The heterogeneous solid-gas reactions comprises of the partial char combustion in the presence of oxidizing agent and gasification reactions. During the process of gasification, both combustion and gasification reactions occur simultaneously.

There are four main solid-gas chemical reactions that have been widely considered in gasification modelling, and these are, char combustion, CO_2, H_2 and steam gasifications, (Wen and Chaung, 1979, Govind and Shah, 1984, Smith and Smoot, 1985). The homogeneous gas-phase reactions, which are dominated by combustion reactions, are CH_4, H_2, CO and tars combustion. For modelling purposes, heavy hydrocarbons or tars released as volatiles are assumed to be mainly benzene (Govind and Shah, 1984, Kasule *et al.*, 2012). The chemical species considered during gasification modelling ranges few components up to 31 components (Zaporowski, 2003). The considered components are mainly composed of 6 elements, which are, carbon, hydrogen, sulphur, oxygen, nitrogen and argon. Apart from gasification and combustion reactions, there are two other important secondary reactions that have a significant impact on the final gas composition produced during coal gasification and these are water-gas shift and steam-methane reforming reactions. The water-gas shift and steam-methane reforming reactions are both reversible reactions. The summary of the reactions that have been widely used in gasification literature, both combustion and gasification, are summarized in **Table 2.3**.

The chemical reactions summarized in **Table 2.3** are global reaction schemes as opposed to elementary reactions. The kinetic data for most of the elementary reactions is not generally

available and hence, researchers involved in coal gasification have preferred global reactions schemes. A number of researchers have studied chemical reactions taking place in the gasifier and published their respective kinetics. The kinetics that have been widely used for solid-gas reactions are those of Wen and Chaung (1979), Westbrook and Dryer (1981) for most of the combustion reactions, Jones and Lindstedt (1981) for hydrogen combustion and Bustamente *et al.* (2004) and Bustamente *et al.* (2005) for water-gas shift reactions.

Table 2.3: Dominant chemical reactions in a gasifier

Stage	Reaction	ΔH_R^o(kJ/kmol)
Gasifcation	$C + 0.5O_2 \rightarrow CO$	-110.525
	$C + H_2O \rightarrow CO + H_2$	131.30
	$C + CO_2 \rightarrow 2CO$	172.459
	$C + 2H_2 \rightarrow CH_4$	-74.9
Combustion	$C + O_2 \rightarrow CO_2$	-393.5
	$H_2 + 0.5O_2 \rightarrow H_2O$	-241.8
	$CO + 0.5O_2 \rightarrow CO_2$	-283.0
	$CH_4 + 2O_2 \rightarrow CO_2 + 2H_2O$	-802.2
	$CH_4 + 1.5O_2 \rightarrow CO + 2H_2O$	-519.3
	$C_2H_6 + 3.5O_2 \rightarrow 2CO_2 + 3H_2O$	-1428.8
	$C_6H_6 + 7.5O_2 \rightarrow 6CO_2 + 3H_2O$	-3169.4
Secondary Reactions	$H_2O + CO \leftrightarrow CO_2 + H_2$	-41.2
	$CH_4 + H_2O \leftrightarrow CO + 3H_2$	206.2

All the chemical reactions described above are considered to be taking place simultaneously in the gasifier. Vamvuka *et al.* (1995) considered both sequencing and paralleling the reactions and discovered that when the reactions are in sequence, only about 10% of carbon conversion could be obtained as compared to over 99% for parallel reactions. Walker *et al.* (1959) studied the solid-gas reactions at relatively low temperatures and pressure (800 ^oC and 0.1 atm) and published their relative reaction rates as shown in **Table 2.4**. The carbon-oxygen reaction is

the fastest reaction while carbon-steam and carbon-carbon dioxide have almost the reaction rate, and the hydro-gasification is the slowest reaction.

Table 2.4: Approximate relative rate of solid-gas

Reaction	Relative rates
$C + O_2$	1.00×10^5
$C + H_2O$	3.00
$C + CO_2$	1.00
$C + H_2$	3.00×10^{-3}

It can be noted though from **Table 2.4** that the difference in relative rates between carbon-steam and carbon-carbon dioxide is very small and reaction kinetics for the two reactions have been considered the same by most researchers in this field, and these are, Wen and Chaung (1979), Govind and Sha (1984), Vamvuka *et al.* (1995) and Xu and Qiao (2012).

2.9 **The Synthesis Gas**

Syngas which also sometime being referred to a synthesis gas can be used in the generation of pure hydrogen, clean diesel or synthetic natural gas (Chiu *et al*., 2009). The chemical composition of a syngas is highly dependent on as coal quality, rank, feeding system (slurry or dry feed), oxidising agent (pure oxygen from ASU or air), temperature, pressure, residence time in the gasifier and the heating rate (Maxim *et al.*, 2010). Although presence of hydrocarbons such as methane on the syngas negatively affects the carbon capture plant capabilities (Maxim *et al.*, 2010), however, it enhances the overall calorific value of the syngas due to methane having a relatively higher heating value. IGCC operating conditions should, therefore, be selected based on the syngas application. The hydrogen to carbon monoxide ratio of the syngas gas varies based on the feed composition and reaction temperature (Raju *et al.*, 2008, Cao *et al.*, 2008). The H_2-to-CO ratio in a gasifiers range depends on the final syngas application, for Fischer-Tropsch liquids production it is an average of 2:1, for synthetic natural gas it is about 3:1 and 10+:1 for hydrogen production (Abughazaleh *et al.*, 2007).

Syngas quality and composition largely depends on the oxidizing agent and the feed type (dry or slurry) used during gasification. Oxygen-blown gasifiers produces syngas with higher CV as opposed to air-blown counterpart and this is because of the high N_2 content in air-blown units (Wang *et al.*, 2008). Silaen and Wang (2005, 2006, 2009 and 2010) concluded that slurry feedstock yielded more H_2 than the dry feed and while dry-fed gasifiers produced more CO. Syngas can be divided into three main categories; high, medium and low calorific value (Btu)

gas (Baughman, 1978). High CV gas is generally used in pipeline systems due to its compatibility with natural gas and its heating value is approximately 37 MJ/m^3 and it primarily consists of methane. Medium heating value gas has a CV ranging between 11 and 26 MJ/m^3, and its main composition is carbon monoxide, hydrogen and other gases. It can be used as an industrial fuel but cannot be used as substitute for pipeline-quality gas. Low CV gas has a heating value less than 11 MJ/m^3, and its main constituents are carbon monoxide and hydrogen. This gas is mainly used as fuel in industry or as a raw material for the production of ammonia, methanol and other compounds.

2.10 **Gasifier Performance**

Published literature has described a number of operating conditions that largely influence the gasifier performance and these includes oxidizing agent-to-fuel ratio and the steam-to-carbon, temperature, pressure, particle size, etc. The key performance indicators of the gasifier are best described by the carbon conversion efficiency, cold gas efficiency (CGE), C-to-H_2 ratio and the syngas exit temperature. The carbon conversion and CGE are described by Equations 2.2 and 2.3, respectively.

$$X_c = \left(1 - \frac{C_{GR}}{C_f}\right) x\ 100 \tag{2.2}$$

$$\eta_{cg} = \left(\frac{1}{Q_c} \sum_{i=1}^{n} x_i CV_i\right)\ x\ \ 100 \tag{2.3}$$

Where C_{GR} and C_f are the amounts of carbon in the gasification residue and in the feedstock, respectively. Q_c is heating value of coal fed to the reactor. The ratio of hydrogen to carbon monoxide is very critical in the syngas composition especially if the gas has to be burn in a gas turbine of the IGCC. While dominance H_2 of in the syngas composition results in more stable flames, it also causes problems on the combustor making it more prone to flash backs and thermo-acoustic instability (Tuncer 2006).

2.10.1 **Effect of temperature**

Gasifiers, particularly the entrained flow gasifiers, are known to operate at higher temperatures to maximize carbon conversion. The severe temperatures affect both mechanical, process design and operation of the gasifier, and consequently, the operating and capital costs of the gasifier. The gasification temperature is determined by the oxidizing agent-to-coal ratio (Chyou *et al.*, 2010). Gasifiers using air as an oxizing agent operates at lower temperature compared to those using almost pure oxygen. This is due to nitrogen acting as a dilution in the reactor.

Operating the gasifier at relatively higher temperatures increases the carbon conversion and as well the concentrations of CO and H_2 in syngas while CO_2, CH_4 and H_2O reduces (Zhou *et. al.*, 2009, Emami *et al.*, 2012 and Puente-Ornelas *et al.*, 2012). The effect of temperature in the syngas yield is also a strong function the gasifying agent used (Hernandez *et al.*, 2012). It is, however, not recommended to operate the entrained flow gasifier below a temperature of 1300ºC as this would negatively affect the carbon conversion and the correct slag flow (Guo *et al.*, 2007).

Lower temperatures also promote the formation of methane gas which might not be desirable depending on the downstream application of syngas (Guo *et al.*, 2007). Excessively high temperatures should also be avoided on the gasifier as these would have a huge impact on the refractory lining integrity and high carbon dioxide concentration on the syngas. An increase in temperature changes the rate-determining step of char gasification from chemical reaction control to pore diffusion hindered (Sun *et al.*, 2012). This may however be neglected in an entrained flow gasifier operating with very fine particle where only surface reactions are considered. The extreme operating condition of the gasifier, especially temperature, may also result in the formation of the nitrogen oxides.

A number of positive developments have recently emerged in low temperature gasification, particularly in fluidized bed gasifiers (Corela *et al*, 2003, 2006 and 2008). The focus has mainly been on increasing H_2 content and reducing the CO_2 in the product gas (Corela *et al.*, 2008). As opposed to the entrained flow gasifier-based IGCC plants which require an additional plant unit to capture CO_2, in-situ CO_2 removal has been studied and proposed (Curran *et al.*, 1969). In-situ CO_2 removal refers to elimination of CO_2 inside the fluidized bed gasifier by chemical reaction where Calcium Oxide (CaO) is added into the bed to react with CO_2 to form Calcium Carbonate (Corela *et al.*, 2006). One of the disadvantages for low temperature gasification was also the presence of tars in the product gas (Beath, 1996). CaO has also been found to eliminate the tars in the product gas in presence of steam (Corela *et al.*, 2003). Thus far, up to 85 vol% H_2 purity and 0 vol% CO_2 have been reported under various operating conditions (Lin *et al.*, 2001, Yoshida *et al.*, 2004, Hanaoka *et al.*, 2005 and Wang *et al.*, 2007).

2.10.2 **Effect of pressure**

Gasifiers can operate at either atmospheric or high pressures. Mondal *et al.* (2011) reported that the pressures up to 2.94 MPa do not exert any significant impact on syngas composition. This is however in contrast to the work presented by Vamvuka *et al.* (1995) which showed that

an increase in operating pressure decreases the amount of CO_2 and increases the amount of CH_4 as shown in **Table 2.5**.

Table 2.5: Composition and syngas heating values (Vamvuka *et al.*, 1995)

Operating pressure (MPa)	Composition (dry basis) (mol%)				Calorific value (MJ/m^3	
	CO_2	CO	H_2	CH_4	*At operating pressure*	*At s.t.p*
0.1	18.97	49.19	31.83	0.01	2.26	8.31
2.0	18.91	43.82	36.62	0.65	62.48	8.95

Ruiz *et al.* (2012) also indicated that pressurized gasifiers are more efficient compared to atmospheric gasifiers, although this may come at a trade-off between efficiency and capital cost. An increase in gasification operating pressure is also associated with the reduction of tars and char in the final syngas produced. Shen *et al.* (2012) also proved that the operating pressure has a significant contribution on the gasifier performance. In their work, they studied the performance of a pressurised entrained flow gasifier (in a pilot scale) and discovered that an increase in pressure from about 4.2 to 8.2 bar was resulting in approximately 12% increase in carbon conversion for their particular feed mixture of coal and petroleum coke.

Wang *et al.* (2008) indicated that the generation of syngas at high pressures is good for subsequent use in end conversion equipment, such as engines and turbines. This is also in agreement with the work of Vamvuka *et al.* (1995) who showed that operating the gasifier at higher pressures increases the production of methane which has a relatively high heating value. The presence of methane in the syngas improves the overall heating value of the syngas and, therefore, its attractiveness and effectiveness if it has to be used in a gas turbine. An increase in pressure, however, decreases the volatile yield during the gasification (Cai *et al.*, 1993, Yeasmin *et al.*, 1999, Wall *et al.*, 2002 and Yu *et al.*, 2007). Similarly to the operating temperature, the operating pressure of the gasifier may have a significant impact on the mechanical design of the gasifier and the down-stream units, especially the gas cleaning unit. Mechanical wall thickness of the pressure vessel increases with the increase in pressure and therefore resulting in increase in capital cost. The gas cleaning unit, which is generally the cold-process and low pressure, will be affected an increase in pressure in the gasifier, and therefore proper economic evaluation and process benefits with regard to pressure need to be properly assessed.

2.11 Existing Mathematical Models

Previous researchers have approached the modeling of chemical reactions taking place in the gasifier as either hydrodynamics or non-hydrodynamics models, as shown in **Figure 2.9**. The non-hydrodynamic models also referred to as thermodynamic equilibrium models are generally used to conduct parametric studies and thermodynamic analysis of the gasification process (Loha *et al.*, 2014). These models are based on minimizing the Gibbs free energy of the gasification process in order to determine the composition of the resulting from gasification (Buragohain 2013). Equilibrium models are relatively easy to implement with rapid convergence and have been widely used during quantitative assessment of the generic gasification process (Sharma, 2011 and Echegaray 2014).

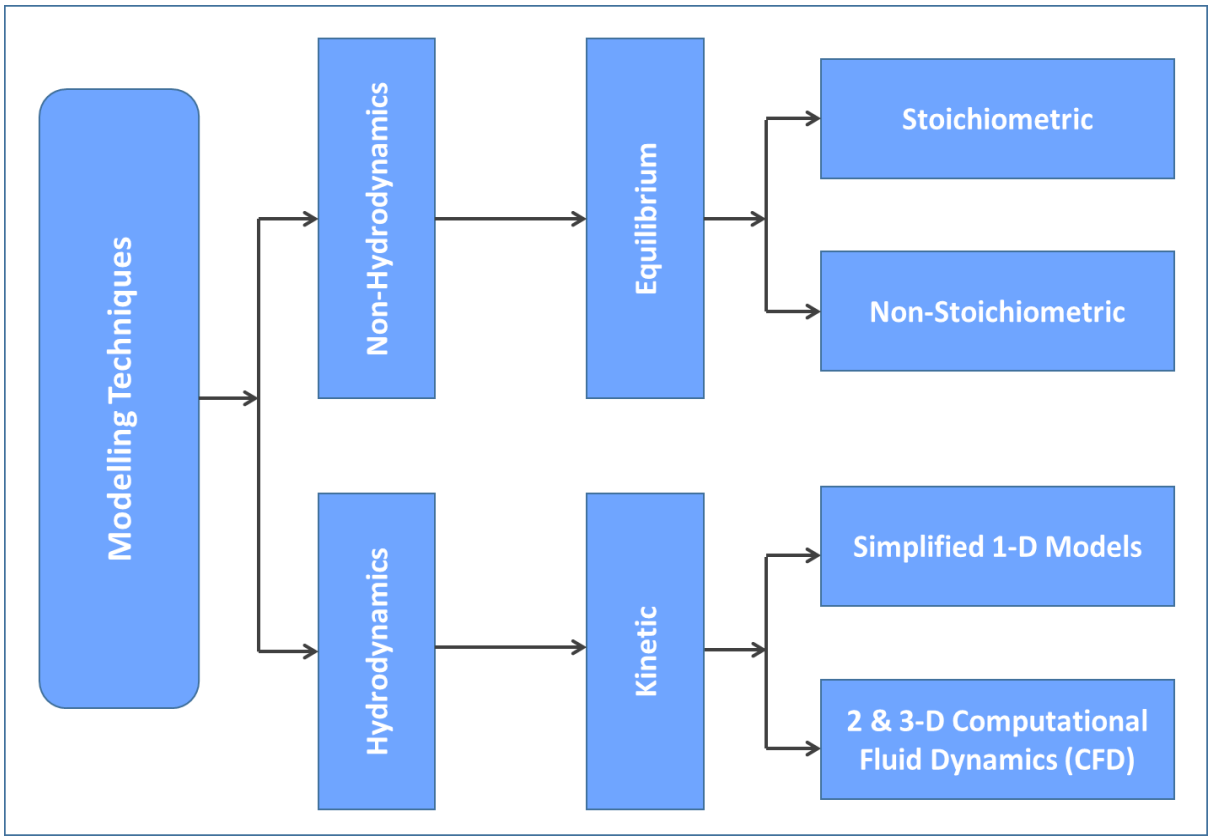

Figure 2.9: Gasifier Modelling Approaches

Equilibrium models are not gasifier design-specific and based on the following summary of assumptions, (Loha *et al.*, 2014):

- Chemical reaction rates proceed fast enough and equilibrium condition can be reached during reactions residence time.
- Gas composition of the gasification process only consists of H_2, CO, CH_4, CO_2, H_2O and N_2.

- Gases produced during the process are at the process temperature and they all obey the ideal gas law.
- Gasification process is at steady state and there is no heat input or output from the gasifier.
- Energies such as kinetic and potential are negligible.

A number of equilibrium models used to study gasification process include those of Sofia *et al*., (2013), Echegaray (2014), Yi *et al*., (2014), and Zhu *et al.,* (2015).

Kinetic models, on the other hand, combines the chemical reaction schemes and hydrodynamics of the gasifier. This, therefore, provides a more comprehensive and realistic insight into the process as opposed to thermodynamic equilibrium models (Loha *et al.*, 2014). The shortcomings of these model generally lies on the availability of chemical reaction kinetics constants over a wide range of operating conditions and as well as coupling of hydrodynamics of the gasifiers and kinetics of reaction scheme (Vamvuka *et al.*, 1995 and Buragohain, 2013). Due to their complexity, kinetic models are computationally expensive.

Existing models can be divided into simulation and optimization. The available mathematical models have focused on both steam and gas paths. Gas path models have been mainly dedicated on the gasifier performance while the steam path models have looked at all the heat recovery units including the steam turbine. Available models for entrained flow gasifiers may be divided according to the gasifier feed type, namely; slurry or dry feed. Modelling tools such as ASPEN PLUS, GTPRO and ANYSYS/FLUENT have been used for both simulation and optimization.

2.11.1 **Simulation Models**

A number of entrained flow gasifier kinetic models have been published in open literature with diverse levels of accuracies. Available models range from simple models such as those of Wen and Chaung *et al.* (1979) and Lee *at al.* (2011) to complex Computation Fluid Dynamic Models recently developed by Ma and Zitney (2012). Previous researchers have approached the modeling of chemical reactions taking place in the gasifier as either equilibrium or simply irreversible chemical reactions, while others have used a combination.

Wen and Chaung (1979) developed a kinetic mathematical model to simulate the Texaco downflow entrainment pilot plant coal gasifier. Mass and energy balances were used to determine the temperature and concentration profiles across the length of the reactor. This was

a simulation model which did not aim at optimizing the gasifier. Although sensitivity analyses were carried out on key parameters such as O_2/fuel and H_2O(g)/fuel ratios, these were carried out one after the other and therefore could not guarantee optimality. Vamvuka *et al.* (1995) proposed a model for the entrained flow gasifier based on mass and energy balances and their model was based on heterogeneous and homogeneous gas-phase equilibria. Their model was solved using modified Euler method in conjunction with a nonlinear algebraic solver. Their model was however limited to pressures between 0.1 and 2 MPa. The model was also focused on maximizing the conversion and this has not been proven if it also results in maximum fuel gas heating value.

Watanabe and Otaka (2006) presented a kinetic mathematical model for a numerical simulation of the entrained flow coal gasifier. Their model was used to predict the effect of air ratio on the gasifier performance. However, this model was evaluated at a constant pressure of 2.0MPa and similar to other published models, sensitivity analysis of the air ratio was performed manually. Chui *et al.* (2009) developed a simulation model for an entrained flow gasifier. In their work the focus was on simultaneous development of the pilot-scale pressurized entrained flow gasifier facility and CFD modelling. The CFD model was developed to predict the performance of the gasifier and the results were compared against the experimental data. This model however over-predicted the carbon conversion, achieving 100% while experiments achieved 84% and this could be attributed to uncertainties in their solid-gas reactions. Jeong *et al. (*2014) presented a CFD model to study the effect of coal gasification in a two-stage commercial entrained flow gasifier. Their modeling was performed using a commercial code, ANYSYS Fluent 14.0. While this was a detailed model for the gasifier and compared well with operational data, it was aimed at studying the impact of particle size in the gasification process and the conclusion was only drawn based on maximum carbon conversion and cold gas efficiency.

Chyou *et al*. (2010) developed a numerical simulation model for a slurry-feed cross-type two-stage gasification unit. In their work, the focus was mainly on the influence of coal slurry concentration and O_2/coal ratio on the gasification process. They found that lower concentration of the slurry was preferred for high H_2 yield at lower syngas temperature while CO was favoured by high slurry concentration with higher syngas temperature. The O_2/fuel ratios, which determine the operating temperature of the gasifier, are investigated at either ends of the temperature scale, and this only reveals the impact on the ratio shift between CO and H_2.

Their work was however a simulation model and therefore did not consider the optimum conditions of the gasification unit that yield the highest CV of the syngas.

Lee *et al.* (2011) proposed a simplified process model for a dry-fed entrained bed coal gasifier based on a 1-D Plug Flow concept. Their model was used to predict the carbon conversion, cold gas efficiency and the temperature profile across the reactor. Their model was however over-simplified, ignoring the important radiation heat transfer mechanism and assuming a simple and uniform heat loss to the gasifier wall. Xu and Qiao (2012) developed a mathematical model for a coal gasification process in a well-stirred reactor. Their model was used to study the effect of devolatilization and moisture content on the gasification performance. Xu and Qiao's model was based on the detailed gas phase chemistry, drying and devolatilization, particle-phase reaction, boundary layer diffusion and pore evolution. Theirs was, however, a numerical simulation model focusing on the conversion time and syngas production. Kasule *et al.* (2012) developed a 1-D steady state model of a slurry-fed entrained flow gasifier to simulate an IGCC process. The differential-algebraic equations of mass, energy and momentum describing the system were considered together with oxygen used as an oxidizing agent. In their model, Kasule and co-workers developed a detailed radiative transfer model taking into account of the solids and all internal gasifier surface interactions and the interactions between surfaces themselves. The model was proposed to give more insight on the gasifier performance using parametric studies subject to feed condition changes. While this was a very detailed 1-D model of the gasifier, similarly to the other simulation models, it investigated optimum conditions in achieving maximum carbon conversion and proposed a range of water-to-coal and oxygen-to-coal ratio to obtain 99% conversion.

Ma and Zitney (2012) proposed a CFD model to simulate the performance of single and two-stage gasification units. Their model was built on the basis of the existing CFD models, particularly that of Shi *et al.* (2006), but incorporated the advanced physical and chemical submodels which included moisture vaporization model and coal devolatilization model which included more species. The model was used to predict the carbon conversion, syngas exit temperature and mole fraction distribution of major species in a gasifier. One of the interesting findings by Ma and Zitney was the fact that the syngas composition at the model exit was not in chemical equilibrium. In both scenarios, single and two stage, the gasifier was operated at an O_2-to-coal ratio that maximize carbon conversion, achieving a 98.2% and 95.1% for single and two stage, respectively. This model was also a simulation model which was aimed at

accurately predicting the performance of the gasifier taking into account the detailed physical and chemical submodels.

2.11.2 **Optimization Models**

Limited work has however been carried on the optimization of the IGCC mostly focusing on the gas circuit. Madzivhandila *et al.* (2009) were amongst the first researchers to focus on the optimization of an IGCC power plant. In their work, they used pinch analysis to optimize the energy generated in an IGCC power plant. The focus on this work was however on improving the plant efficiency with the emphasis on the steam path. Emun *et al.* (2010) proposed a simulation tool aimed at improving the efficiency and minimizing adverse effect on the environment of the IGCC power plant. The optimization of the process flowsheet was carried out by sensitivity analysis which involved selecting variables that were considered to have high impact on the system performance. This work however only considered gasification temperature as the only key variable on the gasifier and this was varied between 1250°C and 1550°C.

Lang *et al.* (2011) proposed the optimization of the IGCC processes using reduced order CFD models. In their comprehensive work, Lang and co-workers considered the integration of the CFD (reduced order) within steady-state process simulators and the subsequent optimization of the integrated system. Two objective functions were proposed; *minimizing heating value* of the syngas and *minimizing the flowrate* of coal feed. The resulting Nonlinear Program (NLP) model was solved using CONOPT3 solver based on O_2/fuel and $H_2O_{(g)}$/fuel as degrees of freedom. Their work was aimed at demonstrating the accuracy of the reduced order models and satisfying the required power demand. This work does not include the effect of pressure, particle size diameter and it operates at a fairly constant temperature of about 1327°C or 1427°C.

Tremel and Spliethoff (2013) developed an entrained flow gasification model to predict the gasifier performance in large scale units. Their work focused on optimizing the cold gas efficiency and fuel conversion. Gas composition and temperature profiles, cold gas efficiency and fuel conversion within a 500 MW gasifier were predicted in validating their model. Sensitivity analysis of fuel particle size and oxygen-carbon ratio was investigated on the cold gas efficiency. The work of Tremel and Spliethoff however ignored the effect of pressure on the conversion and cold gas efficiency. Thus far, there has been no work presented which

proves that maximum fuel conversion amounts to maximum cold gas efficiency and maximum fuel gas heating value.

Complex modelling of major chemical and physical systems continues to facilitate the understanding of processes where experiments have limitations, especially for processes taking place under extreme operating conditions. It has been observed that the gasifier is usually operated at maximum conditions and these conditions impose a severe penalty on the capital cost and as well as the reliability and availability of the gasifier. This current research therefore aims at establishing if the extreme conditions are the optimum conditions that yield the maximum calorific value of the syngas for power generation.

This current work focuses on the entrained flow gasifier used to produce fuel gas for power generation. It therefore aims at establishing whether the extreme conditions above 2000°C (Minchener, 2005) and 5.6MPa (Ma and Zitney, 2012) are indeed the optimum conditions for producing fuel gas of the highest heating value. In the proposed work, a 1-D simulation model for a dry-fed entrained flow gasifier with oxygen as oxidizing agent will be formulated using differential algebraic equations (DAE) of mass and energy balances. An equation orientated flowsheet of the IGCC power plant will be developed on *general Process Modelling and Simulation* (gPROMS) platform for simulation and optimization. Multiflash will be used to obtain the thermodynamic properties of gaseous components. A number of devolatilization, heterogeneous and homogeneous chemical reactions taking place in the gasifier will be selected to model the system under detailed assumptions that will be outlined in *Model Development* section. These selected reactions will be used to study the gasifier performance, more especially in relation to operating conditions and quality of the fuel gas.

References

Aasberg-Petersen, K., Chistensen, T.S., Dybkaer, I., Sehested, J., Ostberg, M., Coertzen, R. M., Steynberg, A. P., *Synthesis gas production for FT synthesis*, Amsterdam, The Netherlands: Elsevier, 2004

Abughazaleh, J., Salazar, N., Ariyapadi, S., *Optimising Hydrogen and Chemicals Production From The Transport Gasifier*^{TM}, International Pittsburgh Coal Conference (Johannesburg, South Africa), 2007

ASME Turbo Expo 2005: Power for Land, Sea, and Air, June 6-9, 2005, Reno-Tahoe, Nevada, USA, ASME, 2005

Beér, J. M., *Higher Efficiency Power Generation Reduces Emissions (MIT)*, National Coal Council, 2009

Bonzani, F., Pollarolo, G., Ferrante, A., Ansaldo V94.2K Gas Turbine Burner *Performance Operating with Steelworks Process Gas-Natural Gas Fuel*. Power-Gen Europe, 2000.

Brdar, R. D., Jones, R. M., *GE IGCC Technology and Experience with Advanced Gas Turbines*, GE Power Systems Schenectad, NY, 2000

Breault, R. W., *Gasification Processes Old and New: A Basic Review of the Major Technologies*, Energies, 2010, 3, 216-240

Burogohain, B., Chakma, S., Kumar, P., Mahanta, P., Moholkar, V. S., *Comparative evaluation of kinetic, equilibrium, and semi-equilibrium models for biomass gasification*, International Journal of Energy and Environment, Volume 4, Issue 4, 2013, 581-614

Cai, H., Guell, A., Dugwell, D., Kandiyoti, R., *Heteroatom distribution in pyrolysis products as a function of heating rate and pressure*, Fuel, 1993,72 (3), 321-327

CATF (Clean Air Task Force), Water usage at IGCC plants, http://www.fossiltransition.org/pages/gasification_page_link2/46.php, (31st Aug), 2014

Choi, Y. C., Li, X. Y., Park, T. J., Kim, J. H., Lee, J. G, *Numerical study on the coal gasification characteristics in an entrained flow coal gasifier*, Fuel, 2001, 80, 2193-2201

Christou, C., Hadjipaschalis, I., Poullikkas, A., *Assessment of integrated gasification combined cycle technology competitiveness*, Renewable & Sustainable Energy Reviews, 2007

Christou, C., Hadjipaschalis, I., Poullikkas, A., *Assessment of integrated gasification combined cycle technology competitiveness*, Renewable & Sustainable Energy Reviews, 2007

Chyou, Y. P., Huang, C.B, Wang, T., *Numerical Simulation of Gasification Process In a Cross-type Two-Stage Gasifier*, International Pittsburgh Coal Conference, Istabul, Turkey, 2010

Corella, J., Caballero, M. A., Aznar, M. P., Brage, C., *Two Advanced Models for the Kinetics of the Varation of the Tar Composition in its Catalytic Elimination in Biomass Gasification*, Ind. Eng. Chem. Res. 2003, 42 (13), 3001-3011

Corella, J., Toledo, J. M., Molina, G., *Steam Gasification of Coal at Low-Medium (600-800ºC)Temperature with Simultaneous CO_2 Capture in Fluidized Bed at Atmospheric Pressure: The Effect of Organic Species. 1. Literature Review and Comments*. Ind. Eng. Chem. Res., 2006, 45 (18), 6137-6146

Corella, J., Toledo, J. M., Molina, G., *Steam Gasification of Coal at Low-Medium (600-800ºC)Temperature with Simultaneous CO_2 Capture in Fluidized Bed at Atmospheric Pressure: 2. Results and Recommendation*. Ind. Eng. Chem. Res., 2008, 47, 1798-1811

COSPP, *Cogeneration & On-Site Power Production, Gas Turbines breaking the 60% efficiency barrier*, http://www.cospp.com/articles/print/volume-11/issue-3/features/gas-turbines-breaking.html, accessed on 10th September 2014

DOE/NETL, 2007/1281, National Energy Technology Laboratory, *Cost and performance baseline for fossil energy power plants study*, 2007, 1 (available on http://www.netl.doe.gov)

Echegaray, M., Rodriguez, R., Castro, M. R., *Equilibrium model of the gasification process of agro-industrial wastes for energy production*, International Journal of Engineering Science and Innovative Technology (IJESIT), 2014, Volume 3, Issue 3

Eskom, Eskom website: http://www.eskom.co.za/AboutElectricity/ElectricityTechnologies/Pages/Electricity_Technologies.aspx , accessed on 09th September 2014

Geositsm R. F., Schmoe, L. A., *IGCC-The Challenges of Integration, Preceeding of GT2005 ASME Turbo Expo 2005*: Power for Land, Sea, and Air, June 6-9, 2005, Reno-Tahoe, Nevada, USA, ASME, 2005

Govind, R., Shah, J., *Modeling and Simulation of An Entrained Flow Coal Gasifier*, AIChE Journal, 1984, (Vol. 30, No. 1), 79-92

Hada, S., Tsukagoshi, K., Masada, J., Ito, E., *Test Results of the World's First 1600ºC J-series Gas Turbine*, Mitsubishi Heavy Industries Technical Review, 2012, (Vol. 49 No. 1)

Higman, C., *The reliability of integrated gasification combined cycle (IGCC) Power Generating Units*, Achema 2008/Frankfurt, 2006

IEA (International Energy Agency), *CO_2 Emissions from fuel combustion highlights*, 2012

Jones, R. H., Thomas, G. J. *Materials for the hydrogen Economy*. CRC Press: Boca Raton, FL, USA, 2008

Kawabata, M., Kurata, O., Iki, N., Furutani, H., Tsutsumi, A., *Advanced integrated gasification combined cycle (A-IGCC) by exergy recuperation – technical challenges for future generations*, Journal of Power Technologies, 2012, 92 (2), 90-100

Korens, N., Simbeck, D. R., Wilhelm, D. J., *Process Screening Analysis of Aletrnative Gas Treating and Sulfur Removal for Gasification*, SFA Pacific, Inc. Engineering & Economic Consultants, 2002

Leung, D. Y. C, Caramanna, G., Maroto-Valer, M. M., *An overview of current status of carbon capture and storage technologies*, Renewable and Sustainable Energy Reviews, 2014, 39, 426-443

Lin, S. Y., Harada, M., Suzuki, Y., Hatano, H., *Hydrogen Production from Coal by Separating Carbon Dioxide During Gasification*, Fuel, 2002, 81, 2079-2085

Loha, C., Gu, S., De Wilde, J., Mahanta, P., Chatterjee, P. K., *Advances in mathematical modeling of fluidized bed gasification*, Renewable and Sustainable Energy Reviews, 2014, 40

Lu, X., Wang, T, *Investigation of Low Rank Coal Gasification in a Two-Stage Downdraft Entrained-Flow Gasifier*, International Journal of Clean Coal and Energy, 2014, (3), 1-12

Madzivhandila, V., Majozi, T., Zhelev, T., *Process integration as an optimization tool in clean coal technology: A focus on IGCC*, Chemical Engineering Transactions, 2009, 941-946

Minchener, A.J., *Coal gasification for advanced power generation*, Fuel 84, 2005, 2222-2235

Mondal, P. Dang, G. S., Garg, M. O., *Syngas production through gasification and cleanup for downstream applications – Recent developments*, Fuel Processing Technology, 2011, 92, 1395-1410

OECD/IEA, *Coal Medium -Term Market Report*, *International Energy Agency*, 2012

OSACVC, *Overview of the South African Coal Value Chain*, *Report*, http://www.sanedi.org.za/archived/wp-content/uploads/2013/08/sacrm%20value%20chain%20overview.pdf, 2011

Pena, F. G., *Operating experience and current status of Puertollano IGCC Power Plant*, International Freiberg Coference on IGCC & XtL Technologies (June 17), 2005

Pouris, A., *Future Sources of Thermal Efficiency in Generation Technology*, Pargamon Journals Ltd, 1985

Pruschek, R., *Enhancement of the efficiency of integrated gasification combined cycle (IGCC) power plants*, Final Report JOU2-CT94-0454, 1998

Puente-Ornelas, R., Lizcano-Zulaica, C. J., Guzman, A. M., Zambrano, P. C., Das-Roy, T. K., *Dissolution of refractories for gasification process of petroleum coke for steel industry*, Fuel, 2012, 93, 581-588

Roth, E., *Efficiency of thermal power plants*, Sealnet, 2005

Sharma, A., *Modeling and simulation of a downdraft biomass gasifier 1. Model development and validation*, Energy Conversion and Management, 2011, 52, 1386 – 1396

Shen, C., Chen, W., Hsu, H., Sheu, J., Hsieh, T., *Co-gasifcation performance of coal and petroleaum coke blends in a pilot pressurized entrained-flow gasifier*, Int. J. Energy Res. 2012, 36, 499-508

Shi, S., Zitney, S. E., Shahnam, M., Syamlal, M., Rogers, W. A., *Modelling coal gasification with CFD and discrete phase method*, J. Energy Institute, 2006, 79 (4), 217-221

Silaen, A., Wang, T., *Comparison of Instantaneous, Equilbriu and Finite Rate Gasification Models in an Entrained Flow Coal Gasifier*, Proceeding of the 26th International Pittsburgh Coal Conferencem Pittsburgh, Pennsylvania, 2009

Silaen, A., Wang, T., *Effects of fuel Injection Angles on Performance of A Two-Stage Coal Gasifier*, Proceeding of the 23rd Pittsburgh Coal Conference, Pittsburgh, Pennsylvania, 2006

Silaen, A., Wang, T., *Effects of Turbulence and Devolatilization Models on Gasification Simulation*, International Journal of Heat and Mass Transfer, 2010, 53, 2074-2091

Smoot, D. L., Smith, P. J., *Coal Combustion and Gasification*, Plenum Press, 1985

SRWE, *Statistical Review of World Energy 2012*, Technical Reports for BP Global: London, UK, June 2012, Available online: http://bp.com/statitisticalreview (accessed on 4 December 2012)

Sofia, D., Guiliano, A., Barletta, D., *Techno-Economic Assessment of Co-gasification of Coal-Petcoke and Biomass in IGCC Power Plants*, Chemical Engineering Transactions, , 2013, Vol. 32

Sun, Z., Dai, Z., Zhou, Z., Xu, J., Yu, G., *Comparative Study of Gasification Perfromance between Bituminious Coal and Petroleum Coke in the Industrial Opposed Multiburber Entrained Flow Gasifie*r, Energy & Fuels, 2012, 26, 6792-6802

Tennant, J. B., *Gasification System Overview v3.0 (Gasifcation System Program – Slide Library),* U. S Department of Energy, 2012

Thompson, J., Clean Air Task Force, *"Integrated gasification combined cycle (IGCC) – Environmental performance*", Presentation at Platts IGCC symposium, Pittsburg, 2005

Tuncer O. *Active Control of Spray Combustion*. *PhD Dissertation, Louisiana State University*, Baton Rouge, LA, 2006.

UNFCCC (*United Nations Framework Conversion of Climate Change*, Copenhagen Accord, Draft decision -/CP.15, 2009

USDoE and Gasification Technology Council, *World Gasification Database*, 2001

van der Riet, M., *Underground Coal Gasification*, Energize, 2008

Walker, P. L. Jr, Rusinko, F. Jr., Austin, L. G., *Gas Reactions of Carbon*, Reprinted from Advances in Catalysis, 1959, Vol. X1, 133-164

Wall, T. F., Liu, G. Wu, H., Roberts, D. G., Benfell, K. E., Gupta, S., Lucas, J. A., Harries, D. J., *The effects of pressure on the reactions during pulverised coal combustion and gasification*, Progress in Energy and Combustion Science 2008, 28, 405-433

Wang L, Weller C. L., Jones D. D., Hanna, M. A., *Contemporary issues in thermal gasification of biomass and its application to electricity and fuel production*. Biomass Bioenergy, 2008, 32, 573-81,

Wang, L., Weller, C. L., Jones, D. D, Hanna, M. A., *Contemporary issues in thermal gasification of biomass and its application to electricity and fuel production*, Biomass & Energy, 2008, 32, 573-581

Wartsila, *Gas Turbine for Power Generation: Introduction*, Power Plants, 2014 (accessed via: http://www.wartsila.com/en/gas-turbine-for-power-generation, 8 October 2014)

WBC (World Bank Commodity), *World Bank Commodity Forecast Price data*, July 2014

Xu, S., Ren, Y., Wang, B., Xu, Y., Chen, L., Wang, X., Xiao, T., *Development of a novel 2-stage entrained flow dry powder gasifier*, Applied Energy, 2014

Xu, S., Ren, Y., Wang, B., Xu, Y., Chen, L., Wang, X., Xiao, T., *Development of a novel 2-stage entrained flow dry powder gasifier*, Applied Energy, 2014

Xu, S., Ren, Y., Wang, B., Xu, Y., Chen, L., Wang, X., Xiao, T., *Development of a novel 2-stage entrained flow coal dry gasifier*, Applied Energy, 2014, 113, 318-323

Yi, Z., Oyedun, A. O., Maojian, W., Gebreegziabher, T., Yu, Z., Jin, L., Wai, H. C., *Modeling, Integration and Optimization of Biomass and Coal Co-gasification*, Energy Procedia, 2014Yeasmin, H., Mathewa, J. F., Ouyang, S., *Rapid devolatilization of Yallourn brown coal at high pressures and temperatures*, Fuel, 1999, 78 (1), 11-27

Yu, J., Lucas, J. A., Wall, T. F., *Formation of the structure of chars during devolatilization of pulverized coal chars produced at elevated pressures and its thermoproperties: A review*. Progress in Energy and Combustion Science, 2007, 33 (2), 135-170

Zaporowski, B., *Analysis of energy-conversion processes in gas-steam power-plants integrated coal gasification*, Applied Energy, 2003, 297-304

Zhu, Y., Simultaneous *Optimization of a Heat Integrated Coal Gasification Process*, Chemical Engineering Research and Design, 2015

3. Model Development

3.1 Introduction

This chapter entails the development of a simulation and optimization models of an entrained flow gasifier. A simulation model developed in this current work is be used to predict the performance of the gasifier in terms of fuel gas composition, gasification temperatures, cold gas efficiency, conversion and the heating value achievable under optimum operating conditions and specified constraints. The developed simulation model is then optimized to ascertain the optimum operating conditions of the gasifier that yields highest possible fuel gas heating value. The model is developed from first principle, using mass and energy equations. A number of chemical reactions that best represent the gasifier both homogeneous (gas-phase) and heterogeneous (solid-gas), is selected to model the system. The model considers the combustion and gasification reactions as a multiphase mixture flowing concurrently in the entrained flow gasifier, which is treated as a Plug Flow Reactor (PFR). The system represented by Differential Algebraic Equations (DAE) is modelled using a state-of-art simulation and modelling tool known as *g*eneral *P*rocess *M*odelling and *S*imulations (*g*PROMS v4.0.0) and the thermodynamic properties of the gaseous mixture are obtained from *Multiflash for Windows* (version 4.1).

The present work only focuses on two major components of the gas path of the IGCC power plant, which are mainly, the gasifier and gas turbine. A dry-fed, oxygen blow, 1 Dimensional gasifier simulation model is first developed and solved in *g*PROMS platform. The results are then compared against other existing models in published literature under similar operating or input conditions. The gasifier model is then be optimised to establish the optimum operating conditions, such as, temperature and pressure that yield the maximum fuel gas heating value. A number of assumptions is be adopted during the development of the current model and they are detailed out in the next subsections of the model development. The existing models that will form a basis of this new model will be those developed by Vamvuka *et al.* (1995), Lee *at al.* (2011) and Sophia *et al*. (2013).

The gas turbine model describes the performance of the gas turbine taking into account the ambient conditions, the compressor and the expander efficiencies. The combustion chamber of the gas turbine is treated as an adiabatic conversion reactor. The key performance indicators predicted by the gas turbine model include expander inlet temperature, power output, exhaust

specific heat capacity and the exhaust temperature. The combined model of the gas turbine and gasifier is used to determine the gas path efficiency.

3.2 **Model description**

3.2.1 **Devolatilization Model**

Devolatilization can be described as a physical distillation of coal into char and volatile matter. This process is a strong function of temperature, heating rate and particle size (Gray *et al.*, 1973). A number of devolatilization models have been proposed in published literature and these range from simple models (Badzioch and Hawksley, 1970) to relatively complex models (Kobayashi *et al.*, 1977) depending on the assumptions undertaken during model development. These models can be classified as either slow or rapid devolatilization models.

Coal devolatilization is characterised by the removal of the volatile components present in the fuel such as CO, CO_2, CH_4 and H_2. In this reaction, coal is broken down into mainly char and volatiles (Beath 1996) and the process begins taking place at temperatures approximately 227°C (Watanabe & Otaka, 2006). The heat of devolatilization is considered almost negligible because the process is assumed to be energetically neutral (Watanabe & Otaka, 2006). At higher temperatures around 1527°C, volatile components are released from coal in a very short period of time (in milliseconds), (Lee et *al.*, 2011). The coal devolatilization process is assumed to be instantaneous and this temperature (above 1500°C) coincides with the peak temperature at which gasification reactions occur (Paul *et al*, 1991 and Biagini *et al*, 2009). When coal is heated up, it physically separates into four main components, as shown in Equation (3.1).

$$Coal = \alpha_1 FC + \alpha_2 VM + \alpha_3 M + \alpha_4 A \tag{3.1}$$

Where *FC*, *VM*, *M* and *A* are fixed carbon, volatile matter, moisture content and ash, respectively.α_i is the respective mass percentage composition. The simplest expression that is widely being used in modelling a devolatilization process is a first order overall reaction as given in Equation (3.2), correlating the kinetics of the volatile yields to the Arrhenius rate constant.

$$r_d = \sum_i k_{ij0}\, exp\left(-\frac{E_{ij}}{RT}\right)\left(V_{ij}^{*} - V_{ij}\right) \tag{3.2}$$

Where V_{ij}^{*} and V_{ij} are the ultimate volatile yied and volatile yield at any given time, respectively. r_d, k_{ij0}, E_{ij}, R, T are rate of devolatilization, pre-exponential factor, activation energy, universal gas constant and the temperature, respectively. In this current work, devolatilization will be treated as a physical process and therefore specific devolatilization

products determined from proximate analysis will be used at their ultimate yields. The minimum particle temperature will be assumed to be above slagging temperature.

3.2.2 **Homogeneous Gas Phase Kinetic Model**

The homogenous gas phase chemical reactions taking place inside the gasifier are mainly dominated by volatile combustion and water gas shift reactions. The volatile compounds present in coal are instantaneously released and subsequently combusted to supply the amount of heat required by endothermic gasification reactions. A number of kinetic models have been published in open literature with different levels of complexities. Modelling combustion reactions can be approached using elementary kinetic reactions which involve all the intermediate reactions and global kinetic reactions. Elementary kinetic reactions generally have a limitation in modelling because the information for all the intermediate chemical reactions steps is not always readily available. On the other hand, global kinetic model is the simplest model which has been widely used in the simulation and modelling environment for combustion reactions. Global kinetic model simulates the overall reaction rate by considering many chemical reactions. Westbrook and Dryer (1981) studied a number of hydrocarbon combustion reactions and published their global kinetic models and chemical reaction rate expressions and these reaction kinetics will be adopted in this work. Other global reactions kinetics used in this work were obtained from Jones and Lindstedt (1981), Bustamante *et al.* (2004) and Bustamante *et al.*, (2005). The reaction rate is expressed as a function of concentrations and rate constant as shown in Equation (3.3).

$$r_j = k_j C_a^x C_b^y \tag{3.3}$$

Where C_a and C_b are the reacting combustible and oxidizing reactants, respectively, and superscripts x and y are the respective reaction orders. The reaction rate constant, k_j is evaluated from Arrhenius equation as shown in Equation (3.4).

$$k_j = A_j exp\left(\frac{-E_{aj}}{RT_g}\right) \tag{3.4}$$

The values of the pre-exponential factors (A_j) and activation energies (E_{aj}) for the selected reactions are summarised in **Table 3.1**. The reacting components respective reaction rate orders (*x* and *y*) are shown in **Table 3.2**. The selected homogeneous phase reactions assume benzene to be the heaviest hydrocarbon present in coal. The reversible water gas shift reaction is treated as two separate chemical reactions for simplicity and this is in agreement with Chen *et al.*, (2000) who studied the water gas shift reaction and concluded that in an entrained flow reactor,

this reaction does not reach equilibrium. The combustion reactions are assumed to be occurring simultaneously on the combustion chamber of the gasifier giving out the energy required by the gasification endothermic reactions. It should also be noted that are more chemical reactions takes place in the gasifier with different kinetic models; however, this work will only focus on the reactions as summarized in **Table 3.1**.

Table 3.1: Homogeneous phase reaction kinetics

Reactions	$E_{a,j}$, (kJ/mol)	A_j $(m-s-kmol)$	*Reference*
$CH_4 + 2O_2 \rightarrow CO_2 + 2H_2O$	202.64	2.1100 x 10^{11}	Westbrook & Dryer (1981)
$C_2H_6 + 3.5O_2 \rightarrow 2CO_2 + 3H_2O$	125.6	3.9029 x 10^{10}	Westbrook & Dryer (1981)
$C_6H_6 + 7.5O_2 \rightarrow 6CO_2 + 3H_2O$	125.6	1.1247 x 10^{10}	Westbrook & Dryer (1981)
$CO + \frac{1}{2}O_2 \rightarrow CO_2$	168.0	2.2387 x 10^{13}	Westbrook & Dryer (1981)
$H_2 + \frac{1}{2}O_2 \rightarrow H_2O$	168.0	6.8000 x 10^{15}	Jones & Lindstedt (1981)
$H_2O + CO \rightarrow H_2 + CO_2$	288.3	2.3400 x 10^{10}	Bustamante *et al.* (2005)
$H_2 + CO_2 \rightarrow H_2O + CO$	190	2.200 x 10^{7}	Bustamante *et al.* (2004)

The first five reactions in **Table 3.1** shows the kinetic data for the combustion reactions of the volatile components that are present in coal while the last two reactions shows the water gas shift reaction presented as two separate chemical reactions.

Table 3.2: Homogeneous gas phase reaction orders

Reactions	x	y	Reference
$CH_4 + 2O_2 \rightarrow CO_2 + 2H_2O$	0.2	1.3	Westbrook & Dryer (1981)
$C_2H_6 + 2O_2 \rightarrow CO_2 + 2H_2O$	1.0	1.65	Westbrook & Dryer (1981)
$C_6H_6 + 7.5O_2 \rightarrow 6CO_2 + 3H_2O$	-0.1	1.85	Westbrook & Dryer (1981)
$CO + \frac{1}{2}O_2 \rightarrow CO_2$	1.0	1.25	Westbrook & Dryer (1981)
$H_2 + \frac{1}{2}O_2 \rightarrow H_2O$	0.25	1.50	Jones & Lindstedt (1981)
$H_2O + CO \rightarrow H_2 + CO_2$	0.5	1.00	Bustamante *et al.* (2005)
$H_2 + CO_2 \rightarrow H_2O + CO$	1.0	0.50	Bustamante *et al.* (2004)

3.2.3 **Heterogeneous Gas-Solid Reactions**

Heterogeneous solid-gas reactions are dominated by four major chemical reactions; *char-*O_2 combustion and gasification, *char-*H_2O, *char-*CO_2 gasification and *char-*H_2 gasification. Depending on the particle size and operating conditions, these reactions can assume three different types of limitations; chemical reaction, pore diffusion and boundary layer diffusion limitation (Biba *et al.*, 1978). Entrained flow reactors have the ability to process very fine coal particles in order to achieve high conversion at a very short residence time and this work will therefore assume that reactions are taking place on the surface of the particle and therefore only chemical reaction limitations will be adopted. Solid-gas reactions have been widely modelled, both as combustion reactions and as gasification reactions (Sundaresan and Amundson (1978), Johnson (1979), Wen and Chaung (1979) and Liu *et al.* (2000)). The reaction kinetics published in published literature does not show any significant variation, and therefore kinetics adopted by Wen and Chaung (1979), as shown in **Table 3.3**, will be used in the current work. The char-oxygen reaction produces both CO and CO_2 depending on the amount oxygen of present in the system. *Methanation* reaction only takes place at higher operating pressures (Guo *et al.*, 2007), however, this is a very important reaction as it produces CH_4, which has a relatively high calorific value but on the other hand, it consumes the present H_2 which has an even better heating value compared to CH_4 and CO.

Two modelling approaches have been adopted in the past when considering the solid-gas reactions, and these are; *Langmuir-Hinshelwood* and *n-order* type approaches. As discussed in Section 2, Langmuir-Hinshelwood is a very complex modelling approach and it involves three adjustable constants that vary from researcher to researcher. In this work, *n-order* type model which assumes chemical reaction limitation will be adopted as shown in Equation (3.5) (Biba *et al.* (1978) and Wen and Chaung (1979)).

$$r_k = ak_k P_a^n \tag{3.5}$$

Where a is the contact area between solid and gas per volume of the reactor, n is the order of the reaction, $P_a$is the oxidizing agent partial pressure and k_k is the reaction rate constant or the pre-exponential factor. Char surface area and porosity are a strong function of the operating conditions such as temperature, pressure and the heating rate, and these are important in determining the conversion of the char particle. A Random Pore Model (RPM) has been developed by Bhatia and Vartak (1996) to estimate or account for the loss of char surface area at different carbon conversion levels. In order to avoid modelling complexity, the RPM *factor* as shown in Equation (3.6) is used to account for the char type and conversion under prevailing reaction conditions

$$RPM_f = (1-x)\sqrt{\left(1 - \Psi_a ln(1-x)\right)} \tag{3.6}$$

Where x and Ψ_a are char conversion and structural parameter of the gasifying agent, respectively. The values of n and Ψ are shown in **Table 3.4.** The values of the structural parameters range from 3 to 14 (Kajitan *et al.*, 2002 and Sun *et al.*, 2012).

Table 3.3: Heterogeneous reaction kinetics

Reactions	***E*$_{a,k}$ *(J/mol)***	***A*$_k$ (kg/m^2.s.amt^n)**	***Reference***
$C + \phi O_2 \rightarrow 2(1-\phi)CO + (2\phi - 1)CO_2$	17,967	87100	Wen & Chaung (1979)
$C + H_2O \rightarrow CO + H_2$	21,060	2470	Wen & Chaung (1979)
$C + CO_2 \rightarrow CO + H_2$	21,060	2470	Wen & Chaung (1979)
$C + 2H_2 \rightarrow CH_4$	127,921	1.200	Wen (1968)

The first reaction in **Table 3.3** indiactes that there are are two possible products that are produced when char reacts with oxygen and those are carbon dioxide and monoxide, depending on the amount of oxygen present in the reaction.

Table 3.4: Heterogeneous reaction parameters

Reactions	***n***	**Ψ**	***Reference***
$C + \phi O_2 \rightarrow 2(1-\phi)CO + (2\phi - 1)CO_2$	1.00	14	Kajitan *et al.* (2002)
$C + H_2O \rightarrow CO + H_2$	1.00	3.0	Kajitan *et al.* (2002)
$C + CO_2 \rightarrow CO + H_2$	1.00	3.0	Kajitan *et al.* (2002)
$C + 2H_2 \rightarrow CH_4$	2.00	3.0	Lee *et al.* (2011)

According to Kajitani *et al.* (2002), the *n* values for H_2O and CO_2 *gasifications* are temperature dependent. In this current model, especially on the Optimization model, average values of these parameters will be used and a sensitivity analysis will be performed in order to quantify their impact on the overall performance of the model.

3.2.4 **Mathematical formulation**

The mathematical expressions of the plug flow reactor and gas turbine, describing the behaviour of the system under different input conditions, have been selected in published literature. The modelling platform used in this work, *g*PROMS, requires a successful simulation model before optimization on the model can be performed. The mathematical model formulation is, therefore, divided into three parts. The first and second parts focus on the simulation of the gasifier and the gas turbine, while the last part will centre on the optimization of the gasifier.

Entrained Flow Gasifier Simulation Model

The entrained flow gasifier has been modelled by a number of researchers as a PFR in different modelling platforms (Ruben *et al.*, 2007, Maxim *et al.*, 2010, Sofia *et al.*, 2012, Park *et al.*, 2015). Due to very steep temperature gradient and discontinuity between the completion of

combustion reaction and the commencement of gasification reactions at reactor, the gasifier was modelled using two reactor configurations, viz, the CSTR and PFR. The selected reactors are placed in series, with the CSTR first then the PFR, and all the feed goes to the first reactor. The CSTR only makes 5% of the total reactor volume and the 95% is the PFR. The mathematical model considers the mass balance, energy balance and pressure drop in both reactors. In this work global kinetics were adopted over elementary reaction kinetics for homogeneous gas-phase reactions. The elementary kinetic reactions generally have a limitation in modelling, because the information for all the intermediate chemical reaction steps is not always readily available.

There are two models generally used for modelling heterogeneous solid-gas reactions and these are Langmuir-Hinshelwood (Klose and Wolki, 2005, Roberts and Harris, 2006, Boreto *et al.*, 2013) and the *n*-order models (Tremel and Spliethoff, 2013, Lee *et al.*, 2014). *n*-order modelling has been selected for this work because of its simplicity and the available reaction kinetics data. Although this is a simplified model, the accuracy is not lost and *n*-order models have been widely used in solid-gas reaction modelling (Vamvuka *et al.*, 1995, Watanabe and Otaka, 2006, Xu and Qiao, 2012). The mass balances of the homogeneous gas-phase and heterogeneous solid-gas phase reactions are shown in Equations (3.7) and (3.8) respectively. The full derivations of these equations are widely published in *Chemical Reaction Engineering* texbooks such Fogler (1999) and Levenspiel (1999) and also as shown in the Appendix.

$$\frac{d\dot{m}_{gi}}{dL} = A_c \sum_{j=1}^{n} \nu_{ij} r_j(T_g, L) + aA_c Mw_i \sum_{k=1}^{m} \nu_{ki} \frac{r_k(T_p, L)}{Mw_c} \tag{3.7}$$

$$\frac{d\dot{m}_c}{dL} = aA_c \sum_{k=1}^{m} r_k(T_p, L) \tag{3.8}$$

Where *j* refers to homogeneous gas phase reactions, *k* refers to solid-gas reactions and *i* is gaseous component in the gas mixture. The gaseous components take part in both homogenous gas phase and heterogeneous solid-gas phase reactions and their generation and consumption is described by Equation (3.7). The first term of the right hand side of Equation (3.7) refers to the gaseous component consumption/generation in combustion reactions while the second term refers to the gaseous component consumption in the gasification reactions. Equation (3.8) describes the mass of the particle or carbon ($\dot{m}_c$) as a function of temperature (T_P) across the

length of the reactor (L). a in Equations (3.7) and (3.8) is the contact surface area of the particle per reactor volume and it is calculated using Equation (3.9), (Wen and Chaung (1979).

$$a = \frac{\dot{m}_c}{A_R v_s}\left(\frac{6}{\rho_p D_p}\right) \tag{3.9}$$

Where $\dot{m}_c$, ρ_p, D_p, v_s is the mass flowrate, density, diameter and velocity of coal or char particle and A_R is the cross-sectional area of the gasifier. The chemical reaction rate expressions for both set of reactions are shown in Equations (3.10) and (3.11).

$$r_j = A_j exp\left(\frac{-E_{aj}}{RT_g}\right) C_a^A C_b^B \tag{3.10}$$

C_a is the concentration of the combustible component, C_b is the concentration of the oxidizing agent in the combustion reaction and the superscripts *A* and *B* are the respective reaction orders. E_{aj} and T_g are the activation energy of the respectively chemical reaction and gas temperature, respectively.

$$r_k = A_k exp\left(\frac{-E_{ak}}{T_p}\right) P_a^n (1 - X_C)\sqrt{1 - \Psi_k \ln(1 - X_C)} \tag{3.11}$$

X_C is the carbon conversion and Ψ_k is the structural parameter, which is based on the gasifying agent and operating temperature (Watanabe and Otaka, 2006). P_a is the partial pressure of the gasifying agent and *n* is the respective reaction order.

Similar to the mass balance model, the energy balance is also formulated using the PFR modelling assumptions. The model only considers two modes of heat transfer in the energy balance. Radiation heat transfer between particle and gas, gas and wall and particle and wall and convection heat transfer between particle and gas and gas-wall have been considered. The model also assumes that the particle and gas exists at different temperatures, and heat transfer is from the particle to the bulk gas. The respective energy balances for gas phase and particles are shown in Equations (3.12) and (3.13), respectively.

$$\dot{m}_g \frac{d\hat{H}_g}{A_R dL} + \dot{q}_{gp,c} + \dot{q}_{gp,r} + \dot{q}_{gw,c} + \dot{q}_{gw,r} = 0 \tag{3.12}$$

$$\dot{m}_p \frac{d\hat{H}_p}{A_R dL} - \dot{q}_{gp,c} - \dot{q}_{gp,r} + \dot{q}_{pw,r} = 0 \tag{3.13}$$

Equations (3.12) and (3.13) indicate that only convection and radiation heat transfer are considered, where subscripts *c* and *r* represent convection and radiation respectively. The subscripts pg and gw mean the heat transfer from the particle to the gas and heat transfer from gas to the walls of the reactor, respectively. The particle-gas radiation and convection heat

transfer terms in Equations (3.12) and (3.13) are calculated as shown in Equations (3.14) and (3.13) respectively.

$$\dot{q}_{pg,r} = a\varepsilon f\sigma\left(T_p^4 - T_g^4\right) \tag{3.14}$$

$$\dot{q}_{pg,h} = ah_{pg}\left(T_p - T_g\right) \tag{3.15}$$

Where ε, σ and f are the emissivity, Stefan's Boltzman's constant and view factor respectively. T_p and T_g are temperatures of the particle and gas, respectively while h_{pg} is the heat transfer coefficient between the particle and gas. The heat transfer by radiation and convection between particle and wall and between gas and wall are determined in Equations (3.16) to (3.18).

$$\dot{q}_{pw,r} = \frac{4}{D_R}\varepsilon f\sigma\left(T_p^4 - T_w^4\right) \tag{3.16}$$

$$\dot{q}_{\mathrm{gw.h}} = \frac{4}{\mathrm{D_R}}\mathrm{h_{gw}}\left(\mathrm{T_g} - \mathrm{T_w}\right) \tag{3.17}$$

$$\dot{q}_{\mathrm{gw,r}} = \frac{4}{D_R}\varepsilon\sigma f\left(T_g^4 - T_w^4\right) \tag{3.18}$$

D_R is the internal diameter of the reactor or gasifier and T_W is the wall temperature of the gasifier. The heat transfer coefficients between particle and gas (h_{pg})and between gas and wall (h_{gw}) are calculated using Equations (3.19) (Ranz and Marshall, 1952) and (3.20) (Babcock and Wilcox, 1978) respectively.

$$h_{pg} = \frac{Nu\ k_g}{D_p} \tag{3.19}$$

$$h_{gw} = \left(0.023\frac{\dot{G}^{0.8}}{D_R^{0.2}}\right)\left(\frac{C_{pg}^{0.4}k_g^{0.6}}{\mu_g^{0.4}}\right)\left(\frac{T_g}{T_w}\right)^{0.8} \tag{3.20}$$

Where $\dot{G}$ is gas flux, D_R is the internal diameter of the gasifier and D_p is the particle diameter. The term $\widehat{H}_g$ and $\widehat{H}_p$in Equations (3.12) and (3.13) is the enthalpies of the gas and particle, respectively and they are defined by Equations (3.21) and (3.22). *g*PROMS allows for the implicit determination of the gas phase enthalpy at a given temperature, pressure and composition.

$$H_g = f\left(T_g, P, y_i\right) \tag{3.21}$$

$$dH_g = \left(\frac{\partial H}{\partial T}\right)_{P,n_i} dT + \left(\frac{\partial H}{\partial P}\right)_{T,ni} dP + \sum\left(\frac{\partial H}{\partial n_i}\right)_{T,P,n_k} dn_i \tag{3.22}$$

$$H_p = \int_{T_{p_in}}^{T_p} (-0.218 + 3.807 \times 10^{-3} T_p - 1.758 \times 10^{-6} T_p^2) dT_p \qquad (3.23)$$

The enthalpy of the particle (H_p) is evaluated using a correlation by Eisermann and co-workers (Eisermann *et al.*, 1980) as shown in Equation (3.23). T_{p_in} is the particle temperature at the inlet of the reactor and $T_p$is particle temperature at any given point in the reactor. The gas heat capacity, viscosity and thermal conductivity are calculated implicitly from *g*PROMS. The pressure drop across the length of the gasifier was calculated from the Ergun expression as shown in Equation (3.24).

$$\frac{dP}{dL} = \frac{G}{\rho g_c D_p}\left(\frac{1-\Phi}{\Phi^3}\right)\left[\frac{150(1-\Phi)\mu}{D_p} + 1.75G\right] \qquad (3.24)$$

Where ρ, G, D_p and Φ are the gas density, superficial mass velocity, particle density and void fraction, respectively.

Gas Turbine Simulation Model

The gas turbine was divided into its subcomponents; compressor (*K*), combustor (*F*) and expander (*X*) as shown in **Figure 3.1**. Air ($\dot{m}_{air}$) from the atmosphere is compressed into the required pressure of the combustion chamber of the gas turbine. The fuel gas ($\dot{m}_{FG}$) from the gas cleaning plant is also compressed and transported to the combustion chamber. N_2 ($\dot{m}_{N_2}$) and steam ($\dot{m}_S$) are added to lower the flame temperature and reduce the formation of NO_x. The produced flue gas is passed through an expander where power is generated. The exhaust gas ($\dot{m}_{Exhaust}$) is passed through a HRSG to produce steam which is then sent to the steam turbine to generate even more power. The combustor is treated as a conversion reactor and 99% conversion of the fuel gas is assumed. A single stage axial compressor was assumed.

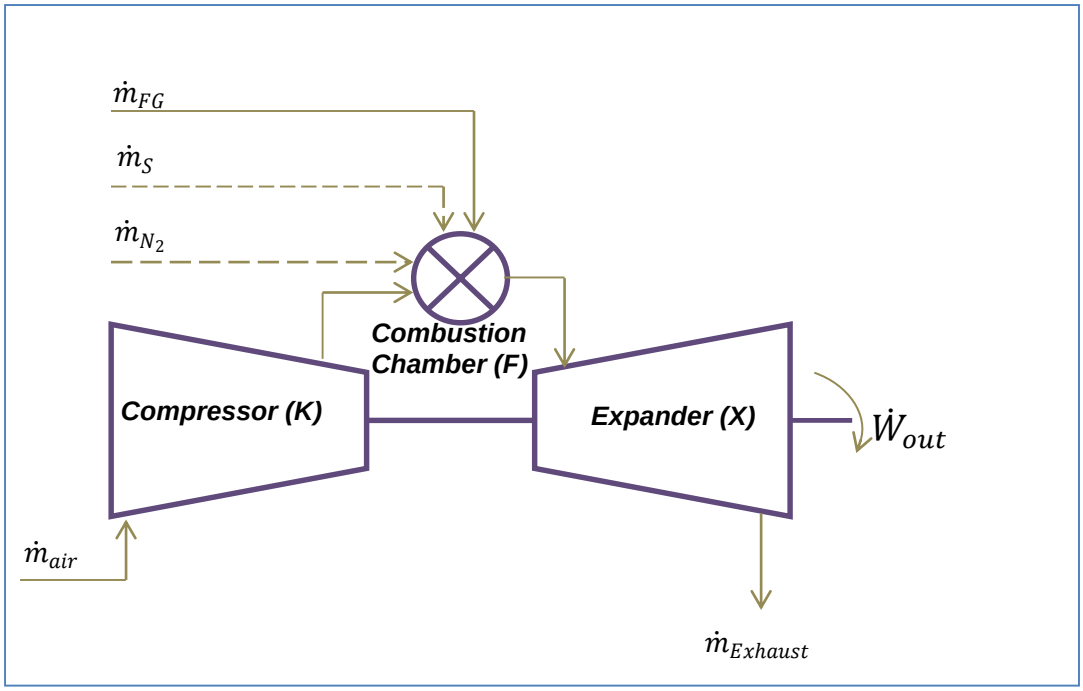

Figure 3.1: Gas turbine unit

The compressor and the turbine are connected by a shaft and the net power produced by the expander is the difference between the total work produced and work required to drive the compressor.

The gas turbine unit was modelled as an open cycle gas turbine. The mass and energy balance of the compressor (*K*) are shown in Equations (3.25) and (3.26), respectively.

$$\dot{m}_{K_in} = \dot{m}_{K_out} \tag{3.25}$$

$$\dot{W}_K = \frac{\dot{m}_{K_in} Cp_{air} (T_{amb} - T_{K_out,is})}{\eta_{K,is}} \tag{3.26}$$

Where $\dot{m}_{K_in}$ and $\dot{m}_{K_out}$ are the inlet air flowrates into and out of the compressor with subscripts *in* and *out* denoting the inlet and outlet of the compressor, respectively. T_{amb} and $T_{K_out,is}$ are the ambient temperature and ideal temperature discharge. The actual and the ideal discharge temperatures of the compressor are given by Equations (3.27) and (3.28) respectively.

$$T_{K_out} = T_{amb} + \frac{(T_{K_out,is} - T_a)}{\eta_{K,is}} \tag{3.27}$$

$$T_{K_out,is} = T_{amb} r_K^{\frac{k-1}{k}} \tag{3.28}$$

T_{K_out}, $T_{K_out,is}$, $\eta_{K,is}$, k, r_K are actual compressor discharge temperature, ideal discharge temperature, isentropic efficiency, the compression specific heat capacity ratio, and the pressure ratio, respectively. The heat capacity of air is obtained from Multiflash via CAPE-

OPEN. The combustion of the fuel gas in the gas turbine assumes only three chemical reactions, i.e., the complete combustions of H_2, CO and CH_4. The model formulated in this work does not consider the gas cleaning unit and assumes that the fuel gas primarily consists of H_2, CO and CH_4. The mass balance across the combustion chamber (*F*) is determined from Equations (3.29) and (3.30).

$$\dot{m}_{F_in} = \dot{m}_{FG} + \dot{m}_S + \dot{m}_{air} + \dot{m}_{N_2} \tag{3.29}$$

$$\dot{m}_{F_out} = \sum_i \left(\dot{m}_{F_in,i} + \sum_j^n \frac{\nu_{ji} X_f \dot{m}_{F_in_i}}{\nu_{ji'}} \right) \tag{3.30}$$

X_f is the conversion of the fuel gas in the combustion chamber of the gas turbine and $\nu_{ji'}$ is the stoichiometric coefficient of the respective fuel gas component i' (CH_4, CO and H_2) in the combustion reaction *j*, while ν_{ji} is the stoichiometric coefficient of other gaseous component *i* taking part in the combustion reaction *j*. $\dot{m}_{F_in}$ and $\dot{m}_{F_out}$ are the inlet and outlet mass flowrates of the combustion chamber, respectively. The subscripts *FG*, *S* and N_2 in Equation (3.29) refer to fuel gas, steam and nitrogen, respectively. The energy balance in the combustion chamber assumes no heat losses and is given by Equation (3.31).

$$\sum_i^n \dot{m}_{F_in,i} \widehat{H}_{F_in,gi} - \sum_i^n \dot{m}_{F_out,i} \widehat{H}_{F_out,gi} = 0 \tag{3.31}$$

Where subscripts *in* and *out* refer to the inlet and outlet streams of the combustion chamber, respectively. The enthalpies of the gases $\widehat{H}_{Fgi}$ are obtained from Multiflash via CAPE-OPEN. The mass and energy balance across the expander (*X*) is shown in Equations (3.32) and (3.33), respectively.

$$\dot{m}_{X_in} = \dot{m}_{X_out} \tag{3.32}$$

$$\dot{W}_X = \dot{m}_{X_in} C_{p,fg} \left(T_{X_in} - T_{X_out} \right) \tag{3.33}$$

$\dot{W}_X$ is the total power produced by the expander and T_{X_out} is the actual expander outlet temperature which is calculated from Equation (3.34) and where the expander efficiency, $\eta_{t,is}$, is calculated using Equation (3.35).

$$T_{X_out} = T_{X_in} - \eta_{t,is} \left(T_{X_in} - T_{X_out_is} \right) \tag{3.34}$$

$$\eta_{t,is} = \frac{T_{X_in} - T_{X_out}}{T_{X_in} - T_{X_out,is}} \tag{3.35}$$

$\eta_{t,is}$ is the turbine isentropic efficiency and $T_{X_out_is}$ is the ideal exit temperature from the gas turbine. In the gas turbine flowsheet, the mass flowrate exiting the compressor is the total air required in the combustion chamber. The flue gas leaving the combustion chamber is the total flowrate to the expander.

3.3 **Gasifier flowsheet and key modelling assumptions**

The process flowsheet of the gasifier model in *g*PROMS is shown in **Figure 3.2** The equation orientated flowsheet is built in *g*PROMS (ModelBuilder 4.0.0) platform and Multiflash 4.3 for Windows is only used to obtain the thermodynamic data of the gases involved. Coal particle data such as proximate and ultimate analysis, density and enthalpy correlations are obtained from various sources and are input or hard-coded on the flowsheet.

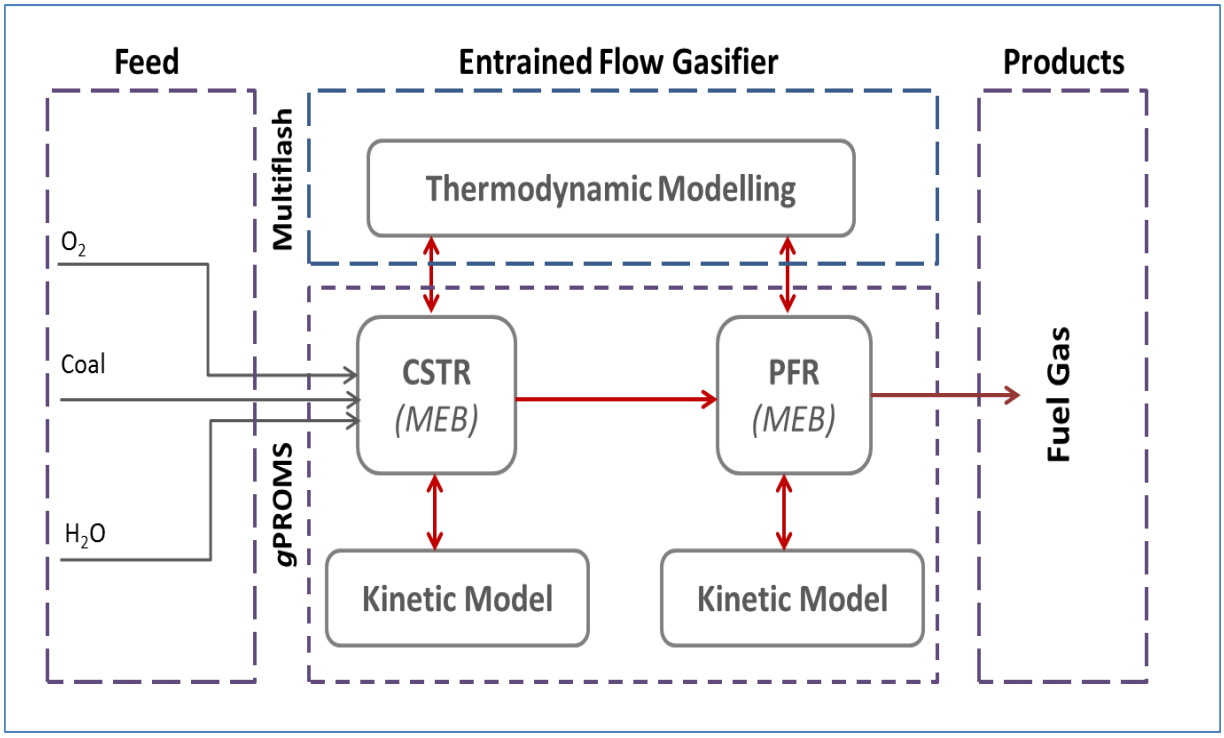

Figure 3.2: Gasifier model process flowsheet

This model has been formulated based on a Plug Flow Reactor configuration, and therefore it will adopt all the assumptions that are used for PFR modelling. Due to very steep temperature gradient and discontinuity between the completion combustion reaction and the commencement of gasification reactions at reactor, the gasifier was modelled using two reactor configurations, viz, the CSTR and PFR. The selected reactors are placed in series, with the CSTR first then the PFR, and all the feed goes to the first reactor. The CSTR only makes 5% of the total reactor volume and the 95% is the PFR. A co-current entrained flow coal gasifier, as shown in Figure 2.8 (a), emulates a Plug Flow Reactor (PFR) arrangement.

The combination of a Continuous Stirred Tank Reactor (CSTR) and PFR was chosen because of difficulty of the modeling platform (gPROMS) in handling the discontinuity in temperature

profile between combustion peak temperature and beginning of an endothermic gasification process. This was found to be appropriate because PFR can also be modeled as multiple CSTRs. The 5%:95% split was determined from combustion peak temperature. Design Equations of CSTR and PFR were therefore applied on the *Combustion* and *Gasification* zones, respectively. The arrangement was also found to be best representing the actual gasifier operation, since the beginning starts with combustion process which best fit the CSTR (throught well mixing and tuburlant at the burner-mount) and then followed by the endothermic gasification reactions. It must also be emphasized that the sequencing of reactors does not entail sequencing of chemical reactions, i.e., combustion reactions only put in the CSTR and gasification reactions on the PFR. The entire chemical reaction scheme is included in both reactors

The published gasification models indicate that the gasifier operates at the extreme conditions, with the gasifier peak temperature of over 2673K and the exit temperature sometimes above 1723K (Tremel and Spliethoff, 2013). Obtaining thermodynamic data such as heat capacity and enthalpy data, from reliable process simulators such as AspenPlus and Multiflash is very crucial to the model accuracy. On the other hand, data provided in handbooks is sometimes limited to certain temperatures for some properties, therefore, may require extrapolation in the region of interest, which could result in compromising the accuracy of the model performance. The enthalpy of the gas, for example, is evaluated implicitly in gPROMS according to Equations (3.21) and (3.22). Similar data for gases such as specific heat capacity, density, viscosity and thermal conductivity can be obtained implicitly on *g*PROMS-Multiflash via CAPE-OPEN.

Literature describes three possible zones when coal is being combusted or gasified. Zone I correspond to reactions taking place throughout the pores of the particle and disregard the mass transfer limitations, Zone II takes into account of the mass transfer and kinetic limitations, while Zone III assumes that the chemical reaction rates are limited by the mass transfer in the boundary layer and that the reactions are taking place on the surface of the particle. In this current work, due to very fine particles considered for the entrained flow reactor, Zone III will form basis of the model. The lists of all the assumptions adopted for a simulation model are summarized below and are divided into mass and energy assumptions.

3.3.1 **Mass balance assumptions**

The basic assumptions for the two reactor configurations have been adopted in the model formulation and these together with other assumptions are summarized below.

(i). There is complete mixing in radial direction of the gasifier.

(ii). The material flow in and out of the gasifier is at steady state.

(iii). The fluid velocity only changes in the axial direction.

(iv). The system is considered to be dilute, and therefore, particle-to-particle collusion is negligible.

(v). There are no tars present in the product gas due to the fact that the gasifier operates at very high temperature, and therefore, the tars will crack or thermally decompose to form light gases.

(vi). The char-gas reactions are considered to be taking place on the surface of the particle, and this is because of the small particle size and high temperature inside the gasifier (Simon, 1984 and Liu *et al.*, 2001).

(vii). All gas-phace chemical reactions are irreversible.

(viii). There is no effect of turbulence on the reactions taking place on the gasifier.

(ix). Coal decomposition takes place in a one step mechanism, $coal \rightarrow char + volatiles$.

(x). Pyrolysis, heterogeneous and homogeneous reactions are only reactions on the gasifier.

(xi). The gas and solid particle velocities are the same (Littlewood, 1977) – small coal particles and high gas velocity

(xii). The chemical reactions taking place inside the gasifier are not in equilibrium (Ma and Zitney, 2012).

(xiii). Syngas only consists of Carbon Monoxide, Hydrogen and Methane gases.

(xiv). Ash does not remain on the reacting coal particles.

(xv). The overall particle-gas reaction rate is proportional to the *n*th power of partial pressure of the gasifying agent and follows Arrhenius equation, (Lee et *al.*, 2011)

(xvi). Char-gas reactions are irreversible and proceed in parallel (Vamvuka *et al.*, 1995).

(xvii). The flow of coal and gasifying agents and product gases generated will be treated as a co-current two-phase flow inside the gasifier.

3.3.2 **Energy Balance Assumptions**

(i). There is no radial variation in gasifier operating temperature

(ii). The energy input and output around the gasifier is at steady state.

(iii). The gasifier wall temperature remains constant as a result of continuous steam generation though gasifier cooling.

(iv). The convection heat transfer coefficients for both particle-gas and gas-wall are a function of temperature.

(v). The particle and gas exist at different temperatures inside the reactor.

(vi). Heat transfer is from particle to the gas.

(vii). The energy into and out of the system is at steady state.

3.4 **Modelling Platform**

3.4.1 ***g*PROMS**

A state-of-the-art modelling tool called *g*eneral *Pro*cess *M*odelling *S*ystems (*g*PROMS – version 4.0.0) will be used to solve the Differential Algebraic Equations (DAE) resulting from mass and energy equations developed above. This tool has the ability to carry out Simulation, Optimization and Parameter Estimation. *g*PROMS has no limit to problem size, unparalleled power for modelling and it can handle dynamic simulation of models with over *100, 000* Differential-Algebraic Equations. Operating procedures can be incorporated into the model and process discontinuities can also be accommodated in this tool. More information about the capabilities of *g*PROMS can be found on the platform manuals, which comes with the software and available on the *Documentation Section* (PSE, 2012).

3.4.2 **Multiflash**

Multiflash is a powerful and versatile system for modelling physical properties and phase equilibria which could be used as a stand-alone program or could be interfaced with other software. It is currently offered by *Infochem Computer Services Ltd* which is based in London. Multiflash for Windows (version 4.1) will be used as a *Physical Property Package* to determine the thermodynamic properties of all the components except for Coal, with Peng Robinson used as an Equation of State. Physical and chemical properties of coal have been obtained from various sources in literature. A User Guide for Multiflash for Windows is also available for more information about system (Infochem Computer Services, 2012).

3.5 **Optimization Model**

As aforementioned, the primary aim of the present work presented is to establish whether the extreme conditions in which the gasifier is generally operated are the optimum conditions for maximum fuel gas heating value. The secondary objective is to develop a gas turbine model and couple it with the gasifier model and perform the overall optimization of the system. The modelling tool used in this work requires a simulation model to be built first and then be optimized. The optimization model is focusing on the key operating conditions such as temperature and pressure, and the *objective function* is maximizing the heating value of the syngas. The Equations (3.36) to (3.42) summarize the formulation of the optimization model. The objective function for the optimization model is to maximize the heating value of the syngas as shown in Equation (3.36). Based on the assumption that there are no tars present in the fuel gas, the primary combustibles in the gasifier product gases are CH_4, CO and H_2. The objective function to be maximized therefore becomes:

$$Maximize\ HV_{FG} = \sum_i x_i HV_i \tag{3.36}$$

This is subject to the following constraints:

$$T_g \leq T_{MAWT} \tag{3.37}$$

$$P_R \leq P_{MAWP} \tag{3.38}$$

$$T_{g,min} \geq T_{AFT} \tag{3.39}$$

$$\sum_i^n x_i = 1 \tag{3.40}$$

$$x_i \geq 0 \tag{3.41}$$

$$X_c < 0.9999 \tag{3.42}$$

$$R_{min} \leq R_{CO/H_2} \leq R_{max} \tag{3.43}$$

In Equation (3.36), x_i is the mass fraction of the contributing gaseous component on the fuel gas heating value and HV_i is the respective heating value of that particular gas component. x_i , which is function of temperature, is determined from the mass and energy balance of the system while HV_i is a constant obtained from literature. T_{MAWT} and P_{MAWP} are the maximum allowable working temperature and pressure, respectively, and they are the design constraints of the gasifier. The ratio of CO-to-H_2 (R_{CO/H_2}) is an optional constraint used in case the gas turbine manufacturers specify the required ratio. The carbon conversion X_C, not exceeding 99.99% in Equation (3.42), is a feasibility constraint owing to the logarithmic term in Equation (3.11).

3.6 **Gasifier Performance**

The performance of a gasifier yield depends mainly on the fuel-to-oxidising agent ratio, operating temperature, particle size and operating pressure. There are two main indicators that are used to measure the performance of the gasifier and these are carbon conversion and cold-gas efficiency as shown in Equations (3.44) and (3.45) respectively.

$$X_c = \left(1 - \frac{C_{GR}}{C_f}\right) x\ 100 \tag{3.44}$$

$$\eta_{cg} = \left(\frac{1}{HV_c}\sum_{i=1}^{n} x_i HV_i\right) x\ \ 100 \tag{3.45}$$

Where C_{GR} and C_f are the amounts of carbon in the gasification residue and in the feedstock, respectively. η_{cg}refers to cold gas efficiency while HV_c refers to the heating value of coal fed into the reactor and HV_i is the heating value of the gaseous species in the product fuel gas. The above indicators are a strong function of the gasifier feedstock, operating temperature and as well as particle size. Another method of calculating the carbon conversion and the cold gas efficiency has also been provided by Xu *et al.* (2014) as shown in Equations (3.46) and (3.47) respectively.

$$\eta_{cg} = \frac{(283[CO] + 888[CH_4] + 286[H_2])\ x\ Q}{F\ x\ SE} \tag{3.46}$$

$$X_C = \frac{\left(m_{CO} + m_{CO_2} + m_{CH_4}\right) x\ 12}{m_{C,feed}} \tag{3.47}$$

The syngas concentrations in Equation (3.46) are on the molar basis (*mol/m*^{3}), the constants (prefixes) are their respective heat of combustion (*MJ/mol*), Q is the normal volumetric flow rate of the fuel gas (*m*^{3}*/hr*), *SE* is the calorific value of the coal fed to the reactor (*MJ/kg*) and *F* is the feed rate of the coal (*kg/hr*). The $m_i$in the numerator of Equation (3.42) is the molar flow rates of the gas species (*kmol/hr*) in the product gas while the denominator is the mass of carbon (*kg/hr*) in the feed.

3.7 **Solution Procedure**

The *g*PROMS modelling platform requires successful simulation of the model before optimization can be performed. The solution procedure for the model is shown in **Figure 4**.

Realistic initial data such as oxygen-to-coal and steam-to-coal ratios have to be obtained from literature. The model also requires input such as proximate and ultimate analysis of coal. At a given oxygen-to-coal ratio, steam-to-coal ratio, inlet temperature and inlet pressure, an estimated combustion zone outlet temperature (flame temperature) has to be made to start the simulation. This process can be repeated until the simulation model converges after solving both combustion and gasification zones. The simulation variables such as simulation fuel gas heating value ($FG_{HV,sim}$), exit temperature, gas composition and conversion are then obtained. The simulation fuel gas heating value is then recorded to be later compared against the optimum fuel gas heating value ($FG_{HV,max}$) that will be obtained during optimization. Other variables such as exit temperature, pressure, steam-to-coal ratio and oxygen-to-coal ratio are used as initial guesses for the optimization model.

The optimization model then commences with the setting of the objective function, which is maximizing fuel gas heating value. The optimum fuel gas heating value is determined by varying the decision variables such as oxygen-to-coal, steam-to-coal ratios, particle size and the inlet pressure to the gasifier while satisfying the design constraints. The obtained optimum fuel gas heating value is then compared against the simulated fuel gas heating value. If the absolute difference between the optimum fuel gas heating value and simulation fuel gas heating value is less than the specified tolerance, the process will stop, indicating optimal solution. If the difference is, however, greater than the tolerance, the process will be repeated until the error is within the tolerances. The simulation uses Backward Finite Differentiation Method together with solvers such as DASOLV for differential equations, LASOLVER (*M48*) for linear algebraic equations, and NLSOLVER for nonlinear equations based on Block Decomposition (BDNLSOL). Optimization is performed using Continuous Vector Parameterization Single Shoot (CVP_SS).

The optimization is only performed on the gasifier where the objective function is set. The produced fuel gas undergoes combustion in the gas turbine to produce power. The gas turbine has no decision variable and it has only one constraint, the expander inlet temperature. This constraint can be satisfied with extraction air, steam or nitrogen which helps in controlling the expander inlet temperature to within design limits.

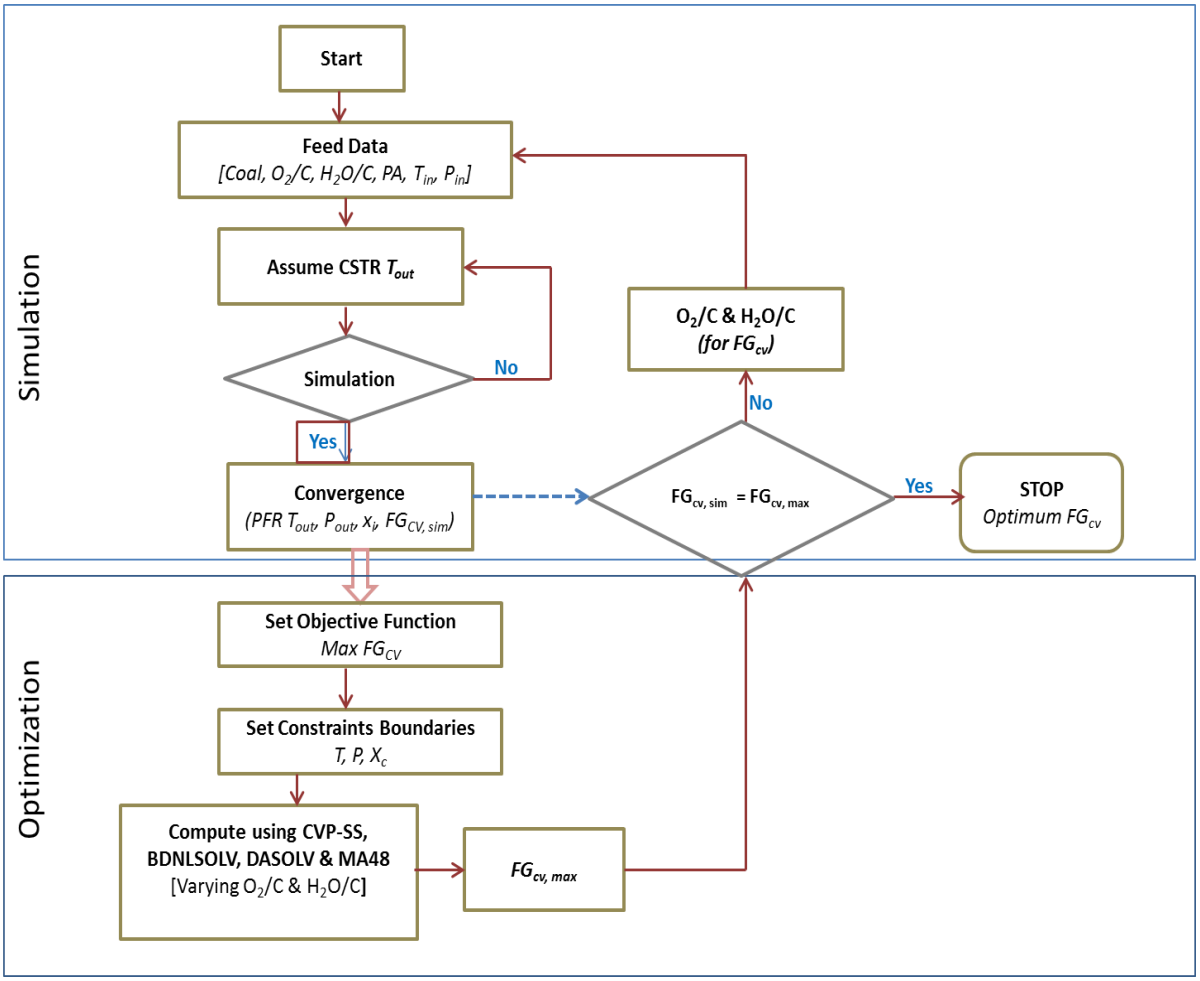

Figure 3.3: Mathematical model solution procedure

The mathematical structure of the model consists of the exponential and bilinear terms thus rendering the model a Nonlinear Programming (NLP) problem. The search for the maximum fuel gas heating value was conducted at the outlet of the gasifier, using steady state optimization.

Reference

Anderson, B., Blatchford, A., Stephanou, T., *Improvements in integrated drying gasification and gas scrubbing and recycle steps*. Australia: HRL Treasury IDGCC Pty Ltd, 2012

Babcock and Wilcox. *Steam: Its generation and use*, Babcock and Wilcox Company, New York, 1978

Babushok, V. I., and Dakdancha, A. N., *Global Kinetic Parameters for High Temperature Gas-Phase Reactions*, Plenum Publishing Corporation, 1994

Badzioch, S., Hawksley, P. G., *Kinetics of Thermal Decomposition of Pulverized Coal Particles*. Ind. Eng. Chem. Process Des. Dev, 1970, 9(4), 521

Biba, V., Marak, J., Klose E. and Malecha J., *Mathematical Model for the Gasification of Coal Under Pressure*, Ind. Eng. Chem. Process Des. 1978, Vol. 17

Chen, C., Horio, M. and Kojima T., *Numerical simulation of entrained flow coal gasifier. Part I: modelling of coal gasification in an entrained flow gasifier*, Chemical Engineering Science, 2000

Fogler, H. S, *Elements of Chemical Reaction Engineering, Third Edition*, Prentice-Hall Internation, Inc, 1999

Howard, J.B., Williams, G. C. and Fine, D. H., *Kinetics of carbon monoxide oxidation in postflame gases*, 1973

Infochem Computer Services, *User Guide for Multiflash for Windows* (Version 4.1), February 2012

Jones, W.P, Lindstedt, R.P, *Global Reaction Scheme for Hydrocarbon Combustion*, Combustion and Flame, 1988

Kajitani, S, Hara, S, Matsuda H, Fuel 2002, 81:539

Kobayashi, H., Howard, J. B., Sarofim, A. F., *Coal devolatilization at high temperatures, 18th Symposium (International) on Combustion*, The Combustion Institute: Pittsburgh, PA, 1977, Vol. 16, 411-425

Lee, H., Choi, S. and Paek, M. *A simple process modelling for a dry-feeding entrained bed coal gasifier*, Proc. IMechE Vol. 225 Part A: J. Power and Energy, 2011

Levenspiel, O., *Chemical Reaction Engineering*, Third Edition, John Wiley & Sons, 1999

Liu, X. J., Zhang, W. R., and Park, T. J. *Modelling coal gasification in an entrained flow gasifier*. Combust. Theory Modelling, 2001, 5, 595-608

Ma, J. and Zitney, S. E. *Computational Fluid Dynamic Modeling of Entrained-Flow Gasifier with Improved Physical and Chemical Submodels*. Energy & Fuels, 2012

Miura, K. and Silverton, L. P., *Analysis of Gas-solid Reaction by use of a Temperature-programmed Reaction Technique*, Energy & Fuels, 1989, Vol. 3, 243-249

Process Systems Enterprise, *gPROMS ModelBuilder Guide* (Release v3.6.0), October 2012

Qiao, L., Xu, J., Sane, A., Gore, J. *Multiphysics modelling of carbon gasification processes in a well-stirred reactor with detailed gas-phase chemistry*. Combustion and Flame, 2012, 159, 1693-1707

Ranz, W. E., and Marshall, W. R., *Evaporation from drops, Part II*, Chemical Engineering Progress, 1952, 48, 173

Silaen, A. and Wang, T. *Investigation of the coal gasification process under various operating conditions inside a two-stage entrained flow gasifier*. Proceeding of the 27th International Pittsburgh Coal Conference, Instanbul, Turkey, October 11-14, 2010

Tomeczek, J. Coal Combustion, Krienger Publishing Company, Florida, 1994

Vilenskii, T. V. and Izmalyan, D. M., *Pulverized Fuel Combustion Dynamics (in Russian)*, Energiya, Moscow, 1978

Wen, C. Y., *Noncatalytic heterogeneous solid fluid reaction models*, Ind. Eng. Chem., 1968

Westbrook, C. K., and Dryer, F. L., *Simplified reaction mechanisms for oxidation of hydrocarbon fuels in flames*, Combust. Sci. Technol., 1981

Xu, J. and Qiao, L. *Mathematical Modeling of Coal Gasification Process in a Well-Stirred Reactor: Effect of Devolatilization and Moisture Content*. Energy & Fuels, 2012

Xu, S., Ren, Y., Wang, B., Xu, Y., Chen, L., Wang, X., Xiao, T., *Development of a novel 2-stage entrained flow dry powder gasifier*, Applied Energy, 2014

4. Case Studies

In chapter III of this dissertation, a one-dimensional steady state simulation model was formulated under detailed assumptions. The model was solved in general Process Modelling and Simulation (*g*PROMS 4.0.0) platform, with Multiflash for Windows used for thermodynamic properties. This chapter will now focus in comparing the developed simulation model against other published simulation models to establish its validity and accuracy. The model validation will also be extended in to predicting the performance of Elcogas power plant. It will then be subsequently optimized to establish if there exist less severe conditions that could result in the highest possible fuel gas heating value. The performance indicators that were considered crucial were fuel gas composition, gasifier peak temperature, exit fuel gas temperature, conversion and fuel gas heating value.

4.1 Entrained Flow Reactor Model

The reactor model developed in this work assumed a continuous stirred tank reactor (CSTR) and a plug flow reactor (PFR) arranged in series. The CSTR was used to model the combustion (flame) zone of the gasifier while the PFR modelled the reduction (gasification) zone of the gasifier. The formulated model was compared against 1-D mathematical models, simulation model developed using commercial packages like Aspen Plus and industrial data of a physical plant. Two mathematical models have been chosen for validation, and these are, the models developed by Vamvuka *et al*. (1995) and Lee *at al*. (2011). A process simulation model of the Elcogas power plant using Aspen Plus version 7.2 developed by Sofia *et al.* (2012) was also used for validation. The last validation was focusing on the industrial published data of the PRENFLO gasifier of Elcogas.

4.1.1 Modelling of an entrained flow gasifier (Vamvuka *et al.*, 1995)

Vamvuka *et al.* (1995) developed a one dimensional, steady-state model for an entrained flow coal gasifier based on mass and energy balances. Their model was solved using a modified Euler method in conjuction with a non-linear algebraic equation solver. The gasifier performance was predicted at low to moderate pressures and constant throughputs. The volatiles presents in coal were assumed to be only CH_4, CO and H_2O in proportions of 2:1:1 and the gas-phase reactions were assumed to be in equilibrium. The parameters for the basis of

comparison are provided in **Table 4.1** and the detailed comparison of the two models is shown in **Table 4.2**.

Table 4.1: Feed data of the gasifier

Parameter	Units	Value
Steam/coal ratio	*kg/kg*	0.20
Oxygen/coal ratio	*kg/kg*	0.80
Feed gas temperature	*K*	630.00
Gasifier pressure	*MPag*	2.00
Gasifier internal diameter	*M*	1.50
Gasifier external diameter	*M*	1.53
Emissivity of wall	-	0.78

It is important to note that a better prediction of a model is a strong function of the chemical reactions selected to model the system, the modelling assumptions undertaken and chemical reaction kinetics. In the comparison of the two models the heterogeneous solid-gas reactions of the original model were adopted however not the homogeneous gas phase reactions. The original model assumes that all gas phase reactions are in equilibrium while the new model assumes these reactions are not reversible, including the water-gas-shift reaction which is also modelled as two separate chemical reactions.

Table 4.2: Gasifier performance model comparison with Vamvuka *et al.* (1995)

KPI	Units	Vamvuka *et al.* (1995)	Current Model
X_c	%	≈ 95	93
y_{CO}	*mol(%)*	49.19	59.05
y_{H_2}	*mol(%)*	31.83	34.43
y_{CH_4}	*mol(%)*	0.01	6.52
$T_{g,P}$	*K*	≈ 2100	2286
$T_{g,out}$	*K*	≈ 850	1073
FG_{HV}	MJ/m^3	62.48	71.14
CO-to-H_2	-	1.55	1.72
η_{CG}	%	-	-
η_{CO+H_2}	%	81.02	93.48

Vamvuka *et al.* (1995) approximated the Nusselt Number to 2.0, while the current model computes the Nusselt Number from Guo *et al.* (2013) and this becomes twice what was approximated. This increase in Nusselt Number doubles the convection heat transfer between the particle and the gas. The current model obtains the thermodynamic properties of the gaseous species from Multiflash and this gives a much better gas-behaviour prediction, more especially at temperatures above 1500K. The original model makes use of thermodynamic properties obtained from Perry Handbook of Engineers which in most cases does not consider supercritical conditions for enthalpies, heat capacities, viscosities, thermal conductivities, etc. The *particle-wall* radiation heat transfer is also not considered in the original model and this is significant and comparable to the *gas-wall* radiation heat transfer. Another uncertainty in the comparison was the fact that the *wall* temperature in the original model was not reported while the current model used a fixed *wall* temperature of 1200K to ensure the slagging envirnoment.

The original model also takes into account of the diffusion although dealing with very fine particles of 41µm. The new model assumes surface reactions for small particle size and this is in agreement with Simon, 1984, Lee *et al.* (2011), Qiao *et al.* (2012) and Liu *et al.*, 2001. The new model also predicted a very low concentration of CO_2 in the exit gas stream (1.16 %) compared to the original model which predicted 18.91% on the mole basis. Low CO_2 concentration is very common for entrained flow gasifier as a result of extreme conditions which promotes the C + CO_2 gasification reaction. Vogt and van der Burgt (1980) reported 0.8% for a Shell-Koppers gasification unit and Ni and Williams (1995) reported *1.63%* for the Shell SCGP-1 plant. These concentrations reported by the latter concur with the current model prediction. The cold gas efficiency is not reported for both models since the heating value of coal was not reported in the original model. The difference in CO-to-H_2 ratio is also attributed to the difference in exit gas temperature. Ratios above *2.0* but less than *3.0* have been reported by Vogt and van der Burgt (1980), Ni and Williams (1995) and Sofia *et al.* (2013); and these also agree with the current model. It is also important to note that the original model predicted more CO_2 which could have further reacted with C to produce CO, and this could have also improved the ratio. In overall, the two models are in good agreement.

4.1.2 **A simple process modelling for a dry-feeding entrained bed coal gasifier (Lee *et al.*, 2011)**

Lee *et al.* (2011) developed a pseudo-two-dimensional (pseudo-2D) model based on the one-dimensional PFR concept. The model was used to predict the carbon conversion, cold gas

efficiency and temperature distribution along the length of the reactor at variable coal-to-oxygen ratio, coal-to-steam ratio and operating pressure. The comparison of the two models prediction is shown in **Table 4.3**.

Table 4.3: Gasifier performance model comparison

KPI	Units	Lee *et al.* (2011)	Current Model
X_c	%	≈ 90	98
R_{CO/H_2}	-	-	2.8
η_{CG}	%	50	48.9
η_{CO+H_2}	%	-	0.98
$T_{g,P}$	*K*	≈ 2050	2105
$T_{g,out}$	*K*	≈ 1750	1114
FG_{HV}	MJ/m^3	-	61.86

Lee *at al.* (2011) model is over simplified in determining the heat transfer across the gasifier length. It does not consider the *particle-gas* convection and radiation heat transfers. It also assumes a heat loss through the wall (*particle-wall* and *gas-wall* heat transfers) with no mentioning or reference to the *wall* temperature which is very critical for the overall performance of the gasifier. Lee *et al.* (2011) model also makes use of Perry Handbook for Chemical Engineers to determine the average values of the heat capacity of the gas mixture. As a result of simplification of their model, there are significant deviations between the two models. While the gasification temperature (peak temperature), final carbon conversion and cold gas efficiency are comparable, the profiles along the length of the reactor differ considerably.

4.1.3 Techno-Economic Assessment of Co-gasification of Coal-Petcoke and Biomass in IGCC Power Plant (Sofia *et al.*, 2013)

Sofia *et al.* (2013) developed a process simulation model of the IGCC power plant of Elcogas using Aspen Plus version 7.2. The model consists of the feed preparation section, a gasification unit, an ASU, a gas cleaning section and a combined cycle power plant. The gasification unit was simulated using a modular-sequence approach based on Bhattacharyya *et al*. (2011); a sequence of a ***yield*** reactor, a ***stoichiometric*** reactor and an ***equilibrium*** reactor. In their model, 5 different types of feedstock (mixture of coal and petcoke) were used and the model results were compared against the experimental results. The model developed in this work will

however be compared with only one feedstock mixture of coal/petcoke (45/55) as shown in **Table 4.4**. Wen and Chaung (1979) kinetics were used for gasification reactions while various reaction kinetics as shown in chapter III were used for combustion reactions.

Table 4.4: Proximate Analysis of fuel (Sofia *et al.*, 2013)

Parameter	Units	Value
Coal/pet-coke mix	*wt (%)*	45-55
Fixed Carbon	*wt (%)*	58.9
Volatiles	*wt (%)*	17.4
Ash	*wt (%)*	20.7
Moisture	*wt (%)*	7.9
HHV	*MJ/kg*	26.8

Sofia *et al.* (2013) operated the gasifier at fixed temperature of 2007K and a pressure of about 2.4MPag. In the current model, the temperature and pressure are variables (changing along the length of the reactor) determined from energy balance and pressure drop respectively. The summary of the gasifiers performances is shown in **Table 4.5**.

Table 4.5: Gasifier performance model comparison with Sofia *et al.* (2013)

KPI	Units	Sofia *et al.* (2013)	Current Model
X_c	*%*	-	97.19
$T_{g,P}$	*K*	2007.15	2816.98
$T_{g,out}$	*K*	2007.15	1420.86
y_{CO}	*vol (%)*	57.4	69.49
y_{H_2}	*vol (%)*	21.3	26.44
y_{CO_2}	*vol (%)*	2.2	0.24
y_{CH_4}	*vol (%)*	-	3.57
R_{CO/H_2}	-	2.69	2.63
η_{CO+H_2}	%	78.7	93.48
FG_{HV}	*MJ/kg*	-	13.92

It is also important to note that the original model includes impurities that are produced in the gasifier such as H_2S, NH_3, COS and HCN while the new model does not consider these. The main focus of the current work is the heating value of the fuel gas to be burnt in the gas turbine.

Sofia *et al.* (2013), however, demonstrated that there is no significant change in the gas heating value prior and post gas cleaning section of the IGCC. It can therefore be concluded that the model developed in this work shows a very good agreement with Sofia *et al.* (2013) model which simulated an Elcogas entrained flow gasification unit.

4.1.4 **Elcogas IGCC power plant**

Simulation model

Elcogas IGCC power plant is the world's largest commercial solid feedstock-based unit that is currently being operated. The plant uses an entrained flow reactor (PRENFLO® technology) to generate fuel gas that is subsequently burnt in the gas turbine after extensive cleaning, to produce power. The gasifier simulation is based on the mixture of coal and petcoke used by Sofia *et al.* (2013) as shown in **Table 4.4**. The gasifier main design data is shown in **Table 4.6**.

Table 4.6: Elcogas Power Plant main operating data (ThyssenKrupp, 2014)

Process Data	Units	Operating Conditions
P_g	*MPa*	40 (+)
$T_{g,P}$	^oC	> 2000
$T_{g,out}$	^oC	1,350 - 1,600
X_c	*%*	> 99
Composition		
y_{CO+H_2}	*vol. %*	> 85
y_{CO}	*vol. %*	2 – 4
y_{CH_4}	*vol. %*	< 0.1

The gasifier input data (coal flowrate, steam flowrate, oxygen flowrate and gasifier inlet pressure) used by Sofia *et al.* (2013) was used to validate the model against Elcogas Plant. The gas composition prior to gas cleaning is shown **Table 4.7** (ThyssenKrupp, 2014).

Table 4.7: Raw gas analysis of Elcogas

Composition	Units	Quantity
y_{CO_2}	*vol.%*	2.9
y_{CO}	*vol.%*	59.9
y_{H_2}	*vol.%*	21.7
y_{N_2+Ar}	*vol.%*	14.4
y_{CH_4}	*vol.%*	<0.1
y_{H_2S+COS}	*ppmv*	1.1
Total Gas	*vol.%*	*100*
LHV, dry	*MJ/Nm*^{3}	10.16

The predicted performance of the Elcogas entrained flow gasifier using the model developed in this current work is presented in **Table 4.8**. When simulating a chemical reactor, selection of chemical reactions, assumptions adopted and chemical reaction kinetics plays an important role in predicting the performance of the reactor.

Table 4.8: Elcogas Power Plant performance data (ThyssenKrupp, 2014)

KPI	Units	Elcogas Gasifier	Current Model
X_C	*%*	> 98	97.8
$T_{g,P}$	*K*	> 2273	2882.42
$T_{g,out}$	*K*	1623	1539.57
y_{CO+H_2}	*vol.%*	> 85	95.80
y_{CH_4}	*%*	< 0.1	3.53
η_{CG}	*%*	-	66.10
η_{CO+H_2}	*%*	81.02	95.80
FG_{HV}	*MJ/kg*	10.69	13.89

The developed model also shows a very good agreement with the data obtained from the physical plant. It should be noted, however, that there are no actual quoted values of the gasifier peak temperature ($T_{p,P}$) and total mole fraction of CO and H_2 (y_{CO+H2}), with only minimum values being stated. The model also predicts the values above these minimum values and therefore concurring with the actual plant data. The fuel gas heating value of the current model is calculated at the exit gasifier conditions. The fuel gas heating of *10.69MJ/kg* reported under

the Elcogas performance data in **Table 4.7**, was calculated using a standard density of the fuel gas (at 298K and 101325Pa) of $0.95kg/m^3$.

Optimization Model

A simulated Elcogas gasifier was then optimized to determine the maximum possible heating value of the fuel gas. The resulting NLP model assumes a constant feed into the gasifier with four degrees of freedom; feed pressure, particle size, oxygen-to-coal and steam-to-coal ratios. The feed temperature is assumed to be constant. The simulation results of temperature, conversion and fuel gas composition profiles along the length of the gasifier are presented in **Figures 4.1** and **4.2**. The optimized gasifier results are presented in **Figures 4.3** and **4.4**. The fuel gas heating value achieved in simulation was 13.9MJ/kg compared to 16.2MJ/kg achieved after optimization.

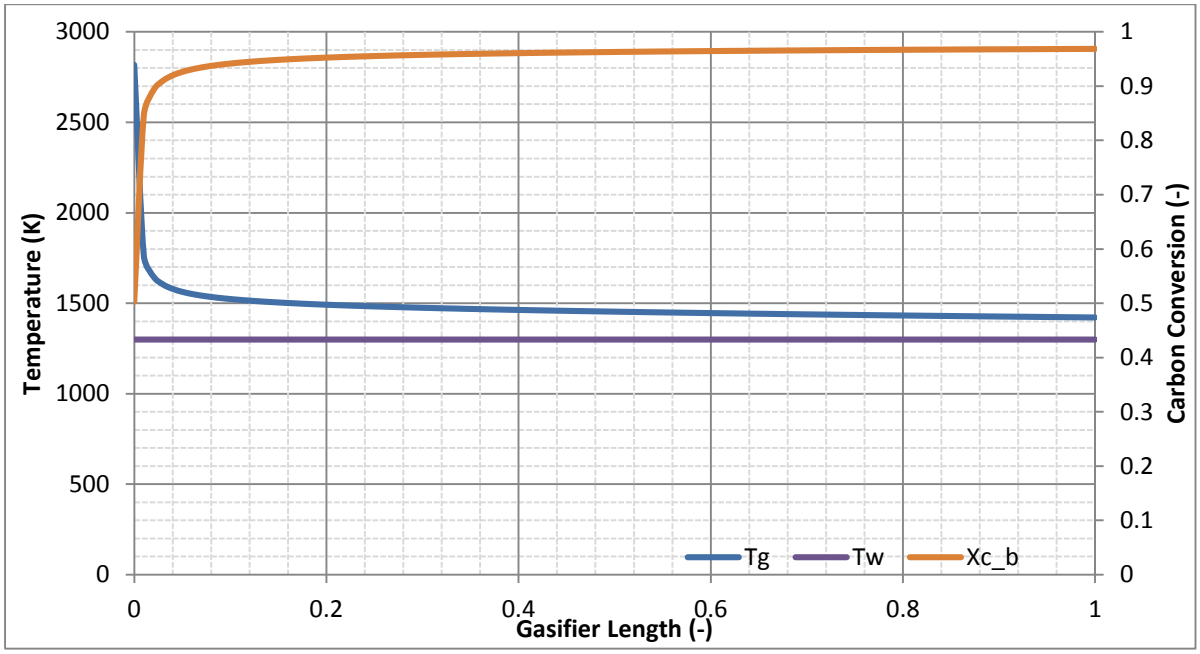

Figure 4.1: **Temperature and Conversion profiles of an original simulated gasifier**

T_g, T_w and $X_{c,b}$ are the gas temperature, wall temperature and baseline carbon conversion, respectively. The peak gas temperature is achieved in the flame zone of the gasifier as a result of volatile combustion. The temperature in the gasification zone (PFR) starts dropping as a result of the endothermic gasification reactions. It is also noted that due to high temperatures in the combustion zone, a larger fraction of char is also converted in the presence of oxygen to form CO and CO_2. A maximum conversion of 97% is achieved with an exit gas temperature of

1480K as shown in **Figure 4.1**. At these conditions, a fuel gas heating value of 13.9 MJ/kg was achieved.

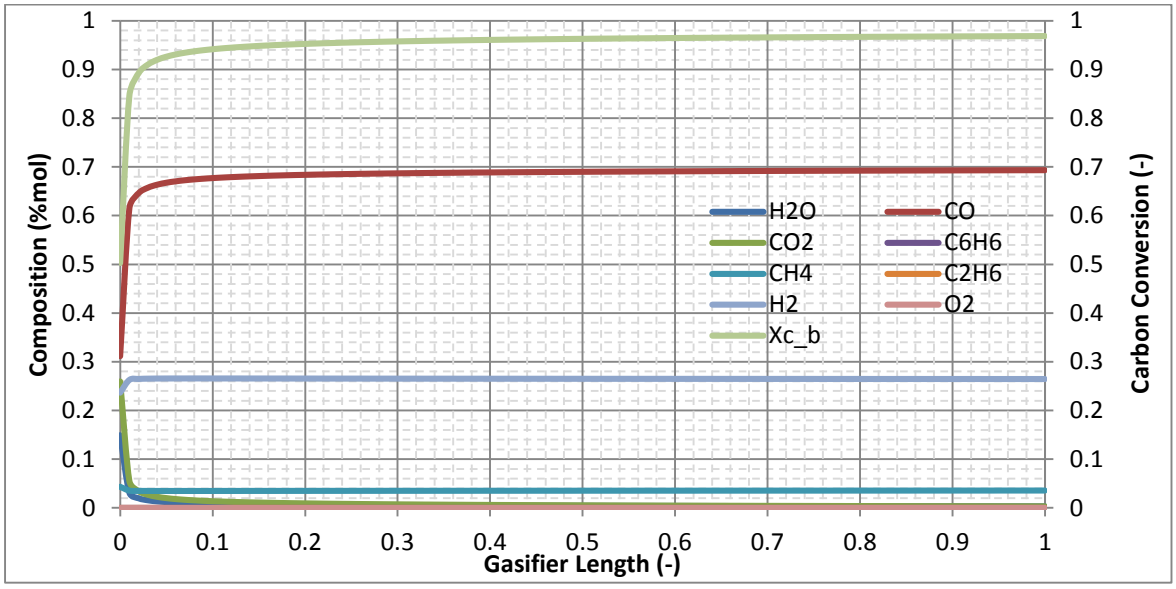

Figure 4.2: Fuel gas composition of the original simulated gasifier

The composition profiles of the fuel gas shown in **Figure 4.3** indicate the total CO and H_2 present in the fuel gas (η_{CO+H2}) is greater than 90%. It is also noted that CH_4 does not change much across the length of the reactor. The exit gas is almost dry and largely dominated by fuel gas.

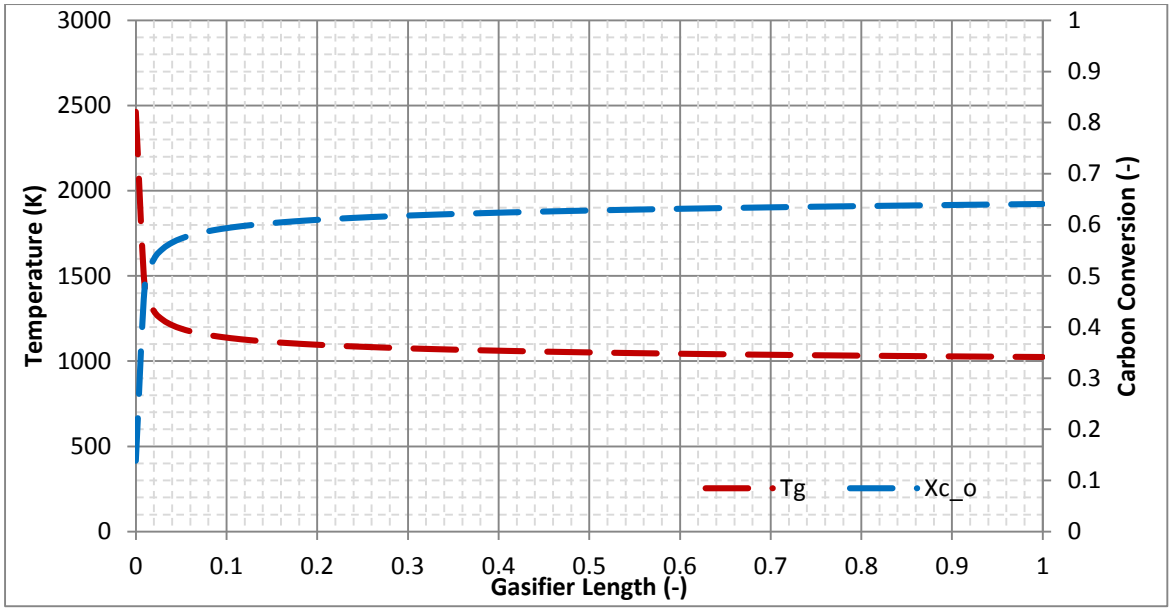

Figure 4.3: Temperature and Conversion profiles of an optimized gasifier

$X_{c,o}$ in **Figure 4.3** is the conversion achieved after optimization. The optimized gasifier indicates a relatively big change in temperature. The peak and exit gas temperatures drop by almost 500K. However, there is also a significant drop in conversion, from 97% to 63%. The fuel gas heating value on the other hand improves by almost 14.26%.

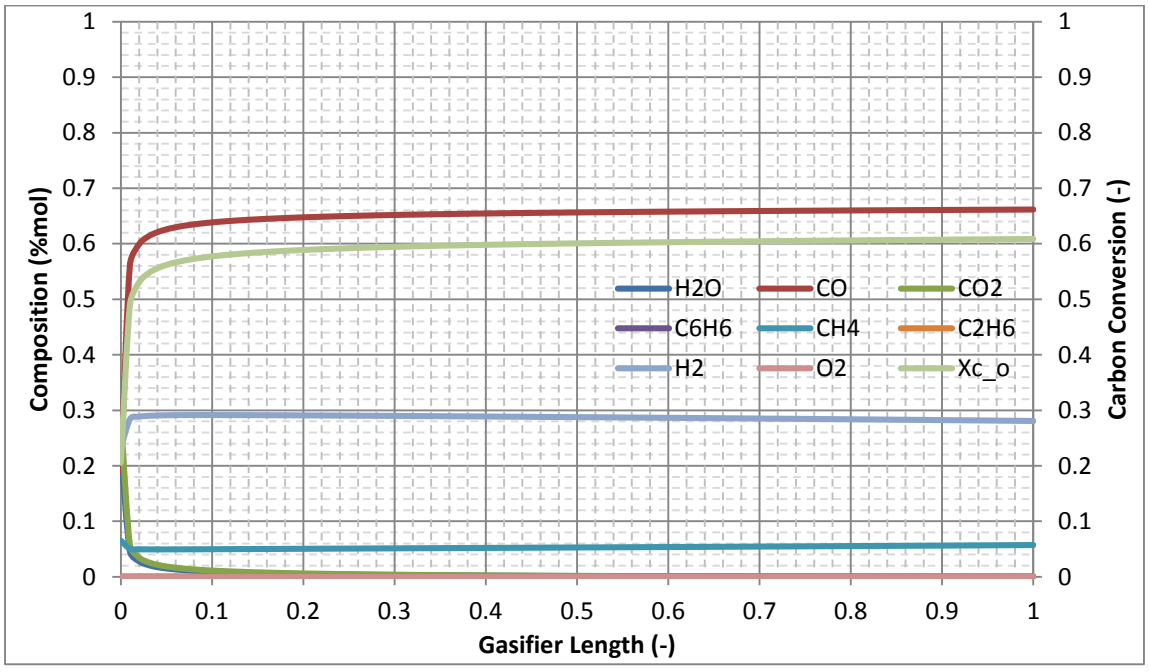

Figure 4.4: Composition profiles of an optimized gasifier

A drop in CO concentration from 69% to 66% was also noted while there was in improvement in the H_2 concentration in gasifier outlet. CH_4 concentration also increased from 3% to 6%.

CH_4 and H_2 have higher heating values of 50.1MJ/kg and 120.1MJ/kg, respectively, compared to CO which has the heating value of 10.9MJ/kg (Bossel, 2003). Therefore an increase in H_2 and CH_4 concentration results in an increase in fuel gas heating value.

It is also important to note that these results were achieved without specifying the range for CO-to-H_2 ratio. This ratio is, however, important if the gasifier stipulates the hydrocarbon mixture required for combustion. The most common CO-to-H_2 ratio produced in the gasifier ranges from 1.0 to about 3.0 (Guo *et al.*, 2007). A CO-to-H_2 ratio of 2.6 was obtained in the simulation and this was increased to 3.0 after the optimization. The maximum possible fuel gas heating value was achieved without specifying the lower and upper bounds of the CO-to-H_2 ratio. It was, however, noted that the model was biased towards the upper bound of the CO-to-H_2 ratio whenever it was not specified. During the initial simulation, a 97% conversion was achieved which subsequently reduced to about 63% after optimization. If bounds for conversion are set between 80 and 99.99%, the model converges towards the lower bound. This, therefore, implies that 63% conversion (which was achieved without bounds) is the minimum conversion that can be achieved for maximum possible fuel gas heating value for this specified gasifier. Carbon conversion can, however, be improved by considering the particle-gas separation and recycling the particles back to the gasifier. Two gasifiers in series can also be considered and these will be operating at moderate conditions, hence the improved operating cycle.

4.2 **Overall performance**

The fuel gas produced from the gasifier during the model simulation and optimization was then burnt in the gas turbine to evaluate the performance of the gas turbine. **Table 4.9** compares the performance of the gas turbine before and after optimization. The ambient air temperature was assumed to be at 25°C, the compressor and expander efficiencies were assumed to be 80 and 83% respectively.

Table 4.9: Performance of the gas turbine

KPI	Units	Simulation	Optimization
$\dot{m}_{FG}$	*kg/s*	41.8	41.8
$\dot{m}_{air}$	*kg/s*	606	606
P_r	-	16.6	16.6
T_{amb}	^oC	15.0	15.0
T_{X_in}	^oC	1189.3	1287.3
T_{X_out}	^oC	564.7	620.9
Cp_{ex}	*kJ/kg.K*	1140.6	1166.3
$\dot{m}_{ex}$	*kg/s*	647.8	647.8
$\dot{W}_C$	*MW*	-339.6	-339.6
$\dot{W}_X$	*MW*	574.9	626.9
$\dot{W}_{NET}$	*MW*	235.3	287.3
η_{GT}	*%*	40.0	41.9

The results presented in **Table 4.9** indicate an improvement in the gas turbine performance and this includes almost 2% increase in efficiency. The expander inlet temperature increases, but still remains within the maximum allowable operating temperature. The exhaust temperature and the specific heat capacity of the exhaust gas also increase and these will potentially increase the amount of heat available for the HRSG. While the focus on this work was only on the gas path of the IGCC, it is, however, understood that the lower temperature in the gasifier will result in less steam generated. The less amount of steam generated can reduce the overall efficiency of the power plant. One of the important assumptions undertaken during optimization was that the coal fed to the gasifier remains the same or could be increased if necessary but could not be decreased. This will therefore imply that a total amount of fuel gas produced will not change, but only its heating value, for the same power output. Burning high heating value fuel gas in the gas turbine will reduce the overall consumption of the gas. The

excess gas can then be considered for a Fired-HRSG instead of the conventional HRSG. This can therefore increase the steam production as well.

The fuel gas composition, which determines the changes in the fuel gas heating value and overall efficieincies in the gas path, is shown in **Table 4.10.** The notable changes in fuel gas compositions are the increase in CH_4 from 3.5% to 5.7%, a decrease in CO, from 69% to 66% while there was also an increase in H_2. These are the changes in fuel gas composition that resulted in an increase in heating value since CH_4 and H_2 have higher heating values compared to CO. This has come as a result of lower gasification temperature which favours an increase in CH_4 and H_2.

Table 4.10: Fuel gas composition

Component	Simulation	Optimization
	%	*%*
CH_4	3.54	5.71
C_2H_6	$1.9x10^{-18}$	$4.7x10^{-30}$
C_6H_6	$1.8x10^{-14}$	$2.4x10^{-14}$
CO	69.33	66.19
CO_2	0.32	0.019
H_2	26.46	28.06
H_2O	0.34	0.016
O_2	$1.4x10^{-23}$	$1.3x10^{-29}$

The overall results of the gas path performance are shown in **Table 4.11**. While there was decrease in carbon conversion, there was a notable increase in cold gas efficiency, the gas path efficiency and as well as the fuel gas heating value. The key performance indicators (KPI) selected in evaluating the gas path performance were; cold gas efficiency (η_{CG}), carbon conversion (X_C), total CO and H_2 in the fuel gas ($\eta_{CO+\,H_2}$) and the gas path efficiency (η_{GP}) as presented in **Table 4.11**.

Table 4.11: Overall performance of the gas path

KPI	Units	Simulation	Optimization
η_{CG}	%	52.0	61.0
X_C	%	96.9	63.5
η_{CO+H_2}	vol%	95.8	91.9
η_{GP}	%	31.5	38.4
FG_{HV}	MJ/kg	13.89	16.2

The gas path efficiency (η_{GP}) and the cold gas efficiency (η_{CG}) were calculated based on the higher heating value (HHV) of the coal/pet-coke mixture as reported by Sofia *et al.* (2013). η_{GP} is defined as the quotient of power generated in the gas turbine to the product of the coal fed into the gasifier and its respective heating value. It can also be noted that although there is a decrease in the η_{CO+H_2}, the CO-H_2 efficiency, which is obtained by summing the CO and H_2 volume percentages, this, however, results in an improvement in fuel gas heating vale. This is mainly because of the water gas shift reaction, in which the CO production is decreased and H_2 increased.

4.3 **Conclusions**

The entrained flow gasifier model developed in Chapter III has been successfully compared against *three* gasifier models published in open literature and also against data obtained from an actual plant. Taking into account of the assumptions adopted and selected chemical reactions, the model shows a very good prediction of the gasifier performance at a given coal quality (based on proximate and ultimate analysis), oxygen-to-feed and steam-to-feed ratios. The model predicts very well the key performance indicators such as gaisification temperature, conversion, CO/H_2 ratio, and the exit gas temperature.

Reference

Bhattacharyya, D., Turton, R., Zitney, S., *Steady-state simulation and optimization of an integrated gasification combined cycle power plant with CO_2 capture*, Ind. Eng. Chem Res., 2011

Bossel, U., *Well-to-Wheel Studies, Heating Values, and the Energy Conservation Principle, European Fuel Cell Forum*, 2003, 1-5

Guo, Y.C., Chan, C.K., and Lau, K.S, *Numerical studies of pulverized coal combustion in a tubular coal combustor with slanted oxygen jet*, Fuel, 2003

Lee, H., Choi, S., and Paek, M., *A simple process modelling for a dry-feeding entrained bed coal gasifier*, Power and Energy (Proc. IMechE), 2011

Ni, Q., and Williams, A., *A simulation study on the performance of entraned-flow coal gasifier*, Fuel, 1995

Qiao, L., Xu, J., Sane, A., and Gore, J., *Mutliphysics modelling of carbon gasification processes in a well-stirred reactor with detailed gas-phase chemistry*, Combustion & Flame, 2012

Sofia, D., Giuliano, A., and Barletta, D., *Techno-Economic Assessment of Co-gasification of Coal-Petcoke and Biomass in IGCC Power Plants*, Chemical Engineering Transactions, 2013

ThyssenKrupp, available at: http://www.thyssenkrupp-industrial-solutions.com/fileadmin/documents/brochures/gasification_technologies.pdf, accessed on 2 December 2014

Vamvuka, D., Woodburn, E. T., and Senior, P. R., *Modelling of an entrained flow coal gasifier (1. Development of the model and general predictions)*, Fuel, 1995

Vogt, E. V., and van der Burgt, *Status of the Shell-Koppers Process*, Chemical Engineering Progress, 1980

5. Conclusions

The objective of this work was to develop a mathematical model for an IGCC power plant, particularly focusing on the gasifier and the gas turbine. The entrained flow coal gasifier, which is widely used in IGCC for power generation, is known to operate under extreme conditions. While these conditions guarantee the highest carbon conversion, they, however, they have a negative impact on the availability, reliability, operating and capital investments of the gasification island. The model was used to establish if the severe operating conditions such as high temperature and pressure are the optimum conditions for producing the maximum fuel gas heating value. The primary focus was therefore centred on the entrained flow gasifier which is the centrepiece of an IGCC power plant. The gas turbine only receives and combusts the fuel gas to produce power. A simulation model was developed and validated against three published models and then extended to Elcogas gas power plant published data. The model showed a very good agreement with published data and even produced better results which were also comparable to that of Elcogas power plant gasifier.

An optimization model was subsequently formulated with the objective function to maximize the fuel gas heating value at the outlet of the gasifier. The optimized model indicated that there are possible moderate conditions at which the entrained flow gasifier can be operated to yield the maximum fuel gas heating value. A maximum fuel gas heating value was achieved with temperatures 500K lower than the extreme temperature reported in literature. During the simulation stage, 13.9MJ/kg of the fuel gas heating value was achieved and this improved by about 14.25% to 16.2MJ/kg at relatively mild conditions. The pressure did not have a significant impact on the fuel gas heating value, with only less than 2.0% increase in heating value being achieved by changing the pressure from 2.0MPa to 5.0MPa.

Owing to a decrease in operating temperature, the conversion was, however, reduced from 97% to about 63%. This, therefore, substantiated that the extreme condition are used to maximize conversion. The minimum conversion of 63% at the maximum heating value was achieved without the bounds of the CO-to-H_2 ratio. It was observed that the model was always biased towards the lower bound of the CO-to-H_2 ratio range, and this therefore indicates 63% conversion is the absolute minimum conversion. A decrease in carbon conversion led to a decrease of almost about 60% in O_2 and 50% in steam used in the gasifier. A decrease on the amount of steam and oxygen will result in the reduced operating cost of the ASU and an

increase in the amount of steam to the steam turbine and therefore more power output. This could also lead to an improved overall thermal cycle efficiency.

An increase in fuel gas heating value of 14.25% also results in an about 14.25% decrease in fuel gas mass flowrate into the gas turbine for the same power requirement. The results also indicate an almost 2% increase in the efficiency of the gas turbine when burning the gas of the higher heating value. This is mainly due to the increase in the expander inlet temperature. The gas turbine exhaust temperature and exhaust gas heat capacity also increases, which increases the amount of heat for the HRSG. The overall gas path efficiency also increased by almost 7%. A reduction in operating temperature and pressure of the gasifier will, therefore, guarantee a longer operating cycle of the gasification unit and relatively lower operating and capital costs.

6. Recommendations

The IGCC has two paths, *viz*., gas and steam paths. The gas path focuses on the fuel gas generation in the gasifier, removal of impurities in the gas cleaning circuit and its combustion in the gas turbine. Steam path involves the heat recovery from gasifier jacketed-walls, gas cooling units and gas turbine exhaust Heat Recovery Steam Generator (HRSG). The total power output and efficiency are, therefore, based on the power generated from the steam and gas turbines. This work has only focused on the path of the IGCC. The optimum operating conditions, which are lower than the extreme conditions at which the entrained flow gasifier usually operates, will potentially result in lower steam production from gasifier wall and raw gas coolers. Less steam production will, therefore, affect the overall power output and efficiency, however, the produced gas has a higher heating value which implies that less fuel gas is burnt in the gas turbine. This will have a further impact on the design of the ash handling system in the IGCC power plant. If the original design of the gasifier could only handle molten ash, operating below the slagging conditions will produce dry ash which should be handled differently. This will therefore require a very a serious assessment during the process conditions evaluation. The excess gas can therefore be considered for Fired-HRSG to produce more steam. Fired-HRSG is different from the traditional HRSG, and will have a Capital and Operational costs implication as a result of mechanical and metallurgical designs and as well as maintenance philosophies. Therefore, a proper financial evaluation must be conducted for both designs of the HRSG.

The carbon conversion achieved at mild condition was 30% lower than the original. This will, therefore, increase the separation cost of the raw gas and unconverted carbon. The cost of adding a separation unit on the existing flowsheet also requires process and financial assessment in order to quantify the gains achieved by lowering the operating conditions. Lower carbon conversion also results in less gas produced from the gasifier. A consideration for two gasifiers in parallel, but operating at mild condition and therefore having an extended life, must also be assessed. Gasifiers in parallel also allows for one gasifier to be shut down for maintenance without having to shut down the entire plant.

A comprehensive financial and overall efficiency evaluation of the IGCC power plant flowsheet must be carried out considering both steam and gas paths. This should include, but not limited to the decrease in steam and oxygen requirements that were observed during

optimization. Reducing the operating conditions could also results in the operation reduced to non-slagging conditions and therefore ash handling system must also be considered. Finally, a detailed CFD model of the plant, especially the gasifier, must be looked at in order to establish if the gasifier might require physical modications.

Nomenclature

Gasifier Nomenclaure

a	contact area of the particle per unit volume of the reactor	m^2/m^3
A_C	cross sectional area of the gasifier	m^2
A_k	chemical reaction rate pre-exponential factor (gas-particle)	$kg/m^2.atm^n.s$
A_j	chemical reaction rate pre-exponential factor (gas phase)	$m^3.s/kmol$
C_a	concentration of the combustible component in the combustion reaction	$kmol/m^3$
C_b	concentration of the oxidizing agent in the combustion reaction	$kmol/m^3$
D_R	gasifier internal diameter	m
D_p	particle diameter	m
G	superficial mass velocity	
g_c	gravitational acceleration	m/s^2
Ea	activation energy	$kJ/kmol$
H_p	specific enthalpy of the particle	kJ/kg
H_g	specific enthalpy of the has mixture	kJ/kg
h_{gp}	convection heat transfer coefficient between particle and gas	$W/m^2.K$
h_{gw}	convection heat transfer coefficient between gas and wall	$W/m^2.K$
HV	heating/calorific value of the fuel gas	MJ/kg
HHV	higher heating/calorific value of the fuel gas	MJ/kg
L	length of the reactor	m
$\dot{m}_{gi}$	mass flowrate of the component *i* in the gas phase	kg/s
$\dot{m}_C$	mass flowrate of carbon	kg/s
Mw_C	molecular weight of component carbon	$kg/kmol$
Mw_i	molecular weight of gaseous component *i*	$kg/kmol$
n	heterogeneous particle gas reaction order	-
n_i	number of moles for component i	$moles$
n_k	total number of moles	$moles$
P_a	partial pressure of the oxidizing agent	Pa
P_{MAWP}	maximum allowable working pressure of the gasifier	Pa
r_j	reaction rate for homogeneous gas phase	$kmol/m^3.s$
r_k	reaction rate for particle-gas	$kg/s.m^2$
R	Universal gas constant	$kJ/kmol.K$

R_{min}	minimum CO-to-H_2 ratio	-
R_{max}	maximum CO-to-H_2 ratio	-
T_{AFT}	ash fusion temperature	*K*
T_g	temperature of the gas	*K*
T_{MAWP}	maximum allowable working temperature of the gasifier	*K*
T_p	temperature of the particle (also refered to as T_s)	*K*
v_s	velocity of the particle	*m/s*
v_g	velocity of the gas mixture	*m/s*
x	mass fraction	-
x_i	mass fraction of the gaseous component	*%wt*
X	combustible gas	$kmol/m^3$
X_c	carbon conversion	*%*
y	mole fraction	-
Y	oxidizing agent	$kmol/m^3$

Gasifier: Subscripts

CG	cold gas
g	gas
i	gaseous component in the gas mixture
i'	combustible gaseous component in the fuel gas mixture
ISO	international standard organizations
j	homogeneous phase reaction
k	heterogeneous phase reaction
out	outlet
p	particle
R	reactor/gasifier
sim	simulation

Gasifier: Superscripts

A	rate order
B	rate order

Gasifier: Greek Symbols

ε_p	emissivity of the particle	-
ε_w	emissivity of the wall	-

η_{CG}	cold gas efficiency	*%*
Φ	void fraction	-
σ	Stefan's Boltzmann Constant	$W/m^2.K^4$
ρ	density	kg/m^3
υ_{ji}	stoichiometric coefficient of component i in reaction j	-

Gas Turbine Nomenclaure

Cp_{air}	specific heat capacity air	*kJ/kg.K*
H_{gi}	specific enthalpy of the gas component i in the gaseous mixture	*kJ/kg*
$\dot{m}_{K_in}$	inlet mass flowrate of air into the compressor	*kg/s*
$\dot{m}_{K_out}$	outlet mass flowrate of air from the compressor	*kg/s*
$\dot{m}_{Exhaust}$	mass flowrate of the gas turbine exhaust	*kg/s*
$\dot{m}_{FG}$	mass flowrate of the fuel gas	*kg/s*
$\dot{m}_{N_2}$	mass flowrate of nitrogen	*kg/s*
$\dot{m}_S$	mass flowrate of the steam	*kg/s*
$\dot{m}_i$	mass flowrate of the component *i* in the gas phase	*kg/s*
T_{amb}	ambient temperature	*K*
T_{K_in}	inlet temperature of the compressor	*K*
T_{K_out}	actual discharge temperature of the compressor	*K*
$T_{K_out,is}$	ideal discharge temperature of the compressor	*K*
T_{X_in}	inlet temperature of the expander	*K*
T_{X_out}	actual discharge temperature of the compressor	*K*
$T_{X_out,is}$	ideal discharge temperature of the expander	*K*
r_K	pressure ratio across the compressor	-
r_X	pressure ratio across the expander	-
$\dot{W}_C$	compressor power requirement	*MW*
$\dot{W}_X$	power produced by the expander	*MW*
$\dot{W}_{NET}$	net power produced by the gas turbine	*MW*
$\dot{W}_{out}$	power produced by the gas turbine	*MW*
x_f	fuel gas conversion	-

Gas Turbine: Subscripts

in	inlet stream to the unit

out	outlet stream from the unit
C	compressor
ex	exhaust
is	isentropic
F	combustion chamber of the gas turbine
X	expander

Gas Turbine: Greek Symbols

η_C	compressor efficiency	*%*
η_t	expander/turbine efficiency	*%*
υ_i	stoichiometric coefficient of the combustible component *i* in combustion reaction	-
υ_{ji}	stoichiometric coefficient of component *i* in reaction *j*	-

APPENDIX A: Mass and Energy Balance

Gasifier Model Derivation

Mass Balance

Consider the control volume as shown in **Figure** AP1.

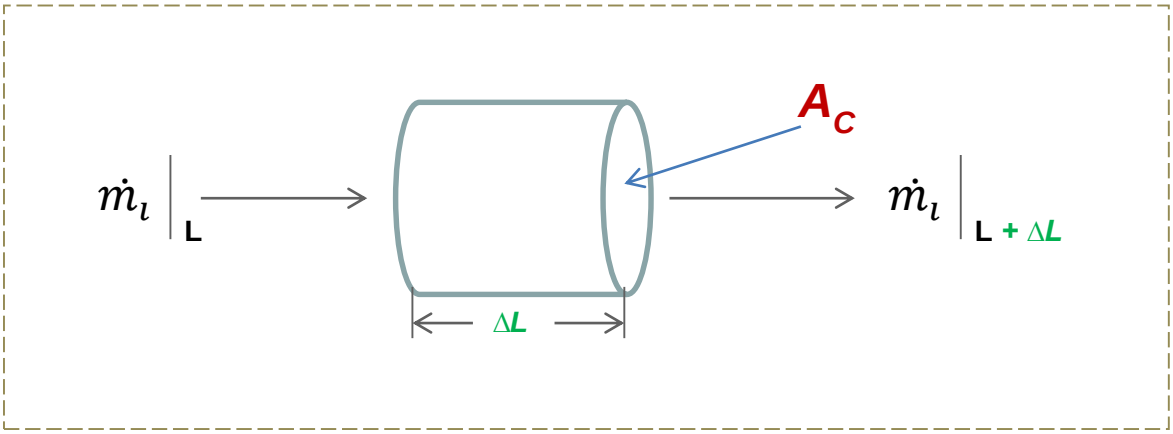

Figure AP1: Control volume of a gasifier for mass balance considerations

The entrained-flow coal gasifier emulates a plug flow reactor configuration and, therefore, the general mass balance of a controlled-volume indicated in **Figure AP1** is given by Equation (i).

$$\dot{m}_{i|L} - \dot{m}_{i|L+\Delta L} + \dot{m}_{iG} - \dot{m}_{iC} = \dot{m}_{iAC} \quad \text{(i)}$$

Where $\dot{m}_{i|L}$ and $\dot{m}_{i|L+\Delta L}$ is mass flowrate of component *i* at the inlet and outlet of the control volume. $\dot{m}_{iG}$ and $\dot{m}_{iC}$ are mass of component *i* generated and consumed in the gasifier. The mass of the component *i* either generated or consumed in the gasifier is given by the chemical reaction rate R_j as shown in Equation (ii).

$$R_j = \sum_{j}^{n} \upsilon_{ji} r_j \quad \text{(ii)}$$

Where υ_{ji} is the stoichiometric coefficient of component *i* in chemical reaction *j*. R_j is net component reaction rate in a set of chemical reactions, i.e., from reaction *j* to *n*. In the PFR, there is no accumulation ($\dot{m}_{iAC}$), and therefore, substituting Equation (ii) in Equation yields Equation (iii).

$$\dot{m}_{i|L} - \dot{m}_{i|L+\Delta L} + (\Delta L) A_C \sum_{j}^{n} \upsilon_{ji} r_j = 0 \quad \text{(iii)}$$

Where A_C is the gasifier cross-sectional area. Dividing Equation (iii) by ΔL on both sides of the Equation and taking limits as $\Delta L \rightarrow 0$ yields Equation (iv).

$$\frac{d\dot{m}_i}{dL} = A_C Mw_i \sum_j^n \upsilon_{ji} r_j \quad \text{(iv)}$$

Where Mw_i is the molecular weight of component *i*. Equation (iv) is a mass balance equation that is used to calculate the gaseous component consumed or generated in the homogeneous gas phase (combustion and WGSR). However, the gasifier has a two-phase mixture, particles and gases. The gaseous components takes place in both combustion and gasification reactions. The particle mass balance is given by Equation (v).

$$\frac{d\dot{m}_C}{dL} = aA_C \sum_k^m \upsilon_{ji} r_k \quad \text{(v)}$$

Where $\dot{m}_C$ and a are the mass flowrate of carbon particle and the contact area of the particle per unit volume of the reactor, respectively. r_k is the chemical reaction rate of the gasification reaction, i.e., reactions *k* to *m*. Since the gases are also consumed and generated in the gasification reactions, the overall gaseous component mass balance is, therefore, given by Equation (vi).

$$\frac{d\dot{m}_i}{dL} = A_C Mw_i \sum_j^n \upsilon_{ji} r_j \; + \; aA_C \sum_k^m \upsilon_{ji} r_k \quad \text{(vi)}$$

Equations (v) and (vi) are used to calculate the mass of all the gaseous components and the carbon particles as they move across the length of the reactor.

Energy Balance

The derivation of the energy balance around the gasifier also follows the same principle as the Mass Balance. It considers all the energy streams into and out of the chosen control volume.

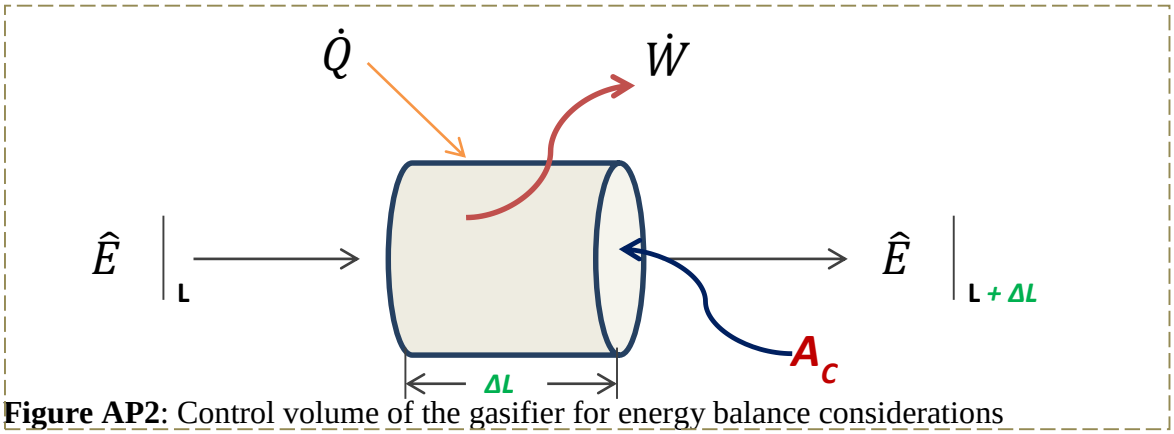

Figure AP2: Control volume of the gasifier for energy balance considerations

The general energy balance around a control volume (as shown in **Figure** AP2) is given by Equation (vii).

$$\sum_{i=1}^{n} \dot{m}_i \hat{E}_{i\,|\,L} - \sum_{i=1}^{n} \dot{m}_i \hat{E}_{i\,|\,L+\Delta L} + \dot{Q} - \dot{W} = \frac{\Delta E}{\Delta t} \qquad \text{(vii)}$$

Where the 1st and 2nd term of Equation (vii) are the energy input and output into the system due to flow (incoming and exit streams), respectively. The term $\dot{Q}$ is the energy input into the system and $\dot{W}$ is the work done on the system. The energy term ($\hat{E}_i$) in Equation (vii) constitutes of internal energy ($\hat{U}_i$), kinetic energy ($\hat{E}_{K,i}$) and potential energy ($\hat{E}_{P,i}$) as shown in Equation (viii).

$$\hat{E}_i = \hat{U}_i + \hat{E}_{K,i} + \hat{E}_{P,i} \qquad \text{(viii)}$$

Assumed that the internal energy is more dominant than the kinetic ($\hat{E}_{K,i}$) and potential energy ($\hat{E}_{P,i}$), therefore, the above equation will reduce to Equation (ix).

$$\hat{E}_i = \hat{U}_i \qquad \text{(ix)}$$

Where the internal energy is defined by Equation (x).

$$\hat{U}_i = \hat{H}_i - PV_i \qquad \text{(x)}$$

The work term in Equation (vii) consists of the shaft work ($\dot{W}_s$), work done by fluid to overcome shear stress ($\dot{W}_\tau$) and work done by fluid to overcome pressure drop ($\dot{W}_\sigma$) as shown in Equation (xi).

$$\dot{W} = \dot{W}_s + \dot{W}_\tau + \dot{W}_\sigma \qquad \text{(xi)}$$

There is, however, no shaft work and since the system only consists of gases, the work to overcome shear stress is negligible and therefore, Equation (xi) reduces to Equation (xii).

$$\dot{W} = \dot{W}_{\sigma} \tag{xii}$$

The work done by the fluid to overcome pressure drop is defined by Equation (xiii).

$$\dot{W}_{\sigma} = \sum_{i=1}^{n} \dot{m}_i (PV_i)_{|\,L+\Delta L} - \sum_{i=1}^{n} \dot{m}_i (PV_i)_{|\,L} \tag{xiii}$$

Substituting Equations (xiii) and (x) in Equations (vii), and assuming steady state yields Equation (xiv).

$$\sum_{i=1}^{n} \dot{m}_i \left(\widehat{H}_i - PV_i + PV_i\right)_{|\,L} - \sum_{i=1}^{n} \dot{m}_i \left(\widehat{H}_i - PV_i + PV_i\right)_{|\,L+\Delta L} + \dot{Q} = 0 \tag{xiv}$$

Dividing by ΔL on both sides Equation (xvi) and taking limits as $\Delta L \rightarrow 0$ yields Equation (xv)

$$\frac{\dot{m}_g d\widehat{H}_g}{dL} + \dot{q} = 0 \tag{xv}$$

Where $\dot{q}$ is energy term representing the heat transfer by conduction and convection between the particle-gas, particle-wall and gas-wall. $\dot{m}_g$ and $\widehat{H}_g$ are the total gas mass flowrates and enthalpy, respectively. Equations (xvi) and (xvii) are the final equations for gas and particle balance across the length of the gasifier.

$$\dot{m}_g \frac{d\widehat{H}_g}{A_R dL} + \dot{q}_{gp,c} + \dot{q}_{gp,r} + \dot{q}_{gw,r} = 0 \tag{xvi}$$

$$\dot{m}_p \frac{d\widehat{H}_p}{A_R dL} - \dot{q}_{gp,c} - \dot{q}_{gp,r} + \dot{q}_{pw,r} = 0 \tag{xvii}$$

Where subscripts *c* and *r* represent convection and radiation respectively, while the subscripts pg and gw mean the heat transfer from the particle to the gas and heat transfer from gas to the walls of the reactor, respectively

APPENDIX B 1: gPROMS Model

Gasifier Model

Kinetic Model

```
#=============================================================
PARAMETER
   components          as  ORDERED_SET
   Gases               as  ORDERED_SET
   Solids              as  ORDERED_SET
   Rxns                as  ORDERED_SET
   Nu                  as  ARRAY(components, Rxns)  of  Real
   Mw                  as  ARRAY(components) of Real
   #   PROXIMATE ANALYSIS
   Ea                  as  ARRAY(Rxns)  of  Real     # kJ/mol
   A                   as  ARRAY(Rxns)  of  Real     # kmol, sec, m^3
   R                   as  Real  Default 0.08206     # atm.l/mol/k
   R1                  as  Real  Default 8.314       # kJ/kmol/K
   PI                  as  Real  Default 3.142857
   mf                  as  Real  Default 1.251827     # Mechanism factor for CO/CO2 Ratio based
on average temperature of 1550K
   n1, n2, n3, n4       as     Real                          #          Pressure order of the n-th order
equation _ Heterogeneous reactions
   psp_OXYGEN, psp_WATER as     Real   #   particle structural parameters _
Heterogeneous chemical reactions
   psp_CARBON_DIOXIDE, psp_HYDROGEN       as     Real   #   particle structural
parameters _ Heterogeneous chemical reactions
   eps                 as  Real Default 0.001
   eps_y               as  Real Default 0.007
   comp_order          as  Array (components) of Real Default 1
   small_mole_fraction   as Real Default 1e-6
   eps_CO              as REAL Default 0.005
   eps_H2O             as REAL Default 0.007
   eps_METHANE          as REAL Default 0.005
   eps_BENZENE          as REAL Default 0.008
#=============================================
   # SCALING
   Tref       as Real Default 1400
   L_scale     as Real Default 1
   E_scale     as Real Default 1
   H_scale     as REAL Default 1e-9
#=============================================================
=============================================================
================

PORT
   info as kinetic_info

VARIABLE
   ko              as  ARRAY(Rxns)  of  rate_constant
   k1              as  ARRAY(Rxns)  of  rate_constant
```

```
   k              as  ARRAY(Rxns)  of  rate_constant
#   lnk            as  ARRAY(Rxns)  of  no_type
   Tp             as  temperature
   Tg             as  temperature
   Xc             as  conversion
   rho_g          as  density
#   vp             as  velocity
   molar_rho_g       as  density
   molar_rho_g1      as  density
   Rxn_rate          as  ARRAY(Rxns) of  base_reaction_rate
#   Rxn_rate_overall   as  ARRAY(Solids) of reaction_rate
   comp_rxn_rate     as  ARRAY(components) of   reaction_rate
   WGSR_Ratio        as  ratio
   mass_flow         as  ARRAY(components) of  bulk_mass_flowrate
   mole_fraction     as  ARRAY(Gases) of  molefraction
   carbon_conversion  as  conversion
   pressure          as  pressure
   P_P               as  ARRAY(Gases) of pressure
   MwAve             as molecular_weight
   Dp             as  length
   Ap             as  area
   contact_area_solid_gas_volReactor as area
#
#   CellVolume        as  Volume

#=================================================================
=================================================================
====================
SET
   components  :=  info.Components;
   Gases := info.Gases;
   Solids     :=   components - Gases;
   Mw := info.Mw;
   Rxns            :=   ['CH4+O2', 'C2H6+O2', 'C6H6+O2',  'CO+O2',          'H2+O2',
'WGSR_F',       'WGSR_R',       'CH4+H2O',     'C+O2',       'C+CO2',       'C+H2O',
'C+H2'];
   Ea('CH4+O2':'C+H2') :=  [202.64E3,   125.6E3,   125.6E3,   {9.76E4}168E3,
{9.76E4}168E3,   288.E3{3.9E5},    {3.96}218E3,     2.51e5{168E3}     ,17967{19244},
21060{29227},   21060{28650},   17921];                  #  Wen & Chaung (1979), Ea/R (the
values represent the quotiant), Combustion reactions Ea = kJ/kmol/K
   A('CH4+O2':'C+H2')  :=  [2.119E11, 3.9029E10, 1.1247E10,   {3.09E11}2.2387E13,
{8.83E11}6.8E15,  2.34E10{2.978E14}, {2.65E-2}5.99E08,   8.0e7{4.4E11},
8710{319},   2470{202},     2470{226},      1.2];      #  Wen & Chaung (1979),
g/cm^2.atm.s
#-------------------------
   n1  :=  0.68;   n2  :=  0.84;
   n3  :=  0.73;   n4  :=  0.5;
   psp_OXYGEN  :=  14;     psp_WATER :=  3.0;
   psp_CARBON_DIOXIDE :=  3.0;    psp_HYDROGEN  :=  3.0;
```

```
#-------------------------------------------------------------------------------------------------------------
-------------------------
#-------------------------------------------------------------------------------------------------------------
-------------------------
      #STIOCHIOMETRIC COEFFICIENTS
#                H2O    CO   CO2    C6H6   CH4   C2H6  H2    O2     N2     C }
{ENTHALPHY OF FORMATION (kJ/mol)}
   Nu(,'CH4+O2') := [ 2,    0,    1,     0,    -1,   0,   0,   -2.0,   0,    0];          {-519.5}
   Nu(,'C2H6+O2') := [ 3,    0,    2,     0,     0,   -1,   0,   -3.5,   0,    0];          {-1471.3}
   Nu(,'C6H6+O2') := [ 3,    0,    6,    -1,     0,    0,   0,   -7.5,   0,    0];
   Nu(,'CO+O2')  := [ 0,   -1,    1,     0,     0,    0,   0,   -0.5,   0,    0];          {-283.1}
   Nu(,'H2+O2')  := [ 1,    0,    0,     0,     0,    0,  -1,   -0.5,   0,    0];          {-242.0}
   Nu(,'WGSR_F') := [-1,   -1,    1,     0,     0,    0,   1,    0.0,   0,    0];          {-41.2}
   Nu(,'WGSR_R') := [ 1,    1,   -1,     0,     0,    0,  -1,    0.0,   0,    0];          {-41.2}
   Nu(,'CH4+H2O') := [-1,    1,    0,     0,    -1,   0,   3,    0.0,   0,    0];          {-41.2}
   Nu(,'C+CO2')  := [ 0,    2,   -1,     0,     0,    0,   0,    0.0,   0,   -1];
   Nu(,'C+H2O')  := [-1,    1,    0,     0,     0,    0,   1,    0.0,   0,   -1];
   Nu(,'C+H2')   := [ 0,    0,    0,     0,     1,    0,  -2,    0.0,   0,   -1];
   Nu(,'C+O2')   := [ 0,   (2-2/mf),  (2/mf-1),    0,     0,    0,   0,   -(1/mf),  0,    -1];

#=============================================================================
=============================================================================
=======
EQUATION
#-------------------------------------------------------------------------------------------------------------
        #   MAIN KINETICS
#-------------Combustion Reactions Rate Constants-------------------

   For i in ['CH4+O2', 'C2H6+O2', 'C6H6+O2','CO+O2','H2+O2','WGSR_F','WGSR_R',
'CH4+H2O'] Do

      ko(i) = A (i) * Exp((-Ea(i)/(R1*Tref))); # /s

   End
   For i in ['C+O2', 'C+CO2', 'C+H2O', 'C+H2'] Do

      ko(i) = A (i) * Exp((-Ea(i)/Tref));

   End
#-------------------------------------------------------------
   For i in ['CH4+O2', 'C2H6+O2', 'C6H6+O2','CO+O2','H2+O2','WGSR_F','WGSR_R',
'CH4+H2O'] Do
      If k(i) > 1e2 Then
        log(k(i)) = log(A(i)*Exp(-Ea(i)/(R1 * Tg))); # /s
      Else
        k(i) = A (i) * Exp(-Ea(i)/(R1 * Tg)); # /s
      End
    End
```

```
    For i in ['CH4+O2', 'C2H6+O2', 'C6H6+O2','CO+O2','H2+O2','WGSR_F','WGSR_R',
'CH4+H2O'] Do
       k1(i) = ko(i)*Exp((-Ea(i)/(R1)*(1/Tg) - (1/Tref))); # /s
    End

    For i in ['C+O2', 'C+CO2', 'C+H2O', 'C+H2'] Do
       k1(i) = 0;
    End
#--------------Gasification Reactions Rate Constants--------------------
   For i in ['C+O2', 'C+CO2', 'C+H2O', 'C+H2'] Do
#       If k(i) > 1e2 Then
#          log(k(i)) = log(A(i) + (-Ea(i)/Tp));
#       Else
         k(i) = A(i)*Exp(-Ea(i)/Tp);
#       End
   End
#---------------------------Misceleneous Variables-----------
      MwAve = sigma(mole_fraction(Gases) * Mw(Gases));
      P_P(Gases) = mole_fraction(Gases) * pressure;
      molar_rho_g1  = pressure/(R*Tg);  # kmol/m^3
      molar_rho_g*MwAve = rho_g;  # kmol/m^3
      Ap = 1e3*PI*(Dp^2); # m^2/g, assuming spherical particles
      WGSR_Ratio = Rxn_rate('WGSR_F')/Rxn_rate('WGSR_R');


#-----------------------CH4 Combustion---------------------------------

   L_scale*Rxn_rate('CH4+O2')*(molar_rho_g * mole_fraction('methane'))      =
L_scale*k('CH4+O2')  * (molar_rho_g  * mole_fraction('methane'))^(1.2) * (molar_rho_g *
mole_fraction('oxygen'))^1.3; # Kinetics from Westbrook & Dryer (1981)

#--------------------C2H6 Combustion---------------------------------

   L_scale*Rxn_rate('C2H6+O2')* (molar_rho_g * mole_fraction('ethane'))    =
L_scale*k('C2H6+O2') * (molar_rho_g * mole_fraction('ethane'))^(1.1) * (molar_rho_g *
mole_fraction('oxygen'))^1.65; # Kinetics from Westbrook & Dryer (1981)

#----------------------C6H6 Combustion---------------------------------

   L_scale*Rxn_rate('C6H6+O2')*(molar_rho_g * mole_fraction('benzene'))     =
L_scale*k('C6H6+O2') * (molar_rho_g * mole_fraction('benzene'))^1.1 * (molar_rho_g *
mole_fraction('oxygen'))^1.85; # Kinetics from Westbrook & Dryer (1981)

#----------------------CO Combustion---------------------------------

   L_scale*Rxn_rate('CO+O2') * (molar_rho_g * mole_fraction('oxygen'))     =
L_scale*k('CO+O2') * (molar_rho_g * mole_fraction('carbon monoxide')) * (molar_rho_g *
mole_fraction('oxygen'))^1.25;    # Kinetics from Rodrigues et. al., 2005 replaced with
Westbrook & Dryer (1981)
```

```
#-------------------H2 Combustion-------------------------------------

   L_scale*Rxn_rate('H2+O2') * (molar_rho_g * mole_fraction('hydrogen'))     =
L_scale*k('H2+O2') * (molar_rho_g * mole_fraction('hydrogen'))^1.25 * (molar_rho_g *
mole_fraction('oxygen'))^1.5;        #  KInetics from Rodrigues et. al., 2005 replaced with
Jones and Lindstedt (1988)

#--------------------Water Gas Shift Forward---------------------------------

   L_scale*Rxn_rate('WGSR_F') * (molar_rho_g * mole_fraction('carbon monoxide'))    =
L_scale*k('WGSR_F') * (molar_rho_g * mole_fraction('carbon monoxide'))^1.5  *
(molar_rho_g * mole_fraction('WATER'));  # Kinetics from Rodrigues et. al., 2005

#--------------------Water Gas Shift Reverse---------------------------------

   L_scale*Rxn_rate('WGSR_R') * (molar_rho_g * mole_fraction('hydrogen'))    =
L_scale*k('WGSR_R')  * (molar_rho_g * mole_fraction('carbon dioxide'))  * (molar_rho_g *
mole_fraction('hydrogen'))^1.5; # Kinetics from Bustamante et. al (2005)

#--------------------Methane Reforming---------------------------------

   L_scale*Rxn_rate('CH4+H2O') * (molar_rho_g * mole_fraction('methane'))    =
L_scale*k('CH4+H2O')  * (molar_rho_g * mole_fraction('methane'))^1.5  * (molar_rho_g *
mole_fraction('WATER')); # Kinetics from Bustamante et. al (2005)

#=================================================================
=================================================================
==============
   #----------------CHAR COMBUSTION/GasIFICATION-------------------
      #kmol/m3.s
#----------------OXYGEN GasIFICATION
      If mass_flow('C') < 0.001 Then
         E_scale*Rxn_rate('C+O2')  =
E_scale*(contact_area_solid_gas_volReactor/Mw('C'))* (mass_flow('C')/0.001) * k ('C+O2')
* (pressure * mole_fraction('oxygen'))*(1 - carbon_conversion)*sqrt(1-
psp_OXYGEN*log(1-carbon_conversion));
      Else
         E_scale*Rxn_rate('C+O2')  = E_scale*(contact_area_solid_gas_volReactor/Mw('C'))
* k ('C+O2') * (pressure * mole_fraction('oxygen'))*(1 - carbon_conversion)*sqrt(1-
psp_OXYGEN*log(1-carbon_conversion));
      End
#----------------CARBON DIOXIDE GasIFICATION
      If mass_flow('C') < 0.001 Then
         E_scale*Rxn_rate('C+CO2') = E_scale*(contact_area_solid_gas_volReactor/Mw('C'))
* (mass_flow('C')/0.001)* k('C+CO2') * (pressure * mole_fraction('carbon dioxide'))*(1 -
carbon_conversion)*sqrt(1-psp_CARBON_DIOXIDE*log(1-carbon_conversion));
      Else
         E_scale*Rxn_rate('C+CO2') = E_scale*(contact_area_solid_gas_volReactor/Mw('C'))
*  k('C+CO2') * (pressure * mole_fraction('carbon dioxide'))*(1 - carbon_conversion)*sqrt(1-
psp_CARBON_DIOXIDE*log(1-carbon_conversion));
```

```
      End
#----------------STEAM GasIFICATION
      If mass_flow('C') < 0.001 Then
          E_scale*Rxn_rate('C+H2O') =
E_scale*(contact_area_solid_gas_volReactor/Mw('C')) * (mass_flow('C')/0.001)*
k('C+H2O') * (pressure * mole_fraction('WATER'))*(1 - carbon_conversion)*sqrt(1-
psp_WATER*log(1-carbon_conversion));
      Else
          E_scale*Rxn_rate('C+H2O') =
E_scale*(contact_area_solid_gas_volReactor/Mw('C')) *  k('C+H2O') * (pressure *
mole_fraction('WATER'))*(1 - carbon_conversion)*sqrt(1-psp_WATER*log(1-
carbon_conversion));
      End
#----------------HYDROGEN GasIFICATION
      If mass_flow('C') < 0.001 Then
          E_scale*Rxn_rate('C+H2') = E_scale*(contact_area_solid_gas_volReactor/Mw('C'))
* (mass_flow('C')/0.001) * k('C+H2') * (pressure * mole_fraction('hydrogen'))*(1 -
carbon_conversion)*sqrt(1-psp_HYDROGEN*log(1-carbon_conversion));
      Else
          E_scale*Rxn_rate('C+H2') = E_scale*(contact_area_solid_gas_volReactor/Mw('C'))
* k('C+H2') * (pressure * mole_fraction('hydrogen'))*(1 - carbon_conversion)*sqrt(1-
psp_HYDROGEN*log(1-carbon_conversion));
      End

# All rxn rates are now consistently in kmol/m3/s, so this allows the comp_rxn_rate to be
elegantly calcuated as:
   For i in components Do
     comp_rxn_rate(i) =  sigma(Nu(i,)* Rxn_rate());
   End

#-----------------------------------------
# Port info
  info.Tg = Tg;
  info.Tp = Tp;
  info.Xc = Xc;
  info.carbon_conversion = carbon_conversion;
  info.density = rho_g;
  info.gasifier_pressure = pressure;
  info.mass_flow() = mass_flow();
  info.mole_fraction() = mole_fraction();
  info.WGSR_Ratio = WGSR_Ratio;
  info.comp_rxn_rate = comp_rxn_rate;
  info.particle_diameter = Dp;
  info.contact_area_solid_gas_volReactor = contact_area_solid_gas_volReactor;
#  info.vp   = vp;
#  info.CellVolume = CellVolume;
```

Combustion Zone (CSTR)

```
#=============================================================
PARAMETER
   phys_prop   as  FOREIGN_OBJECT
   Components  as  ORDERED_SET
   Gases       as  ORDERED_SET
   Solids      as  ORDERED_SET
#   Rxns        as  ORDERED_SET
   Mw          as  Array(Components) of Real
   # FEED
   coal_cv           as  Real
   heating_value   as  Array(Gases) of Real
   Hf_std AS Array(Gases) of Real
   R   as  Real    Default  0.008314 # kJ/mol.K
   PI  as  Real    Default  3.142857
   tref          as  Real  Default 298  #    K
   ViewFactor_wp  as  Real
   emissivity_gp  as  Real
   emissivity_wp  as  Real
   SBC           as  Real  # W m-2 K-4
   Alpha         as  REAL DEFAULT 1
   AlphaR        as  REAL DEFAULT 1
   ExitTemp      as  REAL
#=============================================
   # SCALING
   H_scale     as Real Default 1e-3
   E_scale     as Real Default 1e-3
#   E_Scale     AS REAL DEFAULT 1e-6
   L_scale     as REAL DEFAULT 1e-6
#=============================================================
=============================================================
=================

PORT
   inlet   as Material
   outlet  as Material
   kinetics as kinetic_info

PORTSET
# Start Port Sets
   "streams" AS [inlet, outlet]
# End Port Sets


VARIABLE
   Tin   as  temperature
   Tp  as  temperature
   Tg    as  temperature
   Tw  as  temperature
   O_C as  ratio
```

```
   Xc  as conversion
   WGSR_Ratio        as  ratio
   comp_rxn_rate     as  ARRAY(components) of   reaction_rate
   mass_fraction     as  ARRAY(Gases)   of   massfraction
   mass_flow         as  ARRAY(Components) of   flowrate
   Gas_flow            as  flowrate
   Gas_flux          as  massflux
   total_mass_flow   as  flowrate
   mass_flow_in      as  ARRAY(Components) of flowrate
   mole_flow           as  ARRAY(Components)  of molar_flowrate
   total_mole_flow   as  molar_flowrate
   mole_fraction     as  ARRAY(Gases) of  molefraction
   carbon_out          as  flowrate
   carbon_conversion   as  conversion
   rho_g               as  density
   rho_p             as  density
   CellLength        as  length
   CellDiameter      as  length
   CellArea          as  area
   CellVolume        as  Volume
   Pressure          as  pressure
   gasifier_pressure   as  pressure
   d_P               as  pressure
   contact_area_solid_gas_volReactor  as  contact_area
   CASGPV      as contact_area
   vp     as  velocity
   vp1    as  velocity
   vg     as  velocity
   Re_p   as  ReynoldsNumber
   Pr     as  PrandtlNumber
   Nu     as  NusseltNumber
   Cpg    as  heat_capacity
#  Qgas             AS  energy_rate
   H_p         as  mass_specific_enthalpy
   H_p1        as  mass_specific_enthalpy
   H_p2        as  mass_specific_enthalpy
   H_p3        as  mass_specific_enthalpy
   H_g         as  mass_specific_enthalpy
   Hin_p       as  mass_specific_enthalpy
   Hin_p1      as  mass_specific_enthalpy
   Hin_p2      as  mass_specific_enthalpy
   Hin_p3      as  mass_specific_enthalpy
   Hin_g       as  mass_specific_enthalpy
   Hing        as  mass_specific_enthalpy
   dQg           as  energy_rate
   dQga          as  energy_rate
   dQgr          as  energy_rate
   dQs  as  energy_rate
   dQsa          as  energy_rate
   dQsr          as  energy_rate
```

```
   Qr_pg       as  energy_rate
   Qr_pw       as  energy_rate
   Qr_gw       as  energy_rate
   Qh_pg       as  energy_rate
   Qh_gw       as  energy_rate
#   kg_comp     as  ARRAY(Gases) of conductivity
   kg              as  conductivity
#   kg_m        as   conductivity
   h_gp        as  heat_transfer_Coeff
   h_gp_max    as  heat_transfer_Coeff
   B_factor    as  no_type
   h_gw        as  heat_transfer_Coeff
   viscosity_g  as  viscosity_dynamic
   Dp          as  length # particle diameter
   theta_gw    as  no_type_gezero
   theta_pw    as  no_type_gezero
   porosity    as  no_type_gezero

#Test Variables
   Hfin as array(Gases) of  mass_specific_enthalpy
#=================================================================
=================================================================
====================
SELECTOR
  EnergyBalance   as (general, isothermal) Default general
  SolidsEnergyBal as (general, equilibrium) Default general
  Reactions       as (on,off) Default on

SET
   Components := inlet.Components;
   Solids := inlet.Solids;
   Gases := Components - Solids;
   kinetics.Components := Components;
   kinetics.Gases := Gases;
#   kinetics.Rxns := Rxns;
   phys_prop := inlet.phys_prop;
   Mw(Gases) := phys_prop.molecularWeight();
   Mw(Solids) := inlet.Mw_solids();
   kinetics.Mw := Mw;
   heating_value  := [0,    10.06,   0,    42.66,  50.1,   47.43,  120.04, 0, 0];  # MJ/kg
   Hf_std := phys_prop.IdealGasEnthalpyOfFormationAt25C();
#=================================================================
=================================================================
========
EQUATION
# -----  Inlet port connections -----------------
  mass_flow_in() = inlet.mass_flow();
  Tin = inlet.temperature;
  gasifier_pressure = inlet.pressure;
  Dp = inlet.Particle_diameter;
```

```
  rho_p = inlet.rho_p;
# ----- Outlet port connection ------------------
  outlet.mass_flow() = mass_flow();
  outlet.temperature = Tg;
  outlet.pressure = gasifier_pressure;
  outlet.Particle_diameter = Dp;
# ----- Kinetics conssections -------------------
  kinetics.carbon_conversion = carbon_conversion;
#  kinetics.Rxn_rate = Rxn_rate;
  kinetics.density = rho_g;
  kinetics.gasifier_pressure = gasifier_pressure;
  kinetics.mass_flow() = mass_flow();
  kinetics.mole_fraction() = mole_fraction();
  kinetics.particle_diameter = Dp;
  kinetics.WGSR_Ratio = WGSR_Ratio;
  kinetics.Tg = Tg;
  kinetics.Tp = Tp;
  kinetics.Xc = Xc;
  kinetics.contact_area_solid_gas_volReactor = contact_area_solid_gas_volReactor;
  Case Reactions Of
    When On: comp_rxn_rate = Alpha*kinetics.comp_rxn_rate;
    When Off: comp_rxn_rate = 0;
  End
#-------------------------------------------------------------------------------------------------------------
---------------------------
  #   PARTICLE BALANCE
  carbon_out = mass_flow('C'); # kg/s
  # Contact Area Between Solid & Gas Per Unit Volume of Reactor: m2/m3
#  CellArea*rho_p * vp = mass_flow('C'); # m/s
  vp  = Dp^2 * 9.81 * (rho_p - rho_g)/(18*viscosity_g); # Stoke's Law
  vp1 = 9.81*(Dp^2)*(rho_p - rho_g)/(18*viscosity_g);
  CASGPV  = (mass_flow('C')/(CellArea*vp1))*(6/(Dp * rho_p));
  contact_area_solid_gas_volReactor  = (mass_flow('C')/(CellArea*vp1))*(6/(Dp *
rho_p)){(6/Dp)*(mass_flow('C')/CellVolume/rho_p)};   # m2 of solid gas contact area per
m3 of reactor: Wen & Chaung 1979
  #   Char/Carbon Conversion
  Xc = (mole_flow('methane') + mole_flow('carbon monoxide') + mole_flow('carbon
dioxide'))/mass_flow_in('C');
  carbon_conversion    =   1 - (carbon_out/mass_flow_in('C'));     #   Carbon_in is from
Proximate Analysis / Units: -
#-------------------------------------------------------------------------------------------------------------
---------------------------
   #   GAS BALANCE
#-------------------------------------------------------------------------------------------------------------
-------------------------
  For i in components  Do
    1e-6*mass_flow(i) = 1e-6*(mass_flow_in(i) + (comp_rxn_rate(i) * Mw(i) * CellVolume));
# (kg/s) I multipled by Mw(i) because comp_rxn_rate is in kmol/s.m3
  End
  total_mass_flow = sigma(mass_flow()); # kg/s
```

```
  #   Gas Flow rate (kg/s)
  Gas_flow = sigma(mass_flow(Gases));   # kg/s
  CellArea*Gas_flux = Gas_flow;         # kg/s/m^2
  CellArea* rho_g * vg = Gas_flow;     # m/s
  mass_fraction(Gases) * Gas_flow = mass_flow(Gases); # -
  Mw() * {0.001 *} mole_flow() = mass_flow();  # kmol/s
  total_mole_flow = sigma (mole_flow());       # kmol/s
  sigma(mole_flow(Gases)) * mole_fraction(Gases) = mole_flow(Gases); # -
    # Oxygen to carbon ratio
       O_C = (mass_flow_in('oxygen')/(Mw('oxygen')/2)) / (((54.11/100)*(28 -
28*((8.09+21.77)/100)))/Mw('C'));
#-------------------------------------------------------------------------------------------------------------
-------------------------
    # OTHER EQUATIONS
#-------------------------------------------------------------------------------------------------------------
-------------------------
    # Presssure Drop
       porosity = 1 - (rho_g/rho_p);
       d_P = -(Gas_flux*(1 - porosity)/(rho_g*9.81*Dp*porosity^3))*((150*viscosity_g*(1-
porosity)/Dp) + 1.75*Gas_flux); #Pa [Fogler 1999]
       Pressure = gasifier_pressure*101.325e3 + d_P; # Pa
#   d_P = 32 * viscosity_g * CellLength * vg / CellDiameter^2; # Hagen-Poiseuille Equation
#   Pressure = gasifier_pressure + d_P;

  # GASIFIER CROSS SECTIONAL AREA
  CellArea   =   PI * (CellDiameter^2)/4;   # m^2
  CellVolume =   CellArea*CellLength;       # m^3
  # Dimensionless Groups
  Re_p = rho_g * Dp * abs(vp - vg)/viscosity_g;   # -
  Pr   = viscosity_g*Cpg/kg;    # -
#  Nu   = 2 + (0.4*sqrt(Re_p) + 0.06*(Re_p^(2/3))) *(Pr^(0.4));  # - Can't find the source
  Nu   = 2 + 0.5*sqrt(Re_p); # - Guo et. al., 2013
  B_factor*(PI*Dp*Nu*kg) = -mass_flow('C')*Cpg; # -

  # GAS PHYSICAL PROPERTIES
  kg        =  phys_prop.VapourThermalConductivity(Tg,pressure,mass_fraction(Gases)); #
W/m/k
  Cpg       =  phys_prop.VapourHeatCapacity(Tg,pressure,mass_fraction()); # J/kg.K
  rho_g     =  phys_prop.VapourDensity(Tg,pressure,mass_fraction(Gases)); # kg/m^3
  viscosity_g = phys_prop.VapourViscosity(Tg,pressure,mass_fraction(Gases));  # Pa.s =
kg/m.s

  # CONVECTION HEAT TRANSER COEFFICIENTS
  h_gp      =   Nu * kg/Dp;    # W/m^2/K
  h_gp_max  =   35.8*(kg^0.6)*(rho_p^0.2)/(Dp^0.36);   # W/m^2/K - Zabrodsky (1966)
  h_gw      =   (0.023*(Gas_flux^0.8/(CellDiameter^0.2)))*((Cpg^0.4) * kg^0.6 /
viscosity_g^0.4)*(Tg/Tw)^0.8; # W/m^2/K
```

```
#=================================================================
=================================================================
=======
   #   ENERGY BALANCE
#=================================================================
=================================================================
=======
  # Specific Mass Enthalpies
  L_Scale*H_g    = L_Scale*phys_prop.VapourEnthalpy(Tg,pressure,mass_fraction()); # J/kg
  L_Scale*Hin_g  =
L_Scale*phys_prop.VapourEnthalpy(Tin,pressure,inlet.mass_flow(Gases)/sigma(inlet.mass_
flow(Gases)));   # J/kg
  L_Scale*Hing   =
L_Scale*(phys_prop.VapourEnthalpy(Tin,pressure,inlet.mass_flow(Gases)/sigma(inlet.mass
_flow(Gases))) + sigma(inlet.mass_flow(Gases)/sigma(inlet.mass_flow(Gases))*Hf_std()));
# J/kg
#Test 1
  L_Scale*H_p2    = L_Scale*(0.4979*(Tp^2 - tref^2)  + 731.87*(Tp - tref) - 79021); # J/kg
  L_Scale*Hin_p2  = L_Scale*(0.4979*(Tin^2 - tref^2)  + 731.87*(Tin - tref) - 79021); #
J/kg
#Test 2
    L_Scale*H_p1   = L_Scale*(2.44517e-8*(Tp - Tref)^4 + 2.24636e-5*(Tp - Tref)^3 +
1844.27*(Tp - Tref) - 298000);   # J/kg
    L_Scale*Hin_p1 = L_Scale*(2.44517e-8*(Tin - Tref)^4 + 2.24636e-5*(Tin - Tref)^3 +
1844.27*(Tin - Tref) - 298000);   # J/kg

#  TEST 3: Eisermann et. al., 1980
    L_Scale*Hin_p = L_Scale*((-0.218)*(Tin - Tref) + (3.807e-3/2)*(Tin^2 - Tref^2) -
(1.758e-6/3)*(Tin^3 - Tref^3))*1000; # Eisermaa W., Johanson P., Conger W.L.: Estimating
thermodynamic properties of coal, char, tar and ash. Fuel Processing Technology, 1980, 3,
39-53
    L_Scale*H_p   = L_Scale*((-0.218)*(Tp - Tref) + (3.807e-3/2)*(Tp^2 - Tref^2) - (1.758e-
6/3)*(Tp^3 - Tref^3))*1000; # Eisermann W., Johanson P., Conger W.L.: Estimating
thermodynamic properties of coal, char, tar and ash. Fuel Processing Technology, 1980, 3,
39-53

# Vamvuka et al (1995)
    L_scale*Hin_p3 = L_scale*(0.222*(Tin - Tref) + (2.18E-4/2)*(Tin^2 - Tref^2) +
(9741.666/(Tin - Tref)))*1000*4.1858; # J/kg.K
    L_scale*H_p3   = L_scale*(0.222*(Tp - Tref) + (2.18E-4/2)*(Tp^2 - Tref^2) +
(9741.666/(Tp - Tref)))*1000*4.1858; # J/kg.K

    Hfin() = Hf_std();

#------------------------------ Energy Balance ---------------------------------
    L_scale * dQg  =  L_scale * (-Qr_pg - Qh_pg - Qr_gw - Qh_gw); # W
    L_scale * dQga =  L_scale * (0); # W
    L_scale * dQgr =  L_scale * (Qr_pg + Qh_pg + Qr_gw + Qh_gw); # W
    L_scale * dQs  =  L_scale * (Qr_pg - Qr_pw + Qh_pg);       # W
    L_scale * dQsa =  L_scale * (Qr_pg + Qh_pg);       # W
```

```
   L_scale * dQsr =  L_scale * (Qr_pw);       # W
   theta_gw = Tg/Tw;   # -
   theta_pw = Tp/Tw;   # -
   L_Scale*Qr_gw = L_Scale*CellVolume * (4/CellDiameter) * (emissivity_wp *
ViewFactor_wp * SBC * Tw^4 * (theta_gw^4 - 1));    # W
   L_Scale*Qh_gw = L_Scale*CellVolume * (4/CellDiameter) * h_gw * (Tg - Tw);
   L_Scale*Qr_pw = L_Scale*CellVolume * (4/CellDiameter) * (emissivity_wp *
ViewFactor_wp * SBC * Tw^4 * (theta_pw^4 - 1));    # W
   E_Scale*Qr_pg = E_Scale * CellVolume * contact_area_solid_gas_volReactor *
(emissivity_gp * ViewFactor_wp * SBC * (Tg^4 - Tp^4 ));  # W
   E_Scale*Qh_pg = E_Scale * CellVolume * contact_area_solid_gas_volReactor * h_gp *
(Tg - Tp);    # W

   # Gas energy balance
   Case EnergyBalance Of
     When general:
         # GAS BALANCE
        L_Scale*(sigma(mass_flow_in(Gases))*Hin_g - Gas_flow*H_g + dQga - dQgr)  = 0; #
kW
     When isothermal: Tg = ExitTemp;   # K
   End
   # Solids energy balance
   Case SolidsEnergyBal OF
     When general:
       L_Scale*(mass_flow_in('C') * Hin_p - mass_flow('C') * H_p + dQsa - dQsr)  = 0;  # kW
     When equilibrium:
       Tp = Tg;    # K
       Qr_pg = 0;
       Qh_pg = 0;
   End

INITIALISATION_PROCEDURE Init Default
Start
  Alpha := 0;
  AlphaR := 0;
  Reactions := off;
  EnergyBalance := isothermal;
End
Next
  Jump_To Revert Reactions; End
End
#Next
#  Jump_To Alpha := 0.01; End
#End
Next
  Jump_To Alpha := 0.1; End
End
Next
  Jump_To Alpha := 0.2; End
End
```

```
Next
  Jump_To Alpha := 0.3; End
End
Next
  Jump_To Alpha := 0.4; End
End
Next
  Jump_To Alpha := 0.5; End
End
Next
  Jump_To Revert Alpha; End
End
Next
  Jump_To Revert EnergyBalance; End
End
Next
  Jump_To Revert AlphaR; End
End

#-------------------------------------------------------------------------------------------------------------
```

Gasification Zone (PFR)

```
#============================================================
PARAMETER
   phys_prop   as  Foreign_Object
   Components  as  Ordered_Set
   Gases       as  Ordered_Set
   Solids      as  Ordered_Set
   Mw          as  Array(Components) of Real
#    Rxns       as  Ordered_Set
   # FEED
   coal_cv           as  Real
   heating_value   as  Array(Gases) of Real
   R   as  Real    Default  0.008314 # kJ/mol.K = MPa.m3/kmol.k
   PI  as  Real    Default  3.142857
   tref          as  Real  Default 298  #    K
   Patm          as  Real  Default 101325 #Pa
   ViewFactor_wp  as  Real
   emissivity_gp  as  Real
   emissivity_wp  as  Real
   SBC           as  Real  # W m-2 K-4
   Alpha         as  REAL DEFAULT 1
   roughness      as  Real Default 1.2e-4

#=============================================
   # SCALING
   H_scale     as Real Default 1e-3
   R_scale     as Real Default 1e-3
   E_Scale     as REAL DEFAULT 1e-6
   L_scale     as REAL DEFAULT 1e-9
```

```
#=============================================================
=============================================================
=================

PORT
   inlet as Material
   outlet as Material
   kinetics as kinetic_info_array

PORTSET
# Start Port Sets
   "streams" AS [inlet, outlet]
# End Port Sets

DISTRIBUTION_DOMAIN
   Axial  as  [0  :  1]

VARIABLE
   Tin  as  temperature
   Tp  as  Distribution(Axial) of temperature
   Tg   as  Distribution(Axial) of temperature
   Xc  as  Distribution(Axial) of conversion
   Tw  as  temperature
   tres as Distribution(Axial) of residence_time
   WGSR_Ratio          as  Distribution(Axial) of ratio
   comp_rxn_rate       as  Distribution(components,Axial) of   reaction_rate
   mass_fraction       as  Distribution(Gases,Axial)   of   massfraction
   mole_fraction_o     as  Distribution(Gases) of molefraction
   mass_flow           as  Distribution(Components,Axial) of   flowrate
   Gas_flow            as  Distribution(Axial) of flowrate
   Gas_flux            as  Distribution(Axial) of massflux
   total_mass_flow     as  Distribution(Axial) of flowrate
   mass_flow_in        as  Array(Components) of flowrate
   mole_flow           as  Distribution(Components,Axial)  of molar_flowrate
   total_mole_flow     as  Distribution(Axial) of molar_flowrate
   mole_fraction       as  Distribution(Gases,Axial) of  molefraction
   carbon_out          as  Distribution(Axial) of flowrate
   carbon_conversion   as  Distribution(Axial) of conversion
   cold_gas_efficiency as  Distribution(Axial) of efficiency
   syngas_cv           as  Distribution(Axial) of energy_rate
   obj_cv              as  Distribution(Axial) of mass_specific_enthalpy
   obj_cv_out          as  mass_specific_enthalpy
   obj_eff             as  Distribution(Axial) of efficiency
   CO_H2_ratio         as  Distribution(Axial) of ratio
   rho_g               as  Distribution(Axial) OF density
   rho_g_st            as  Distribution(Axial) OF density
   MassFlowC0          as  flowrate
   rho_p               as  density
   ZoneLength          as  length
   ZoneDiameter        as  length
```

```
   ZoneArea           as  area
   ZoneVolume         as  Volume
   Pressure           as  Distribution(Axial) of pressure
#   Pressure1         as  Distribution(Axial) of pressure
   gasifier_pressure   as  pressure
   contact_area_solid_gas_volReactor  as Distribution(Axial) of contact_area
   vp     as  Distribution(Axial) of velocity
   vg     as  Distribution(Axial) of velocity
   Re_p   as  Distribution(Axial) of ReynoldsNumber
   Re_g   as  Distribution(Axial) of ReynoldsNumber
   Pr     as  Distribution(Axial) of PrandtlNumber
   Nu     as  Distribution(Axial) of NusseltNumber
   Cpg    as  Distribution(Axial) of heat_capacity
   H_p          as  Distribution(Axial) of mass_specific_enthalpy
   H_p1         as  Distribution(Axial) of mass_specific_enthalpy
   H_g          as  Distribution(Axial) of mass_specific_enthalpy
   dQg             as  Distribution(Axial) of energy_rate
   dQga            as  Distribution(Axial) of energy_rate
   dQgr            as  Distribution(Axial) of energy_rate
   dQs   as  Distribution(Axial) of energy_rate
   dQsa            as  Distribution(Axial) of energy_rate
   dQsr            as  Distribution(Axial) of energy_rate
   Qr_pg        as  Distribution(Axial) of energy_rate
   Qr_pw        as  Distribution(Axial) of energy_rate
   Qr_gw        as  Distribution(Axial) of energy_rate
   Qh_pg        as  Distribution(Axial) of energy_rate
   Qh_gw        as  Distribution(Axial) of energy_rate
   kg              as  Distribution(Axial) of conductivity
   h_gp         as  Distribution(Axial) of heat_transfer_Coeff
   h_gp_max     as  Distribution(Axial) of heat_transfer_Coeff
   B_factor     as  Distribution(Axial) of no_type
   h_gw         as  Distribution(Axial) of heat_transfer_Coeff
   viscosity_g  as  Distribution(Axial) of viscosity_dynamic
   Dp           as length # particle diameter
   theta_gw     as Distribution(Axial) OF no_type_gezero
   theta_pw     as Distribution(Axial) OF no_type_gezero
   d_P         as DISTRIBUTION(Axial) of pressure
#   alpha_p     as Distribution(Axial) OF no_type_gezero
#   friction_factor as Distribution(Axial) of ReynoldsNumber
   porosity    as Distribution(Axial) OF no_type_gezero
   HV_fg       as Distribution(Axial) of energy_rate
   MwAve       as Distribution(axial) of molecular_weight
#   MwAve       as Distribution(Axial) of molecular_weight
#   Mwg         as Distribution(Gases) of molecular_weight
#============================================================
============================================================
====================
SELECTOR
  EnergyBalance as (general, isothermal) Default general
  SolidsEnergyBal as (general, equilibrium) Default general
```

```
  Reactions     as (on,off) Default on

SET
    Components := inlet.Components;
    Solids := inlet.Solids;
    Gases := Components - Solids;
    kinetics.Components := Components;
    kinetics.Gases := Gases;
    phys_prop := inlet.phys_prop;
    Mw(Gases) := phys_prop.molecularWeight();
    Mw(Solids) := inlet.Mw_solids();
    kinetics.Mw := Mw;
#    kinetics.Rxns := Rxns;
    heating_value  := [0,     10.06,   0,     42.66,  50.1,   47.43,  120.04, 0, 0];                #
MJ/kg
    kinetics.Axial := Axial;

#================================================================
================================================================
========
EQUATION
# -----  Inlet port connections -----------------
  mass_flow_in() = inlet.mass_flow();
  Tin = inlet.temperature;
  gasifier_pressure = inlet.pressure;
  Dp = inlet.Particle_diameter;
  rho_p = inlet.rho_p;
# ----- Outlet port connection ------------------
  outlet.mass_flow() = mass_flow(,1);
  outlet.temperature = Tg(1);
  outlet.pressure = gasifier_pressure;
  outlet.Particle_diameter = Dp;
# ----- Kinetics connections -------------------
  kinetics.gasifier_pressure = gasifier_pressure;
  kinetics.particle_diameter = Dp;
  For z:= 0 To 1 Do
#    kinetics.Rxn_rate(z) = Rxn_rate(z);
    kinetics.carbon_conversion(z) = carbon_conversion(z);
    kinetics.density(z) = rho_g(z);
    kinetics.mass_flow(,z) = mass_flow(,z);
    kinetics.mole_fraction(,z) = mole_fraction(,z);
    kinetics.WGSR_Ratio(z) = WGSR_Ratio(z);
    kinetics.Tg(z) = Tg(z);
    kinetics.Tp(z) = Tp(z);
    kinetics.Xc(z) = Xc(z);
    kinetics.contact_area_solid_gas_volReactor(z) = contact_area_solid_gas_volReactor(z);
    Case Reactions Of
      When On: comp_rxn_rate(,z) = Alpha*kinetics.comp_rxn_rate(,z);
      When Off: comp_rxn_rate(,z) = 0;
    End
```

```
  End
#-------------------------------------------------------------------------------------------------------------
---------------------------
  #   PARTICLE BALANCE
  carbon_out = mass_flow('C',);    # kg/s
  tres() = ZoneLength/vg();
  # Contact Area Between Solid & Gas Per Unit Volume of Reactor: m2/m3
#  rho_p * vp() = mass_flow('C',)/ ZoneArea; # m/s
  vp() = 9.81 * (Dp^2) * (rho_p - rho_g())/(18*viscosity_g()); # Stoke's Law
  contact_area_solid_gas_volReactor()  = (mass_flow('C',)/(ZoneArea*vp()))*(6/(Dp *
rho_p));
#  contact_area_solid_gas_volReactor()  = 6/Dp;   # m2 of solid gas contact area per m3 of
reactor: Wen & Chaung 1979

#-------------------------------------------------------------------------------------------------------------
---------------------------
   #   GAS BALANCE
#-------------------------------------------------------------------------------------------------------------
---------------------------
  mass_flow(,0) = inlet.mass_flow();    # kg/s
  For z := 0|+ to 1 Do
    For i in components  Do
      1e-6*partial(mass_flow(i,z), Axial) =  1e-6*ZoneVolume * comp_rxn_rate(i,z) * Mw(i);
# kg/s
    End
  End
  For z := 0 To 1 Do
    total_mass_flow(z) = sigma(mass_flow(,z));  # kg/s
    #   Gas Flow rate (kg/s)
    Gas_flow(z) = SIGMA(mass_flow(Gases,z));    # kg/s
    ZoneArea*Gas_flux(z) = Gas_flow(z);         # kg/s/m^2
    ZoneArea*rho_g(z) * vg(z) = Gas_flow(z);  # m/s
    mass_fraction(Gases,z) * Gas_flow(z) = mass_flow(Gases,z);  # (-)
    Mw() {* 0.001} * mole_flow(,z) = mass_flow(,z); # kmol/s
    total_mole_flow(z) = sigma (mole_flow(,z));     # kmol/s
    sigma(mole_flow(Gases,z)) * mole_fraction(Gases,z) = mole_flow(Gases,z);    # (-)
  End
#-------------------------------------------------------------------------------------------------------------
---------------------------
    # OTHER EQUATIONS
#-------------------------------------------------------------------------------------------------------------
---------------------------

  # GASIFIER CROSS SECTIONAL AREA
  ZoneArea   =   PI * (ZoneDiameter^2)/4;   #   m2
  ZoneVolume =   ZoneArea*ZoneLength;       #   m3

  For z := 0 To 1 Do
    # Dimensionless Groups
```

```
#    friction_factor(z) = 0.25
/(log(1/(3.7*ZoneDiameter/roughness))+(5.74/(Re_g(z)^0.9)))^2; # Swamee & Jain
   Re_g(z) = rho_g(z) * vg(z) * ZoneDiameter/viscosity_g(z);
   Re_p(z) = rho_g(z) * Dp * ABS(vp(z)- vg(z))/viscosity_g(z);   # - Guo et. al., 2013
   Pr(z)   = viscosity_g(z)*Cpg(z)/kg(z);  # -
#    Nu(z)   = 2 + (0.4*sqrt(Re_p(z)) + 0.06*(Re_p(z)^(2/3))) *(Pr(z)^(0.4));    # - Can't find
the reference
   Nu(z)   = 2 + 0.5*sqrt(Re_p(z));     # - Guo et. al., 2013
   B_factor(z)*(PI*Dp*Nu(z)*kg(z)) = -mass_flow('C',z)*(Cpg(z));   # -
   # GAS PHYSICAL PROPERTIES
   kg(z)   =
phys_prop.VapourThermalConductivity(Tg(z),pressure(z),mass_fraction(Gases,z));   #
W/m/K
   Cpg(z)  = phys_prop.VapourHeatCapacity(Tg(z),pressure(z),mass_fraction(,z));  # J/kg/K
   rho_g(z)= phys_prop.VapourDensity(Tg(z),pressure(z),mass_fraction(Gases,z));   #
kg/m^3
   rho_g_st(z)= phys_prop.VapourDensity(tref,Patm,mass_fraction(Gases,0));   # kg/m^3
   viscosity_g(z) = phys_prop.VapourViscosity(Tg(z),pressure(z),mass_fraction(Gases,z));
# Pa.s = kg/m.s
   # CONVECTION HEAT TRANSER COEFFICIENTS
   h_gp(z) = Nu(z) * kg(z)/Dp; # W/m^2/K
   h_gw(z) = (0.023*(Gas_flux(z)^0.8/(ZoneDiameter^0.2)))*(Cpg(z)^0.4 * kg(z)^0.6 /
viscosity_g(z)^0.4)*(Tg(z)/Tw)^0.8;    # W/m^2/K
   h_gp_max(z) = 35.8*(kg(z)^0.6)*(rho_p^0.2)/(Dp^0.36);   # W/m^2/K
  End
  # Pressure Drop [Usually the pressure drop for gases flowing through pipies without
packing can be neglected (Fogler (1999), Page 173)]
  For z := 0 To 1 Do
     porosity(z) = 1 - (rho_g(z)/rho_p);
     d_P(z) = -(Gas_flux(z)*(1 -
porosity(z))/(rho_g(z)*9.81*Dp*porosity(z)^3))*((150*viscosity_g(z)*(1-porosity(z))/Dp) +
1.75*Gas_flux(z)); #Pa [Fogler 1999]
     Pressure(z) = gasifier_pressure*101.325e3 + (d_P(z)); # Pa
#      Pressure1(z) = gasifier_pressure* (1 - alpha_p(z)*ZoneVolume)^0.5;
#      alpha_p(z)  = 4 *
(friction_factor(z)*(rho_g(z)*vg(z))^2)/(ZoneArea*rho_g(0)*gasifier_pressure*101.325e3*Z
oneDiameter);
#      d_P(z) = 32 * viscosity_g(z) * ZoneLength * vg(z) / ZoneDiameter^2; # Pa [Hagen
Poiseuille Equation, Laminar, steady, incompressible and fully developed; Newtonian and
behaves like a continuum
#      (((gasifier_pressure*101.325e3)^2) - (Pressure1(z)*101.325e3)^2) = 4 *
friction_factor(z) *(gasifier_pressure*101.325e3/rho_g(0)) *(ZoneLength/ZoneDiameter) *
(rho_g(z)*vg(z))^2;
  End

#=============================================================
=============================================================
=======
   #   ENERGY BALANCE
```

```
#=================================================================
=================================================================
=======
  # Specific Mass Enthalpies
    # Gas Enthalpy
  For z := 0 To 1 Do
    E_Scale*H_g(z) =
E_Scale*phys_prop.VapourEnthalpy(Tg(z),pressure(z),mass_fraction(,z));   # J/kg
    # Particle Enthalpy
       #  TEST 3: Eisermann et. al., 1980
    E_Scale*H_p(z)   = E_Scale*((-0.218)*(Tp(z) - Tref) + (3.807e-3/2)*(Tp(z)^2 - Tref^2) -
(1.758e-6/3)*(Tp(z)^3 - Tref^3))*1000; # Eisermann W., Johanson P., Conger W.L.:
Estimating thermodynamic properties of coal, char, tar and ash. Fuel Processing Technology,
1980, 3, 39-53
       # Vamvuka et al (1995)
    E_scale*H_p1(z)  = E_scale*(0.222*(Tp(z) - Tref) + (2.18E-4/2)*(Tp(z)^2 - Tref^2) +
(9741.666/(Tp(z) - Tref)))*1000*4.1858; # J/kg.K
  End
##------------------------------ Energy Balance ---------------------------------
  E_Scale*dQg()  =  E_Scale*(-Qr_pg() - Qh_pg() - Qr_gw() - Qh_gw());   # W
  E_Scale*dQga() =  E_Scale*(0);   # W
  E_Scale*dQgr() =  E_Scale*(Qr_pg() + Qh_pg() + Qr_gw() + Qh_gw());   # W
  E_Scale*dQs()  =  E_Scale*(Qr_pg() - Qr_pw() + Qh_pg());          # W
  E_Scale*dQsa() =  E_Scale*(Qr_pg() + Qh_pg());          # W
  E_Scale*dQsr() =  E_Scale*(Qr_pw());          # W
  theta_gw() = Tg()/Tw; # -
  theta_pw() = Tp()/Tw; # -
  E_Scale*Qr_gw() =  E_Scale*ZoneVolume*(4/ZoneDiameter) * (emissivity_wp *
ViewFactor_wp * SBC * Tw^4 * (theta_gw^4 - 1)); # W
  E_Scale*Qh_gw() =  E_Scale*ZoneVolume*(4/ZoneDiameter) * h_gw() * (Tg() - Tw);    #
W
  E_Scale*Qr_pw() =  E_Scale*ZoneVolume*(4/ZoneDiameter) * (emissivity_wp *
ViewFactor_wp * SBC * Tw^4 * (theta_pw^4 - 1)); # W
  E_Scale*Qr_pg() =  E_Scale*ZoneVolume*contact_area_solid_gas_volReactor() *
(emissivity_gp * ViewFactor_wp * SBC * (Tg()^4 - Tp()^4 ));  # W
  E_Scale*Qh_pg() =  E_Scale*ZoneVolume*contact_area_solid_gas_volReactor() * h_gp()
* (Tg() - Tp()); # W

  # Boundary conditions
  Tg(0) = Tin;
  Tp(0) = Tin;
  # Gas energy balance
  For z := 0|+ To 1 Do
    Case EnergyBalance Of
      When general:
        # Gas Balanc
        E_Scale*(partial(Gas_flow(z) * H_g(z),Axial) - dQga(z) + dQgr(z)) = 0 ;    # W
      When isothermal: Tg(z) = Tin; # K
    End
    # Solids energy balance
```

```
    Case SolidsEnergyBal Of
      When general:
        E_Scale*(partial(mass_flow('C',z) * H_p(z),Axial) -dQsa(z) + dQsr(z)) = 0;  # K
      When equilibrium:
        Tp(z) = Tg(z);  # K
    End
  End
#-----------------------Performance Indicator----------------
  #  Char/Carbon Conversion
    Xc() = 12*(mole_flow('methane',) + mole_flow('carbon monoxide',) + mole_flow('carbon
dioxide',))/(10*MassFlowC0);
    carbon_conversion()*MassFlowC0  =   MassFlowC0 - mass_flow('C',);     #   (%)
Carbon_in is from Proximate Analysis
  # Cold Gas Efficiency
  For z := 0 To 1 Do
    cold_gas_efficiency(z) =
(sigma(mass_fraction(Gases,z)*heating_value(Gases))/coal_cv)*100;
#    cold_gas_efficiency(z) = ((mass_fraction('carbon monoxide',z)*heating_value('carbon
dioxide')
#                        + mass_fraction('methane',z)*heating_value('methane')
#                        + mass_fraction('hydrogen',z)*heating_value('hydrogen'))/coal_cv)*100;
    syngas_cv(z) = sigma(mass_fraction(Gases,z)*heating_value(Gases));
    obj_cv(z) = mass_fraction('hydrogen',z)*heating_value('hydrogen') +
mass_fraction('carbon monoxide',z)*heating_value('carbon monoxide')  +
mass_fraction('methane',z)*heating_value('methane');
    obj_eff(z) = obj_cv(z)/21*100; # %
    CO_H2_ratio(z) = mole_flow('carbon monoxide',z)/mole_flow('hydrogen',z);
    MwAve(z) = sigma(mole_fraction(Gases,z) * Mw(Gases));
  End

  # Syngas CV at the outlet of the gasifier
      mole_fraction_o(Gases) = mole_fraction(Gases,1);
      obj_cv_out = obj_cv(1);          # MJ/kg
      HV_fg() = syngas_cv()*rho_g_st(); # MJ/Nm^3
#-------------------------------------------------------------


INITIALISATION_PROCEDURE Init DEFAULT
Start
  Alpha := 0;
  Reactions := off;
  EnergyBalance := isothermal;
End

Next
  Jump_To Revert Reactions; End
End
Next
  Jump_To Alpha := 0.1; End
End
```

```
Next
  Jump_To Alpha := 0.2; End
End
Next
  Jump_To Alpha := 0.3; End
End
Next
  Jump_To Alpha := 0.4; End
End
Next
  Jump_To Alpha := 0.5; End
End
Next
  Jump_To Revert Alpha; End
End
Next
  Jump_To Revert EnergyBalance; End
End
#=============================================================
```

Gas turbine Model

Compressor Model

```
PARAMETER
   components     as  Ordered_Set
   phys_prop      as  Foreign_Object
   Mw             as  Array(components) of Real
   k              as  Real  Default 1.4 # J/kg.K
   F              as  Real  Default 2100
   Ta             as  Real  Default 288.15 # K (ambient temperature)
   Pk_i           as  Real
   mass_fraction  as  Array(components) of Real
   air_flow       as  Real
#=============================================
#PORT
#    info AS Combustor_info

VARIABLE
   Tk_o      as   temperature
   Tk_os     as   temperature
   Pk_o      as   pressure
   Pk_r      as   ratio
#    n         as   no_type
   rho_air   as   density
   k_air     as   conductivity
   u_air     as   viscosity_dynamic
   Cp_air    as   heat_capacity
   Wc        as   energy_rate
#    Wp        as   energy_rate
   nc        as   efficiency # Compressor efficiency
```

```
EQUATION
   # Properties of Air
   rho_air =   phys_prop.VapourDensity(Ta, Pk_i*101325,mass_fraction);
   k_air   =   phys_prop.VapourThermalConductivity(Ta, Pk_i*101325,mass_fraction);
   u_air   =   phys_prop.VapourViscosity(Ta, Pk_i*101325,mass_fraction);
   Cp_air  =   phys_prop.VapourHeatCapacity(Ta, Pk_i*101325,mass_fraction);
   # Compressor Model
#   Wp    =    air_flow * (Pk_i *101325e-6* n/(rho_air * (n -1))) * (Pk_r^((n - 1)/n) - 1); #
MW
   Wc    =    1e-6*air_flow * Cp_air * (Ta - Tk_os)/nc;   # MW
#   np    =    0.017*log(F) + 0.7; # %
#   n     =    np * (k)/(1 + np * k - k); # -
   Pk_r  =    Pk_o/Pk_i;
   Tk_os =    Ta * (Pk_r)^((k - 1)/k);
   Tk_o  =    Ta + (Tk_os - Ta)/nc;
#=================================================================
```

Combustor Model

```
PARAMETER
   components     as  Ordered_set
   Rxns           as  Ordered_set
   Nu             as  Array(components, Rxns) of Real
   phys_prop      as  Foreign_object
   Mw             as  Array(components) of Real
#  Fuel Gas
#   fuel_flow     as   Real
#   fuel_frac     as   Array(components) of  Real
#  Air Flow
   air_flow      as   Real
   air_frac      as   Array(components) of  Real
#  Steam Flow
   steam_flow    as  Real
   steam_frac    as  Array(components)  of  Real
#  Percentage Pressure Drop
   dP            as  Real
#   Tcr_i        as  Real

#================================================
VARIABLE
   Tcr_i         as   temperature
   Tcr_ii        as   temperature
   Tcr_o         as   temperature
   Pcr_i         as   pressure
   Pcr_o         as   pressure
   total_flow_i  as   mass_flowrate
   fuel_flow     as   mass_flowrate
#   x22          as   Array(components) of  mass_flowrate
#   feed_flow    as   Array(components) of  mass_flowrate
   fuel_frac     as   Array(components) of  massfraction
```

```
   mass_flow_i    as   Array(components) of  mass_flowrate
   mass_frac_i    as   Array(components) of  massfraction
   mole_flow_i    as   Array(components) of  molar_flowrate
   mass_flow_o    as   Array(components) of  mass_flowrate
   mass_frac_o    as   Array(components) of  mass_fraction
   mole_flow_o    as   Array(components) of  molar_flowrate
   mole_frac_i    as   Array(components) of  molefraction
   mole_frac_o    as   Array(components) of  molefraction
   total_mass_i   as   mass_flowrate
   total_mass_o   as   mass_flowrate
   total_mole_i   as   molar_flowrate
   total_mole_o   as   molar_flowrate
   Xf             as   Array(Rxns) of conversion
   Hin            as   mass_specific_enthalpy
   Hout           as   mass_specific_enthalpy

SET
   Rxns := ['CO + O2', 'CH4 + O2', 'H2 + O2'];
#                  H2O      CO     CO2     C6H6       CH4      C2H6    H2        O2          N2
   Nu(,'CO + O2')  := [0.0,   -1.0,    1.0,    0.0,      0.0,     0.0,    0.0,     -0.5,   0.5*(0.79/0.21)];
   Nu(,'CH4 + O2') := [2.0,    0.0,    1.0,    0.0,     -1.0,     0.0,    0.0,     -2.0,   2.0*(0.79/0.21)];
   Nu(,'H2 + O2')  := [1.0,    0.0,    0.0,    0.0,      0.0,     0.0,   -1.0,     -0.5,   0.5*(0.79/0.21)];

EQUATION
   # Combustion Chamber Inlet Temperature
         Tcr_ii = ((fuel_flow/(air_flow + fuel_flow))*300) + ((air_flow/(air_flow +
fuel_flow))*Tcr_i);
#          x22 = outlet.mass_flow();
   #   Pressure Drop
         Pcr_o = Pcr_i - dP * Pcr_i;
   # Properties of Gas Fluid
     # Inlet
         Hin    =   phys_prop.VapourEnthalpy(Tcr_i, Pcr_i*101325, mass_frac_i);
         Hout   =   phys_prop.VapourEnthalpy(Tcr_o, Pcr_o*101325, mass_frac_o);

   # Material Balance

   total_flow_i = fuel_flow + air_flow + steam_flow;
   For i in components Do
      mass_flow_i(i)= (fuel_frac(i) * fuel_flow) + (air_frac(i)*air_flow) +
(steam_frac(i)*steam_flow);
   End

   For i in components -'nitrogen' Do
   mole_flow_o(i) = mole_flow_i(i) - mole_flow_i('carbon monoxide') * Xf('CO + O2') *
(Nu(i,'CO + O2')/(Nu('carbon monoxide','CO + O2')))
                        - mole_flow_i('methane') * Xf('CH4 + O2') * (Nu(i,'CH4 +
O2')/(Nu('methane','CH4 + O2')))
                        - mole_flow_i('hydrogen') * Xf('H2 + O2') * (Nu(i,'H2 +
O2')/(Nu('hydrogen','H2 + O2')));
```

```
   End
   mass_flow_o('nitrogen') = mass_flow_i('nitrogen');
   mole_flow_i() = mass_flow_i()/Mw();
   mole_flow_o() = mass_flow_o()/Mw();
   total_mole_i  = sigma(mole_flow_i());
   total_mole_o  = sigma(mole_flow_o());
   total_mass_i  = sigma(mass_flow_i());
   total_mass_o  = sigma(mass_flow_o());
   mass_frac_i() = mass_flow_i()/sigma(mass_flow_i());
   mass_frac_o() = mass_flow_o()/sigma(mass_flow_o());
   mole_frac_i() = mole_flow_i()/sigma(mole_flow_i());
   mole_frac_o() = mole_flow_o()/sigma(mole_flow_o());

   #  Energy Balance
   sigma(mass_flow_i()) * Hin - sigma(mass_flow_o()) * Hout = 0;

#============================================================
```

Expander Model

```
PARAMETER
   components     as  Ordered_Set
   phys_prop      as  Foreign_Object
   Mw             as  Array(components) of Real
   R              as  Real  Default 8.314462e3 # J/kmol.K
   kg             as  Real  Default 1.333
   LHV            as  Array(components) of Real
#============================================
VARIABLE
   Tx_i        as   temperature
   Tx_o_is     as   temperature
   Tx_o_tr     as   temperature
   Px_i        as   pressure
   Px_o        as   pressure
   Px_r        as   ratio
   rho_fg      as   density
   k_fg        as   conductivity
   u_fg        as   viscosity_dynamic
   Cp_fg       as   heat_capacity
   rho_ex      as   density
   k_ex        as   conductivity
   u_ex        as   viscosity_dynamic
   Cp_ex       as   heat_capacity
   mass_fract_i as Array(components) of massfraction
   mass_fract_o as Array(components) of massfraction
   mole_fract_i as Array(components) of molefraction
   mole_fract_o as Array(components) of molefraction
   FG_flow      as   mass_flowrate
   fuel_flow    as   mass_flowrate
   fuel_frac    as   Array(components) of  massfraction
#   Cpg         as   heat_capacity
   MwAve        as   molecular_weight
```

```
#   Wc          as   energy_rate
    Wt          as   energy_rate
    Wc          as   energy_rate
    Wnet        as   energy_rate
    nt          as   efficiency # Turbine efficiency
    Therm_eff   as   efficiency # Thermal efficiency
#-----------------------------------------------
SET
    LHV  := [0,     10.06,   0,     42.66,  50.1,   47.43,  120.04, 0, 0];              # MJ/kg

#===============================================
EQUATION
    # Properties of Fuel Gas
    rho_fg =   phys_prop.VapourDensity(Tx_i, Px_i*101325,mass_fract_i);
    k_fg   =   phys_prop.VapourThermalConductivity(Tx_i, Px_i*101325,mass_fract_i);
    u_fg   =   phys_prop.VapourViscosity(Tx_i, Px_i*101325,mass_fract_i);
    Cp_fg  =   phys_prop.VapourHeatCapacity(Tx_i, Px_i*101325,mass_fract_i);
    mole_fract_i() = (mass_fract_i()*FG_flow/Mw())/sigma(mass_fract_i()*FG_flow/Mw());
    mole_fract_o() = mole_fract_i();
    MwAve          = sigma(mole_fract_i() * Mw());

#   Mass Balance
     mass_fract_i() = mass_fract_o();

    # Properties of Flue Gas
    rho_ex =   phys_prop.VapourDensity(Tx_o_tr, Px_o*101325,mass_fract_o);
    k_ex   =   phys_prop.VapourThermalConductivity(Tx_o_tr, Px_o*101325,mass_fract_o);
    u_ex   =   phys_prop.VapourViscosity(Tx_o_tr, Px_o*101325,mass_fract_o);
    Cp_ex  =   phys_prop.VapourHeatCapacity(Tx_o_tr, Px_o*101325,mass_fract_o);

    # Turbine Model
    Wt      =   -FG_flow * Cp_fg * (Tx_o_tr - Tx_i)*1e-6; # MW
    Px_r    =   Px_i/Px_o;
    Tx_o_is =   Tx_i/(Px_r)^((kg - 1)/kg);
    Tx_o_tr =   Tx_i - nt*(Tx_i - Tx_o_is);

    # Net Turbine Power
    Wnet = Wt + Wc;

    # Thermal Efficiency
    Therm_eff = Wnet/(fuel_flow*sigma(fuel_frac()*LHV()))*100;
#    Therm_eff = Wnet/(28*27)*100;
```

APPENDIX B2: Optimization Model

```
PROCESS NewGasifier

OPTIMISATION_TYPE
POINT

TIME_INVARIANT
Flowsheet.Feed.Dp
INITIAL_VALUE
4.1E-5 : 4.1E-5 : 1.0E-4

TIME_INVARIANT
Flowsheet.Feed.oxygen_rate
INITIAL_VALUE
10.25 : 5.0 : 15.0

TIME_INVARIANT
Flowsheet.Feed.Pressure
INITIAL_VALUE
20.0 : 1.0 : 50.0

TIME_INVARIANT
Flowsheet.Feed.steam_rate
INITIAL_VALUE
5.75 : 2.0 : 10.0

TIME_INVARIANT
Flowsheet.Gasifier.Tw
INITIAL_VALUE
1100.0 : 1100.0 : 1100.0

ENDPOINT_INEQUALITY
Flowsheet.Gasifier.gasifier_zone.carbon_conversion(1)
0.0001 : 1.0

#ENDPOINT_INEQUALITY
#Flowsheet.Gasifier.gasifier_zone.carbon_out(1)
#0.0 : 3000.0
#
ENDPOINT_INEQUALITY
Flowsheet.Gasifier.gasifier_zone.mole_fraction_o(1)
0.001 : 1.000001

ENDPOINT_INEQUALITY
Flowsheet.Gasifier.gasifier_zone.Tg(1)
300.0 : 3000.0

ENDPOINT_INEQUALITY
Flowsheet.Gasifier.gasifier_zone.Tp(1)
```

300.0 : 3000.0

MAXIMISE
Flowsheet.Gasifier.gasifier_zone.obj_cv_out

APPENDIX C: Model Input data

Figure C1 shows feed stream data. Physical properties of gases were obtained in Multiflash for Windows. The volatiles breakdown was also assumed as shown in Figure C1.

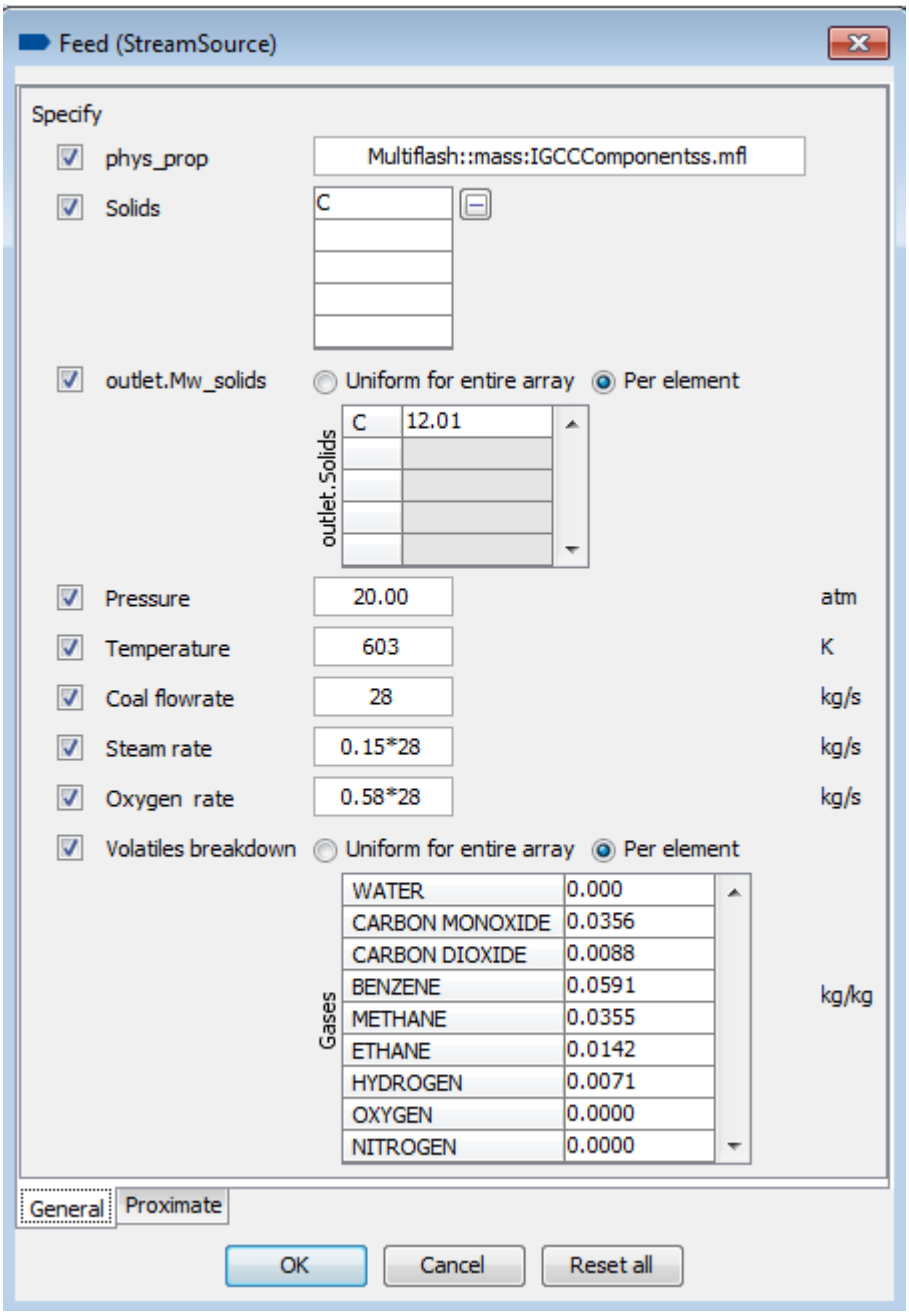

Figure C1: Gasifier inlet conditions

Figure C2 shows the particle size diameter, particle density in kg/m^3 and the Proximate Analysis of the coal used in the modeling.

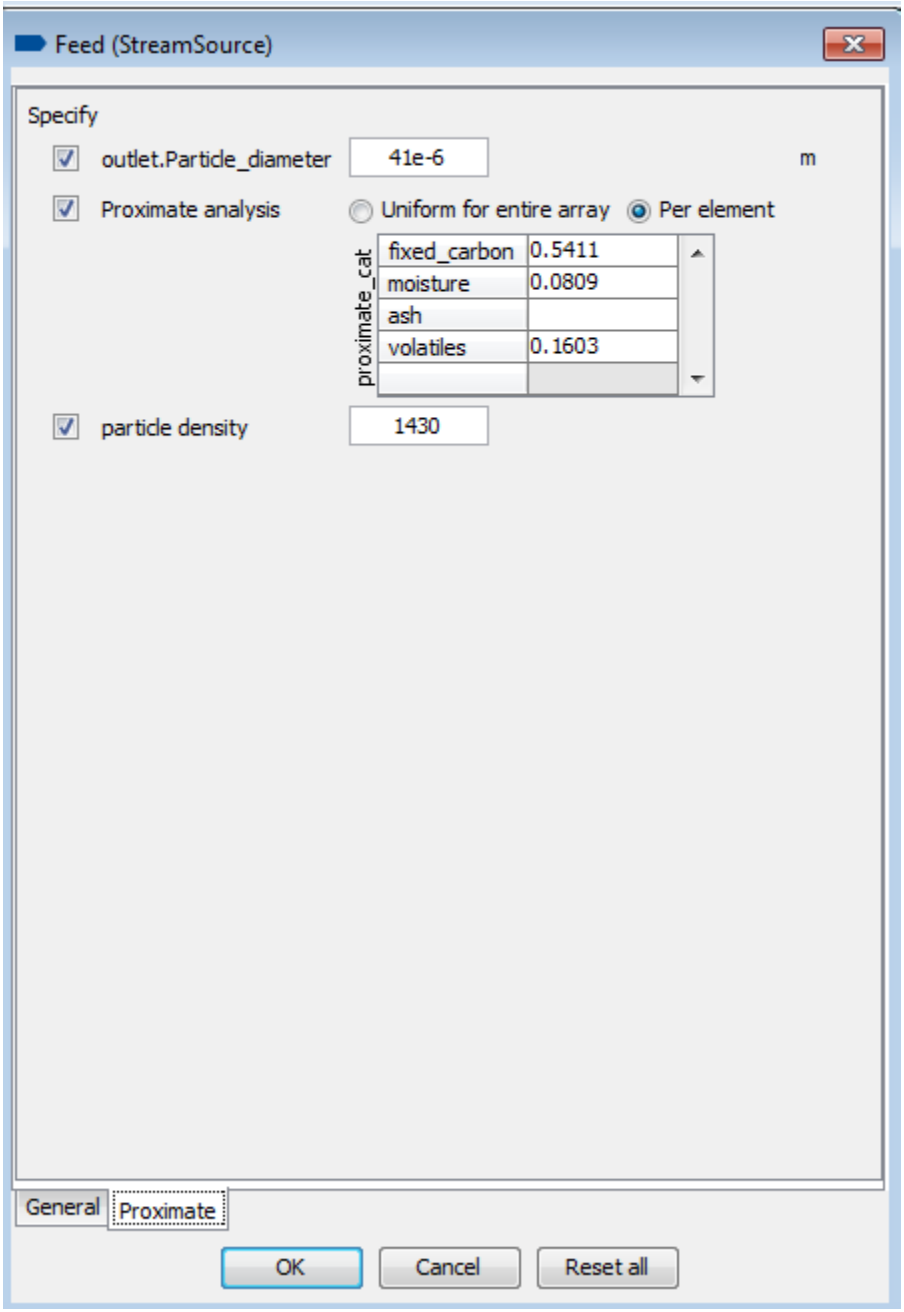

Figure C2: Gasifier Proximate Analysis

Figure C3 shows the gasifier dimensions used in the model.

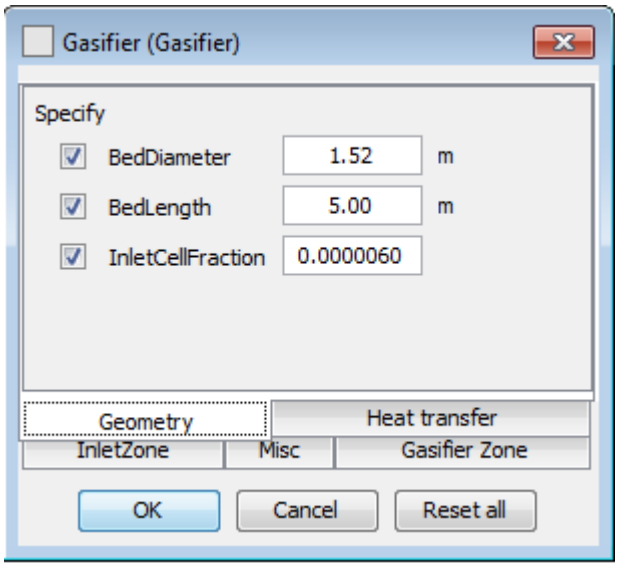

Figure C3: Gasifier Dimensions

Figure C4 shows the heat transfer data used in the model. *emissivity_gp* is the emissivity of gas-particle while *emissivity_wp* is the emissivity of wall-particle. *ViewFactor_wp* is the view factor of the wall-particle. T_w is the wall temperature of the gasifier.

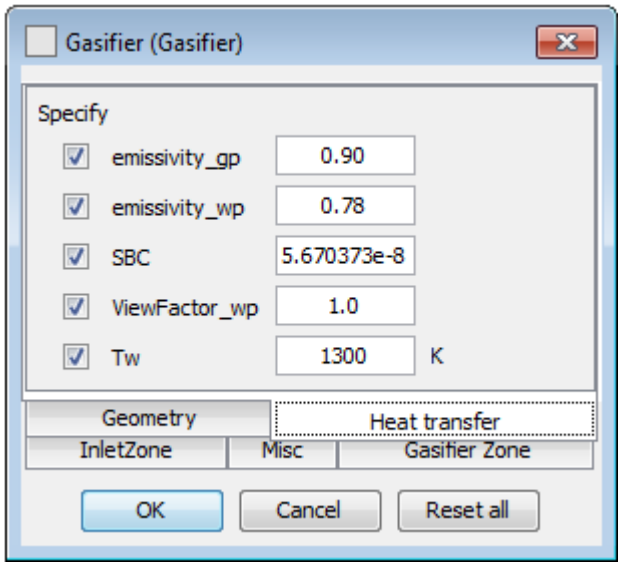

Figure C4: Heat Transfer Data

Figure C5 indicate the coupling of the energy balance in combustion chamber (CSTR) of the gasifier and initial of gas of the combustion chamber exit temperature.

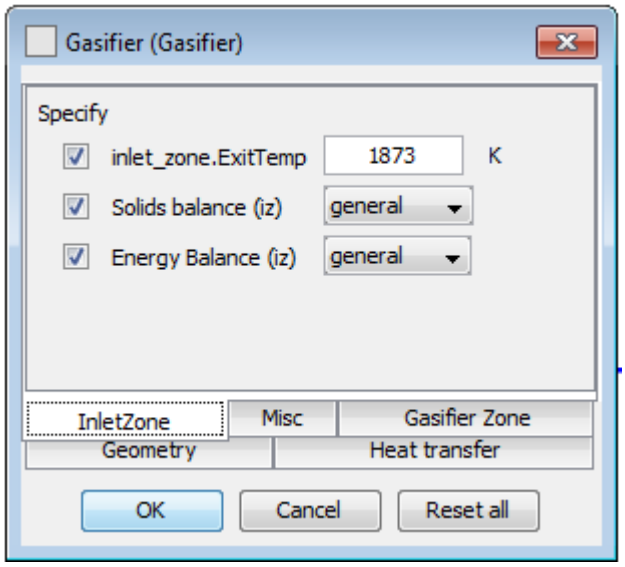

Figure C5: CSTR Energy Balance Coupling

Figure C6 indicating the heating value of the coal. This was obtained from Sofia et al., (2013).

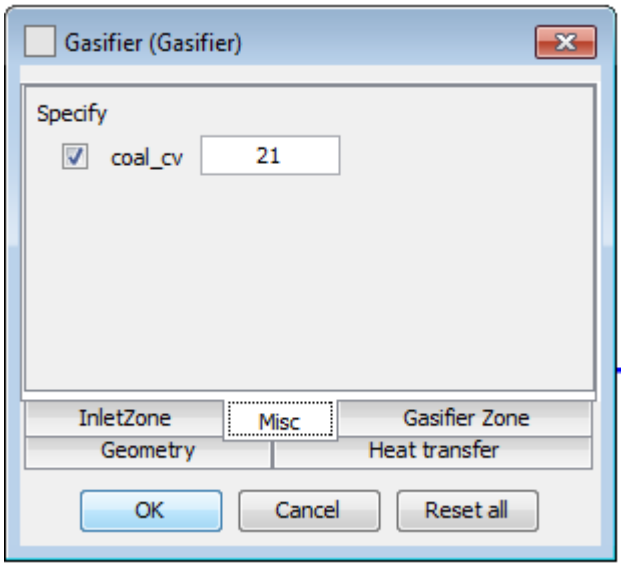

Figure C6: Feed stream heating value

Figure C7 shows the coupling of the energy balance in the gasification zone (PFR) of the gasifier.

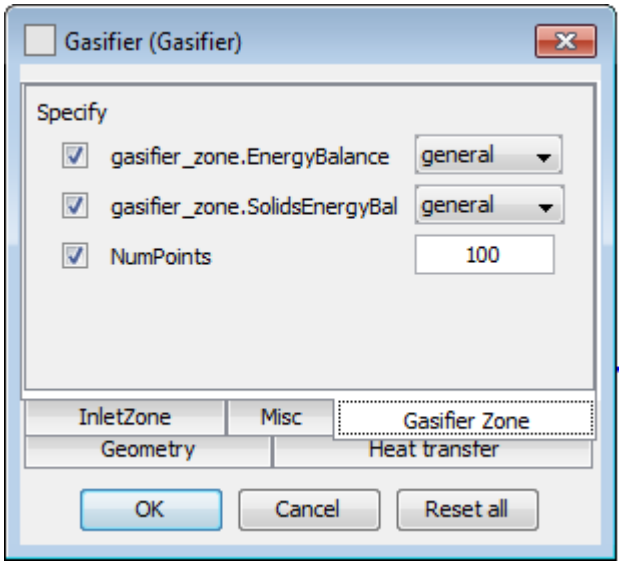

Figure C7: PFR Energy Balance Coupling

APPENDIX D: gPROMS Results

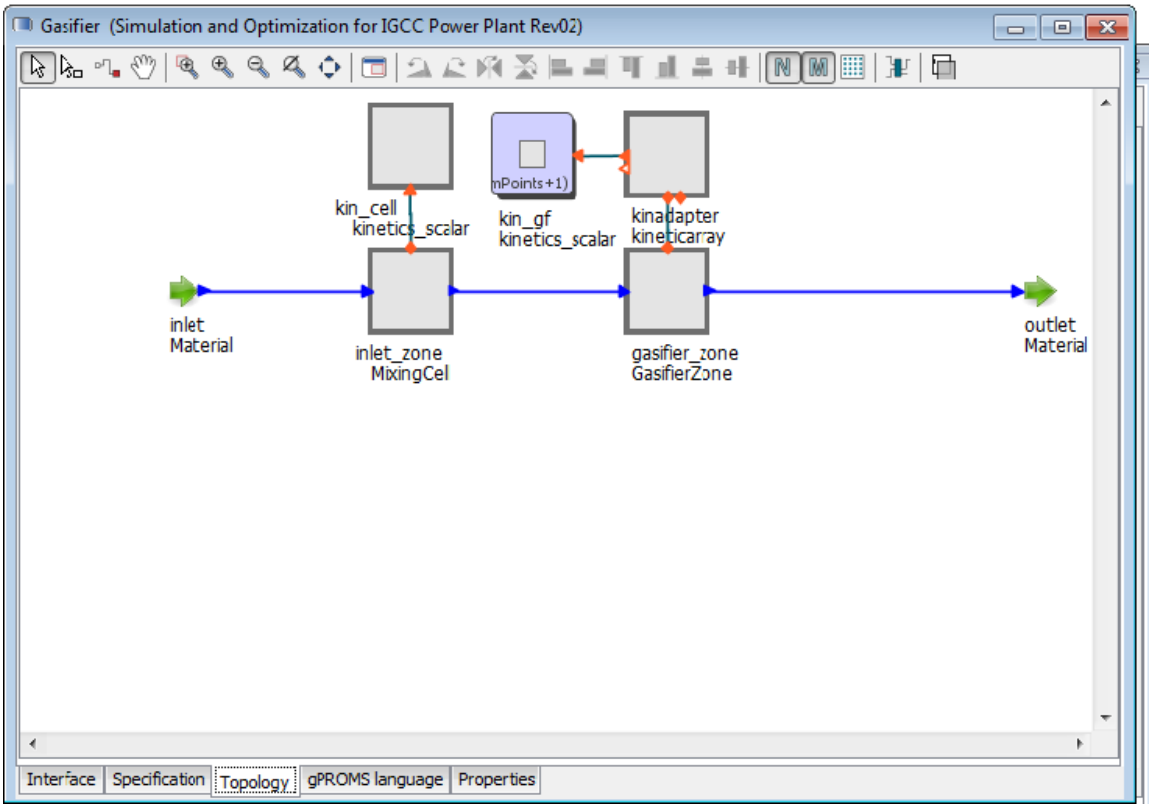

Figure D1: Model flowsheet in gPROMS

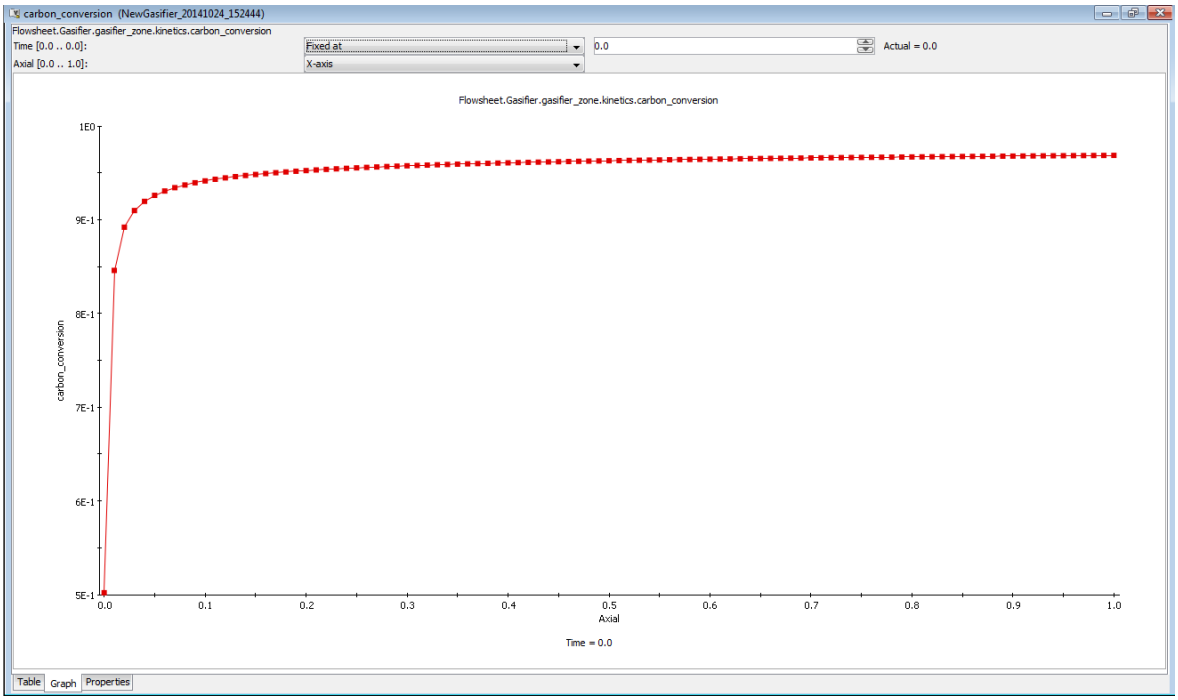

Figure D2: Simulation Model Carbon Conversion (*Simulation*)

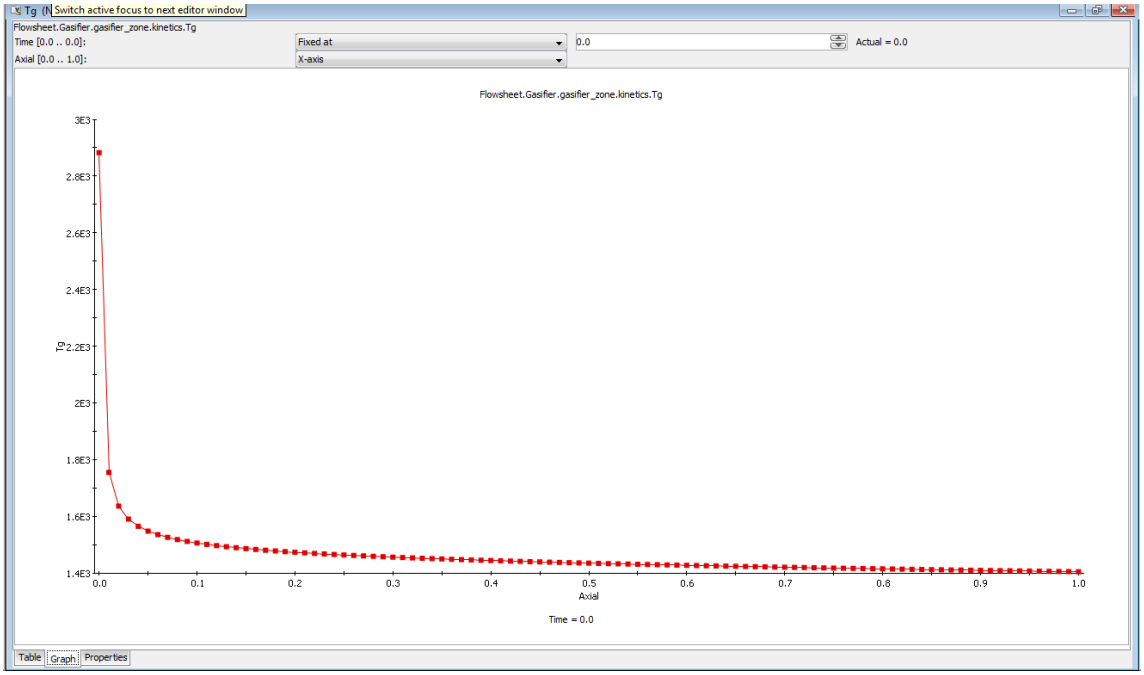

Figure D3: Gasifier Temperature profile (*Simulation*)

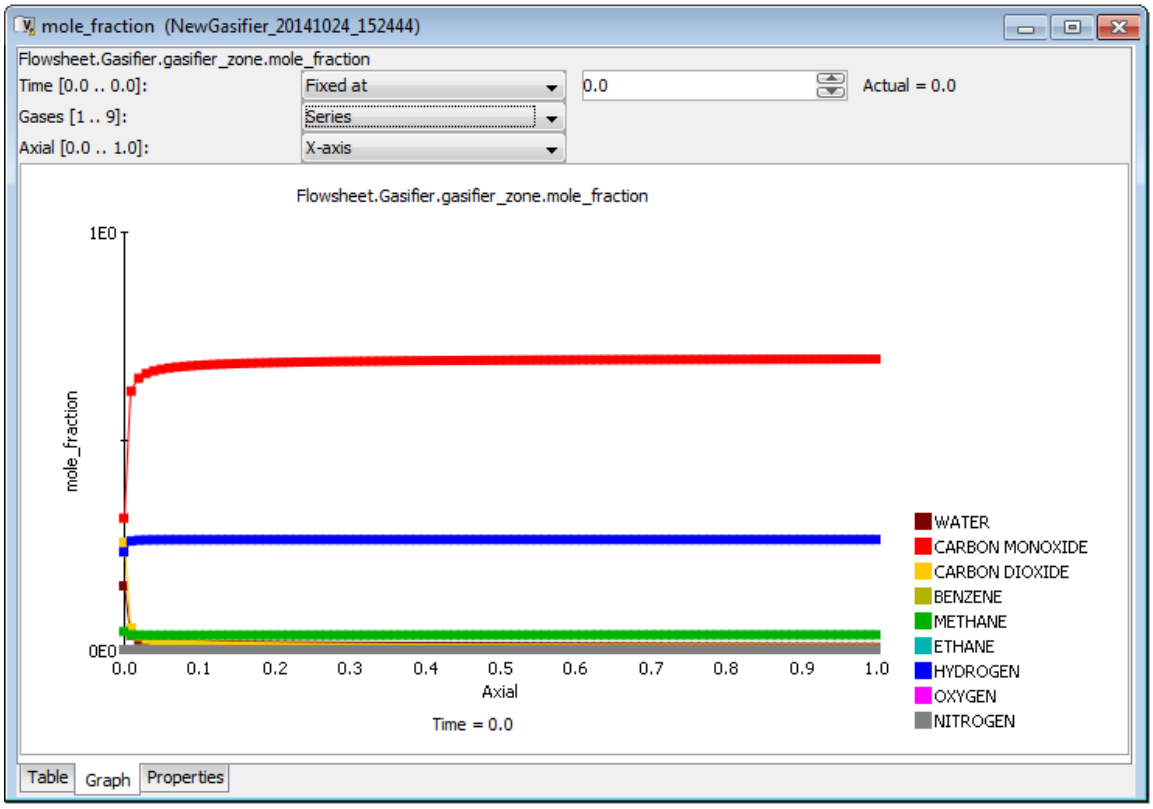

Figure D4: Mole fraction of the gases produced across the length of the gasifier

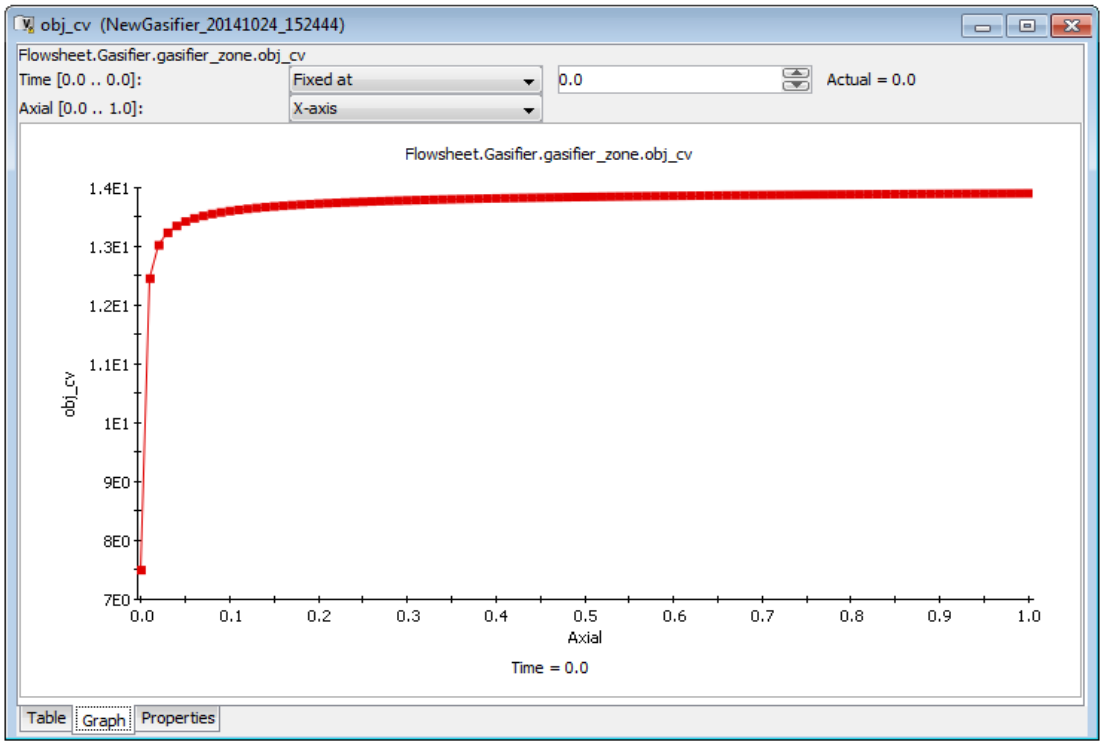

Figure D5: Heating value of the fuel gas (*Simulation*)

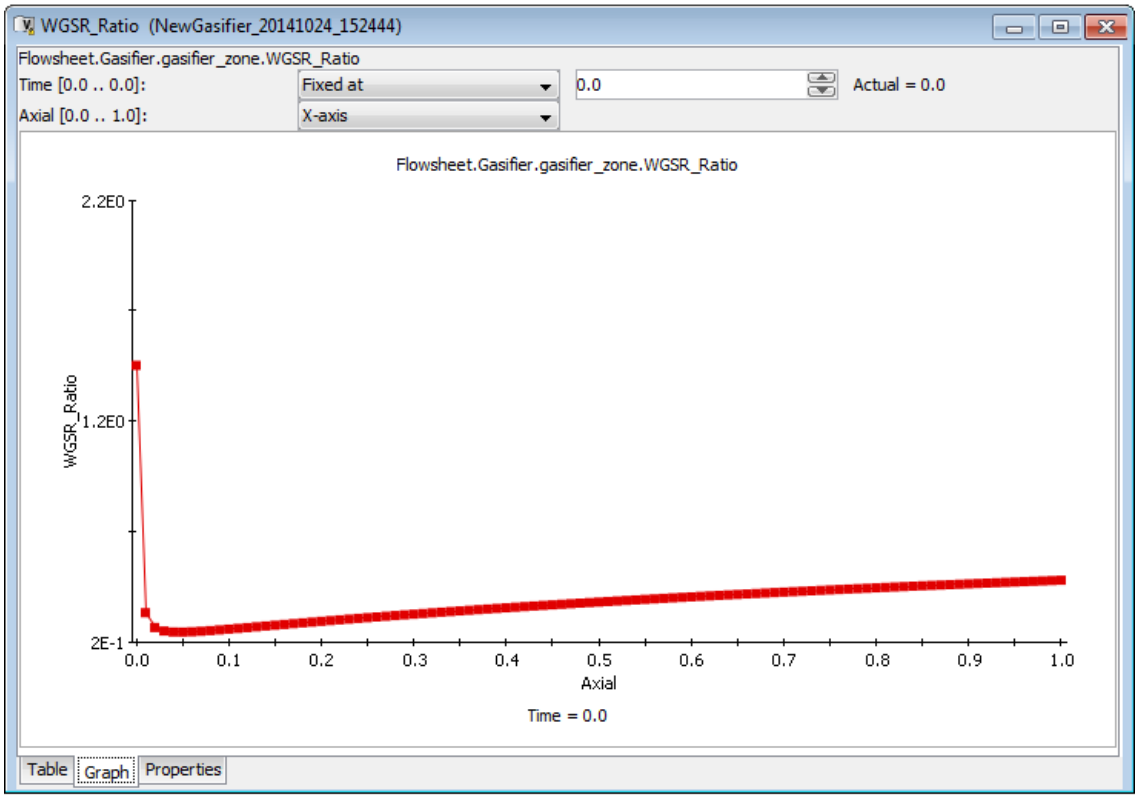

Figure D6: Ratio of the Forward WGSR to the Reverse WGSR (*Simulation*)

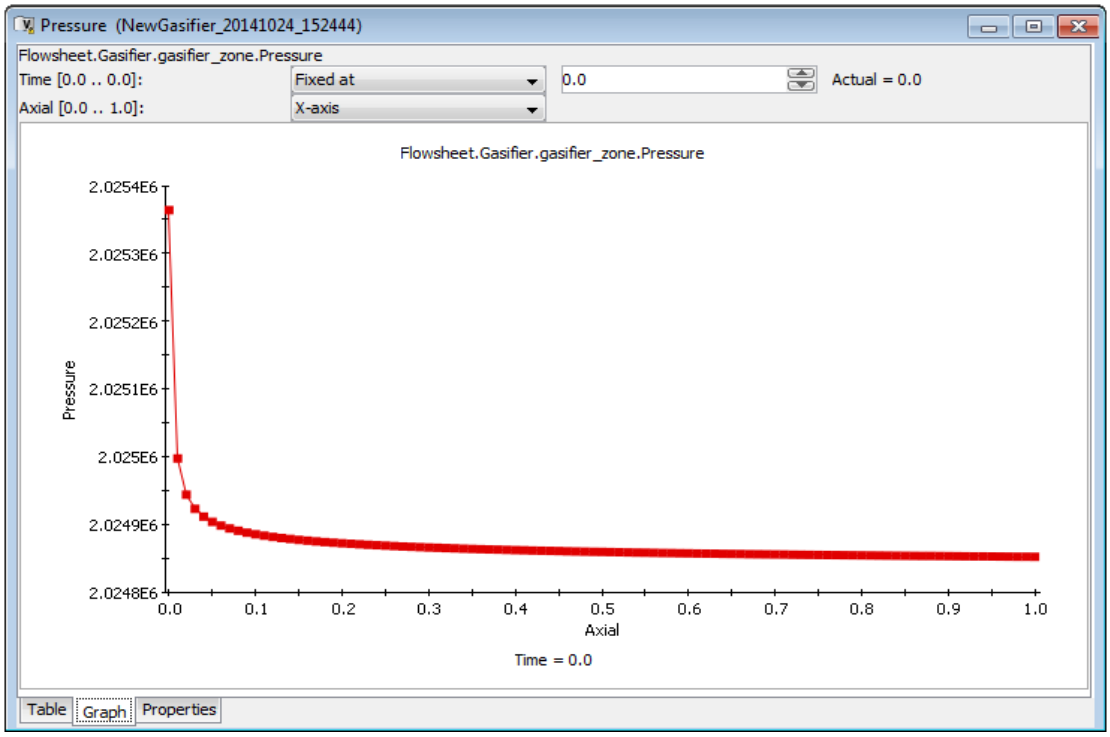

Figure D7: Pressure Drop across the length of PFR (*Simulation*)

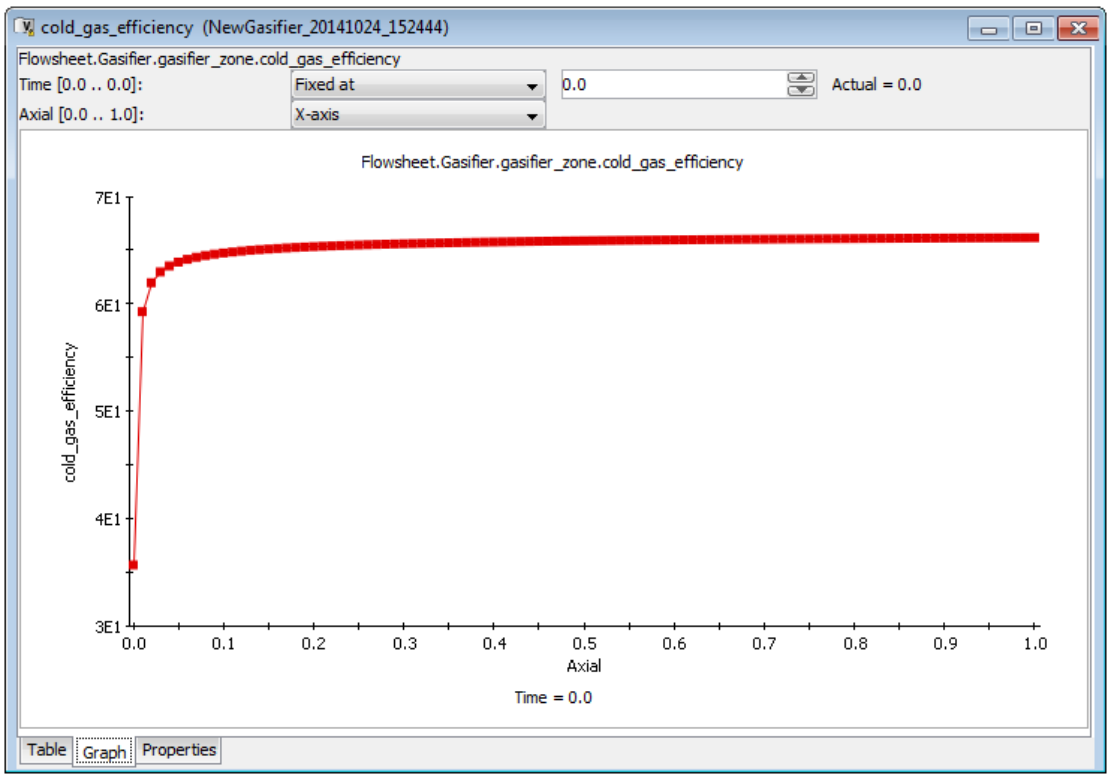

Figure D8: Cold gas efficiency (*Simulation*)

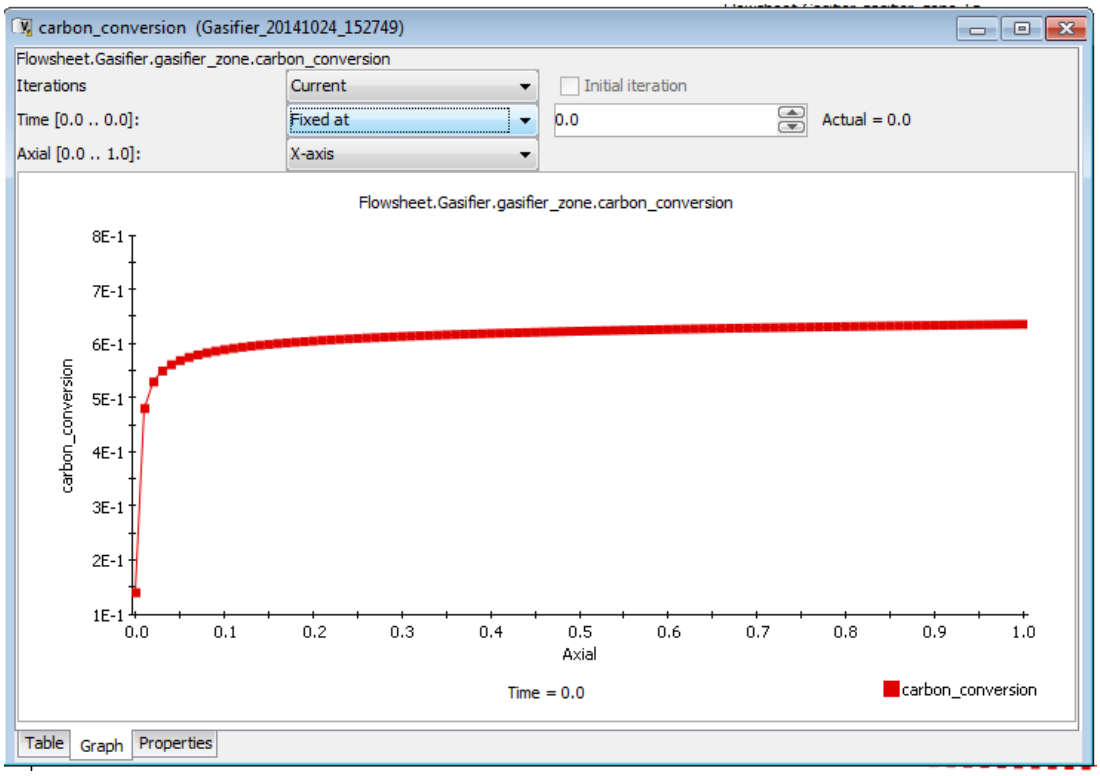

Figure D9: Carbon Conversion (*after optimization*)

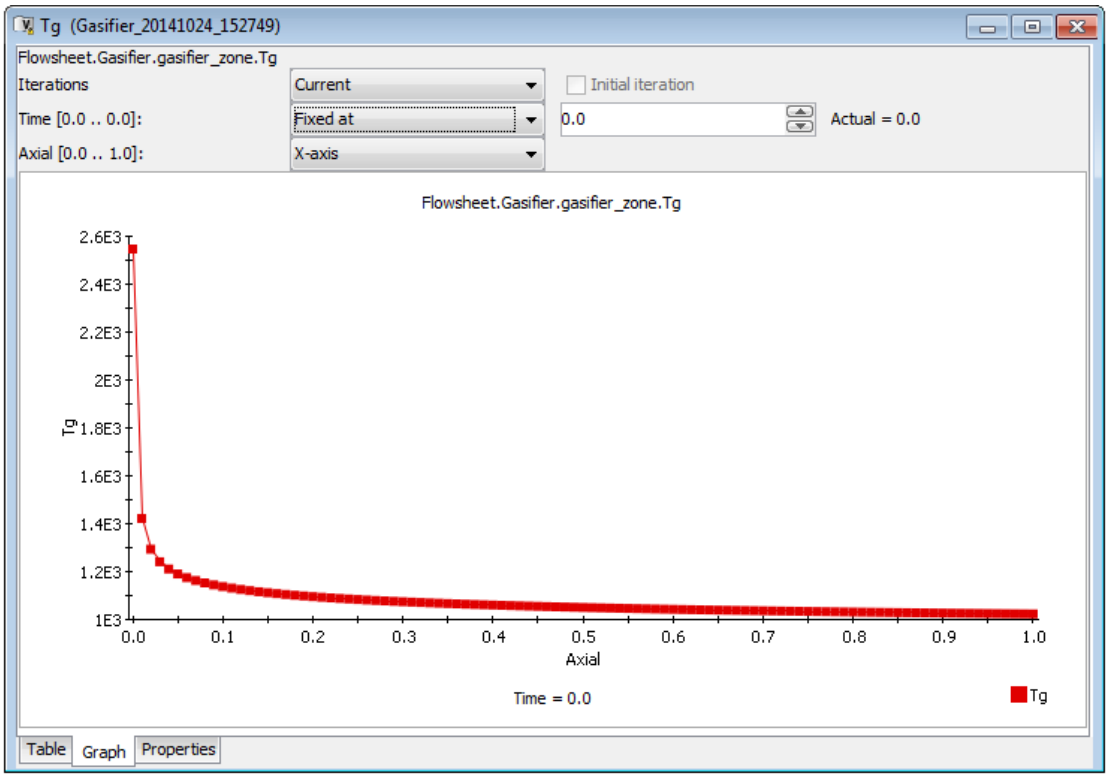

Figure D10: Gasifier temperature (*after optimization*)

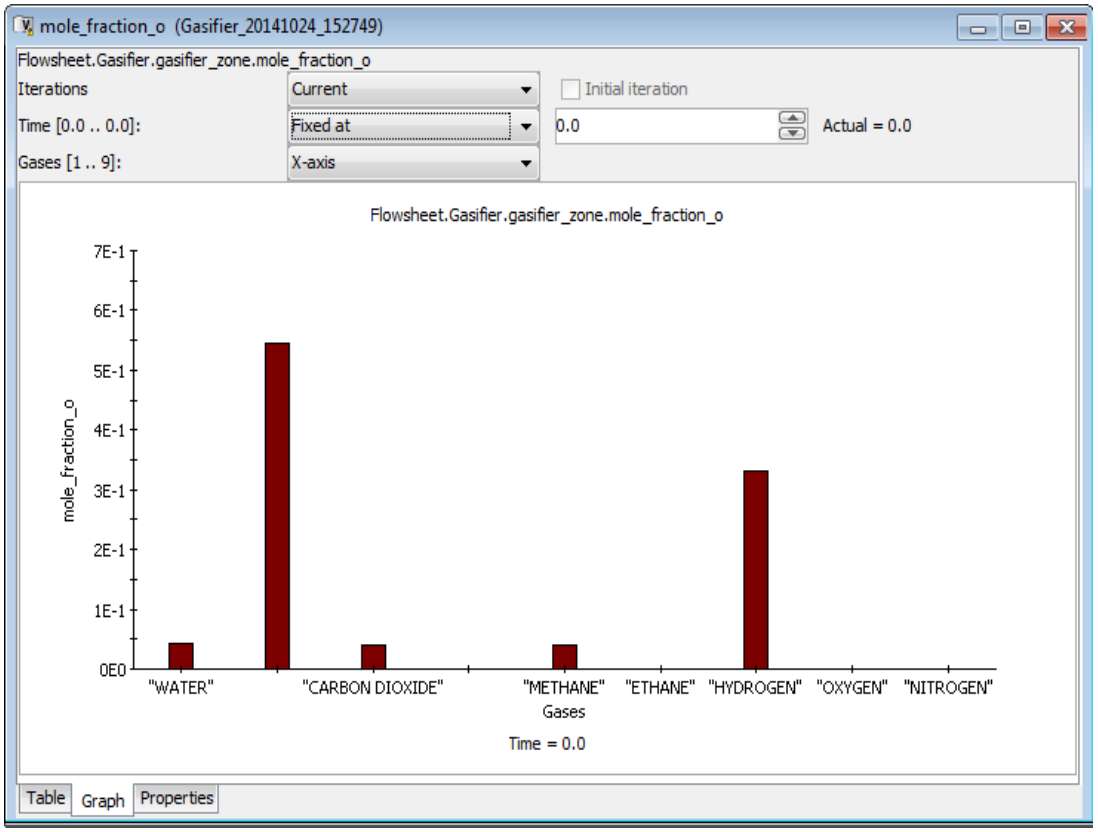

Figure D11: Mole fraction of the product gas at the gasifier outlet (*after optimization*)

Appendix E: Lee *et al.* (2011) Model Results

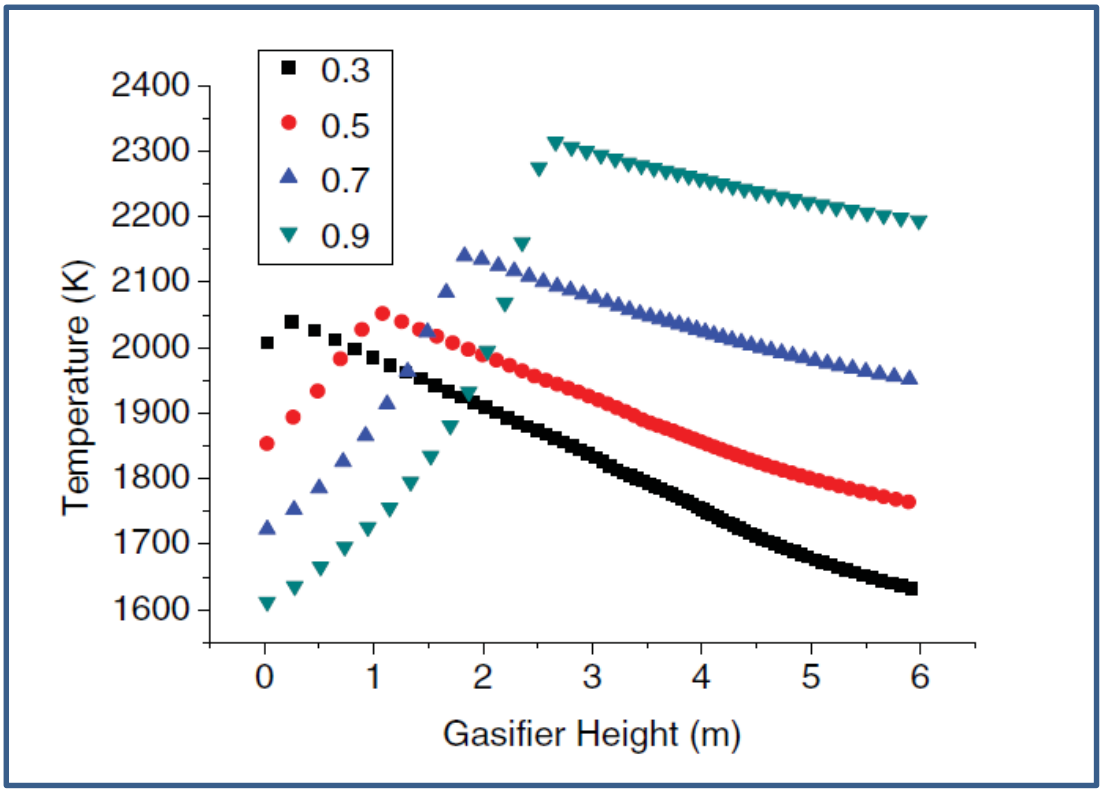

Figure E1: Effect of oxygen to coal ratio on gas temperature

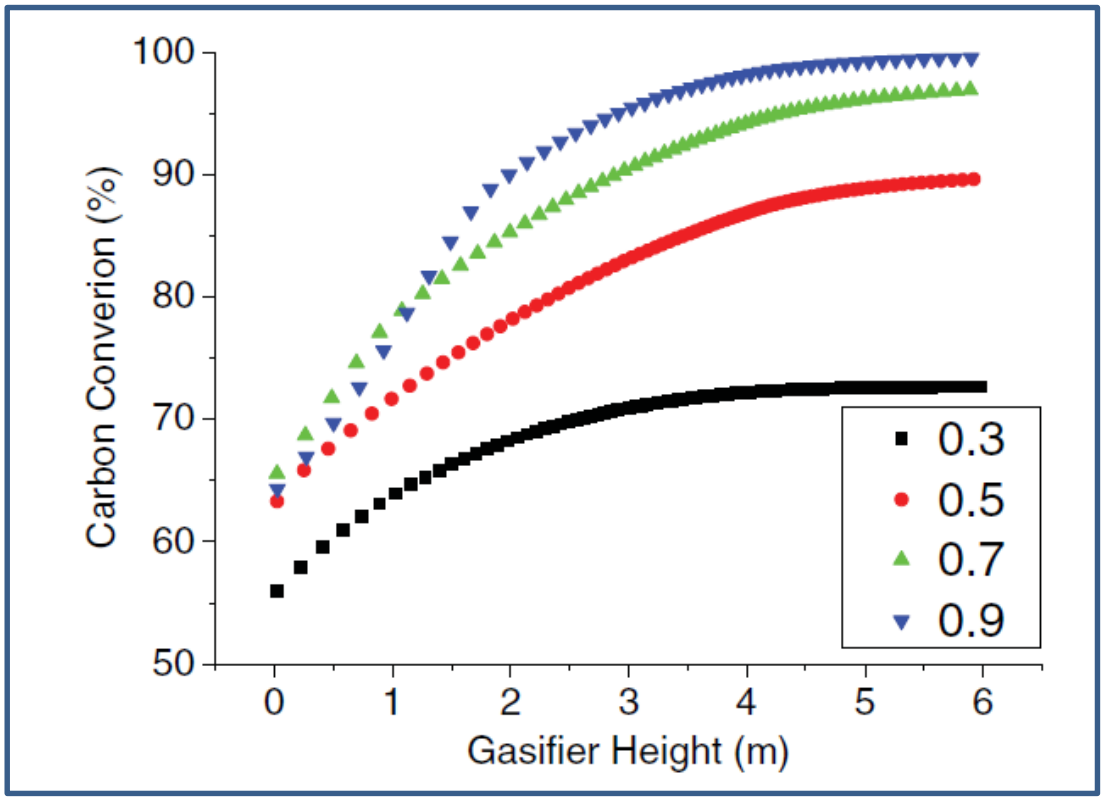

Figure E2: Effect of oxygen to coal ration on carbon conversion

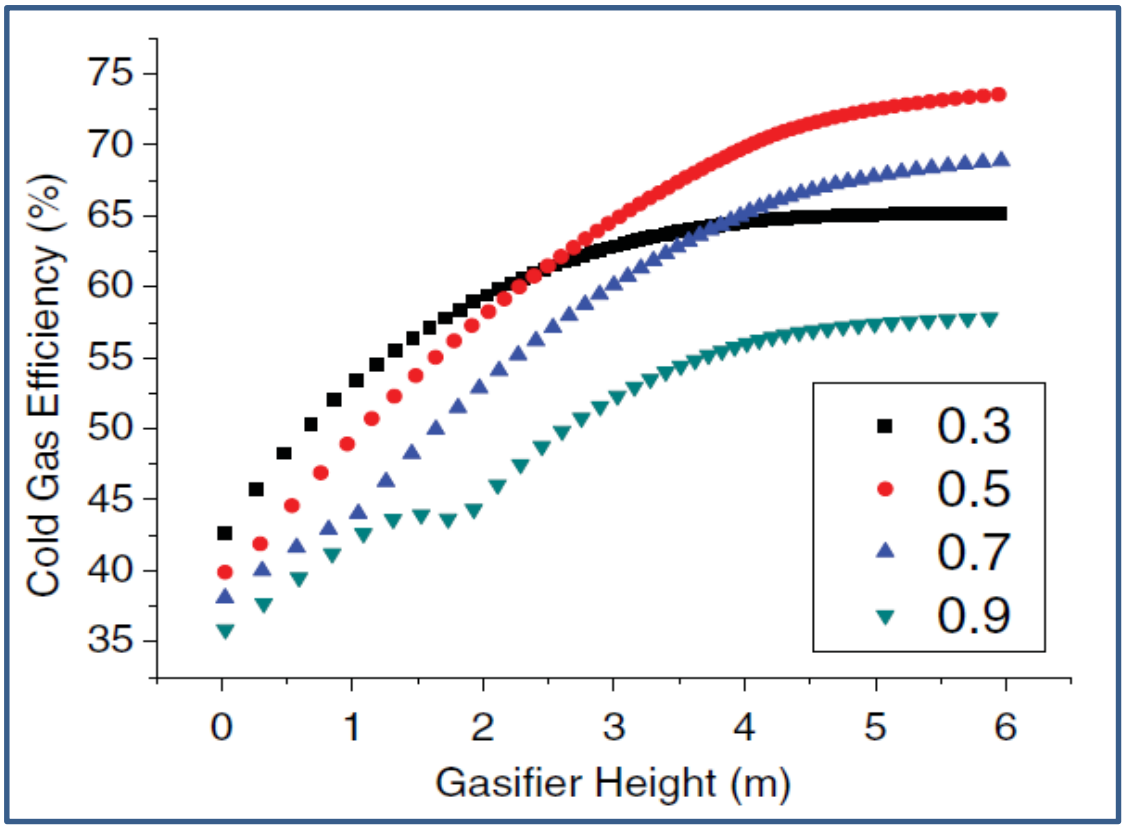

Figure E3: The effect of oxygen to coal ratio on coal gas efficiency